NTNU – Trondheim
Norwegian University of
Science and Technology

Damage Assessment of Sevan FPSO Subjected to Impacts From Shuttle Tankers

Meilin Ma

Marine Technology
Submission date: July 2014
Supervisor: Jørgen Amdahl, IMT

Norwegian University of Science and Technology
Department of Marine Technology

Title:	Delivered:
Damage assessment of Sevan FPSO subjected to impacts from shuttle tankers	July 31, 2014
	Availability: Open
Student: Meilin Ma	**Number of pages:** 86

Abstract:

Non Linear Finite Element Analysis (NLFEA) models of the Sevan SSP300 platform and a shuttle tanker are created, with the correct mass, added mass and rotational inertial. Different impact scenarios are chosen. In the integrated analysis, both the platform and the tanker are free moving. When it comes to internal mechanics analysis, the platform is set to be fixed spatially. Both integrated NLFEA analysis and internal analysis are performed on the structures using the explicit NLFEA solver LS DYNA. Important results obtained from the NLFEA are the energy dissipation and the force displacement relationship.

External mechanics analysis is performed to calculate the dissipated energy and the velocity of the FPSO and shuttle tanker after the impact. Liu's method is utilized in this thesis. A fully three dimension solution is proposed for the analysis and a Matlab program based on the Stronge 3D program is used to achieve this goal. Both the correct mass and the added mass are included in the external mechanics analysis.

Liu's method is considered as one of the simplified methods. Two other simplified methods are utilized to calculate the dissipated energy and then compare them with the results from NLFEA analysis. One is from the DNV-RP-C204 and the other one is from T.de Jonge&L.laukeland's report. The latter one is an optimized method compared to the one from DNV rules, which includes the effect of roll motion.

Two additional jobs are conducted in the end. One is changing the loading conditions of the two bodies, and the other is changing the friction coefficient. Only the energy dissipation is analyzed in this section.

Keyword:

Finite element modeling, LS DYNA
Platform-ship collision
Simplified method

Advisor:

Professor Jørgen Amdahl

MASTER THESIS SPRING 2014

for

Stud. techn. Meilin Ma

Damage assessment of Sevan FPSO subjected to impacts from shuttle tankers
Skadevurdering av Sevan FPSO utsableatt for støt fra skytteltankere

In deep water - drilling for and production of oil and gas - use of floating platforms/FPSOs are the only viable solutions. The Sevan marine design has proved to be an efficient concept. In many remote fields the only practical possibility for oil transfer to shore is via off take tankers based on tandem offloading or via a single point mooring system. Tandem offloading has shown to be the most economical alternative in this respect. In tandem offloading, the shuttle tanker is moored to the FPSO by hawsers and/or Dynamic Positioning (DP), while the cargo is off loaded through floating hoses. Comment: For the Sevan concept the base case offloading scenario is with a shuttle tanker on DP – i.e. no hawser – and in addition the offloading hose is not a floating hose.

The use of tankers for offshore loading implies risk for various types of collision:

- Collision of powered or drifting tanker with installation (FPSO). This can be treated as for collisions for other passing vessels with platforms, defining the tanker route as part of the shipping traffic data. This scenario is treated as a passing vessel.

- Collision of shuttle tanker with FPSO during offloading. This may be due to human error or machinery failure on approach or due to a mooring or Dynamic Positioning (DP) failure during offloading operations.

The latter scenario will be studied here for the Sevan 300 FPSO. This platform was analysed for ship impacts in 2005 by means of simplified, plastic analysis. The idea of the present Project/Master thesis work is to conduct more advanced analysis based on the non-linear finite element method (NLFEA) and to compare the results with those obtained with simplified methods.

Scope of work for project/master thesis:

General

The 2005 investigation showed that the Sevan 300 design has significant resistance against local deformation in terms of global structural collapse. Consequently, the local damage to the platform hull in terms of penetration distance and number of punctured compartments, and the global response in terms of collision-induced offset will be important parameters.

The aim of the work is to evaluate the collision consequences in a realistic manner without over-conservative assumptions, thereby enabling the establishment of realistic operational

constraints around the platform. This is especially challenging with glancing impacts between vessel and platform, and cannot be solved with simple methods without significant conservative assumptions. By utilizing non-linear finite element analysis with advanced structural and material modelling, a realistic consequence assessment can be conducted.

Establishment of impact scenarios:

Likely impact scenarios are related to ship operations in the approach stage and during offloading. In extreme cases this may lead to a head on impact with the platform, in which the highest level of kinetic energy will have to be dissipated during collision. However, normal operating procedures dictate that the incoming vessel approach at an angle to the platform, thereby making a glancing impact more probable. For the approach phase the ballast draft and displacement will be used.

Assessment of penetration versus impact speed

For head-on collisions the bow will be pushed into the platform allowing penetration up to several meters involving puncturing of tanks. The energy dissipation is expected to be considerably larger than 100 MJ. The penetration levels, and hence the critical impact speed for puncturing of tanks, will be back calculated by means of external mechanics principles (conservation of momentum and energy).

If the same principles shall be used for glancing bow impacts, the ship will have to be pushed into the platform in a constant direction while the platform is kept fixed. This does not simulate the actual motions of the ship and platform, where focus is placed on surge, sway and yaw motions. Hence, for simulation of glancing bow impacts, a complete model of the ship and the platform will be made. A very crude finite element model will be created outside the impact area, so as to take into account inertia and hydrodynamic forces for in-plane motions (surge, sway, yaw). The simulation will have to be carried out for a given initial speed of the ship.

Finite Element Modelling

Finite element analyses will be carried out with the non-linear program LS-DYNA. The structures are modelled with shell elements, with a mesh size of 5-10 x plate thickness. A representative part of the Sevan 300 will be modelled in detail. Existing finite element models of two tankers will be used for the simulations. Fracture in steel plating will be modelled using the RTCL fracture criterion.

It is recommended to carry out the work in the following steps:

1) Describe the structural configuration of the Sevan 300 platform side structure

2) Describe the structural configuration of a realistic offloading tanker

3) Select relevant impact scenarios in terms of impact geometry and speed of the two bodies

4) Establish a detailed finite element model of the *Sevan 300* side structure connected to a coarse global model of the entire platform. The finite element model for the platform shall be sufficiently fine to capture the governing deformation mechanisms in way of the impact zone,

but still meet requirements with respect to acceptable CPU consumption. The mass (including added mass) of the global platform model should be representative of the actual platform in terms of magnitude, center of gravity and radii of gyration.

5) Establish a model of a large tanker for use in the integrated collision simulations. An existing detailed bow model should be extended. The mass (including added mass) of the global vessel model should be representative of a reference vessel in terms of magnitude, centre of gravity and radii of gyration

6) By means of external impact mechanics, estimate the amount of impact energy that must be dissipated as strain energy for the selected impact scenarios.

7) Conduct impact simulations of the global tanker model with the global *Sevan 300* model for the selected scenarios. Compare the results of the global impact analysis with those based on simplified methods. To the extent time permits the following assumptions may be varied:

a. Friction steel-steel friction coefficient

b. The added mass coefficients

c. Fracture strain

8) Conclusions and recommendations for further work.
Literature studies of specific topics relevant to the thesis work may be included.

The work scope may prove to be larger than initially anticipated. Subject to approval from the supervisors, topics may be deleted from the list above or reduced in extent.

In the thesis the candidate shall present his personal contribution to the resolution of problems within the scope of the thesis work.

Theories and conclusions should be based on mathematical derivations and/or logic reasoning identifying the various steps in the deduction.

The candidate should utilise the existing possibilities for obtaining relevant literature.

Thesis format

The thesis should be organised in a rational manner to give a clear exposition of results, assessments, and conclusions. The text should be brief and to the point, with a clear language. Telegraphic language should be avoided.

The thesis shall contain the following elements: A text defining the scope, preface, list of contents, summary, main body of thesis, conclusions with recommendations for further work, list of symbols and acronyms, references and (optional) appendices. All figures, tables and equations shall be numerated.

The supervisors may require that the candidate, in an early stage of the work, presents a written plan for the completion of the work. The plan should include a budget for the use of computer

and laboratory resources, which will be charged to the department. Overruns shall be reported to the supervisors.

The original contribution of the candidate and material taken from other sources shall be clearly defined. Work from other sources shall be properly referenced using an acknowledged referencing system.

The report shall be submitted in two copies:

- Signed by the candidate
- The text defining the scope included
- In bound volume(s)

- Drawings and/or computer prints which cannot be bound should be organised in a separate folder.

- The report shall also be submitted in pdf format along with essential input files for computer analysis, spreadsheets, Matlab files etc in digital format.

Ownership

NTNU has according to the present rules the ownership of the thesis. Any use of the thesis has to be approved by NTNU (or external partner when this applies). The department has the right to use the thesis as if the work was carried out by a NTNU employee, if nothing else has been agreed in advance.

A Sevan Marine design will be utilized in the thesis work. With the intention of allowing the results of the thesis work publicly available, Sevan Marine reserves the right to ensure that commercially sensitive information is not included in the public part of the thesis. If such issues should arise, confidential information is suggested to be included as an appendix, which is omitted from the openly available thesis.

Thesis supervisor

Prof. Jørgen Amdahl

Contact person at Sevan Marine: Ragnar Thunes

Deadline

July 31, 2014

Trondheim, February 12, 2014

Jørgen Amdahl

Summary

Platform-ship collisions are fortunately rare events, but as the development of the offshore and oil industry and the gradually frequently used offloading operation, accidents become more and more frequent. The consequences of collisions are always severe, which includes loss of life, property and environmental damage. Thus It is important to predict the outcome of collision scenarios and assess the damage that may happen to the platform as well as the shuttle tanker.

Collisions are always analyzed by means of the principle of the principle of energy conservation. Initial kinetic energy is dissipated by the two contact bodies as strain energy and in viscous force generation. There is also energy remained as the kinetic energy after the impact for both the striking and struck bodies, both for translational and rotational degrees of freedom. The external mechanics of the collision is easily evaluated, but the strain energy absorption can be rather difficult to evaluate in a correct way.

In this thesis, A Samsung shuttle tanker and the Sevan SSP300 platform are analyzed as the striking and struck bodies, respectively. Structural configurations are described for both structures. Different impact scenarios are then discussed in the report, some of which are chosen to analyze in the thesis work. Non Linear Finite Element Analysis (NLFEA) model of the SSP300 platform is created. The shuttle tanker model is an exist one. One-sixth of the platform is modeled in detail with the correct stiffeners and other details, while for the other part, only the outer shell and the main bulkheads are modeled. For the tanker, adjustments are made in order to increase the calculation efficiency. Only the bow is remained in details. For the hull, only the outer shell is remained. For both structural models, adjustments are made to obtain the correct mass, added mass and inertial. Both models have a user defined material with the fracture criterion included.

Integrated analysis is mainly performed. Then the integrated analysis is split into internal mechanics and external mechanics. Among these, integrated analysis and internal mechanics analysis are performed with finite element method, using the explicit NLFEA solver LS-DYNA. For the collision scenarios, only bow impact with different headings is considered. Two different impact velocities are chosen in both head on collision and collision with the glancing angle of 30 degrees. Energy absorption and force-displacement relationship can be obtained. Damage on the platform is also evaluated.

Internal mechanics are then analyzed by changing the boundary condition and making the impact velocity constant. The purpose is to evaluate the damage with internal mechanics and then compare it with the results from integrated analysis.

Liu's method, which is based on Stronge theory, is mainly used in external mechanics as a simplified method. Herein a Matlab program is established to calculate the energy dissipation and the velocity after the impact. Two other simplified methods are utilized to calculate the dissipated energy and then compare them with the results from NLFEA analysis. One is from

the DNV-RP-C204 and the other one is from T.de Jonge&L.laukeland's report. The latter one is an optimized method compared to the one from DNV rules, which includes the effect of roll motion.

Results from the simplified methods and NLFEA method show good correlation. All the simplified methods overestimate the absorbed energy, which is conservative. Among these, Liu's method gives the best correlation with the NLFEA method.

Two additional jobs are conducted in the end. Only the energy dissipation is analyzed in this section. One is changing the loading conditions of the two bodies. The energy dissipation becomes smaller after changing. The other one is changing the friction coefficient. The energy dissipated by the tanker is smaller, while by the platform is larger. But from the overall view, the energy does not show big difference with friction coefficient 0.15 and 0.4.

Preface

This report is the result of the Master Thesis for student Meilin Ma at The Norwegian University of Science and Technology (NTNU), spring 2014. This project has been carried out from February to July. All the compulsive requirements in the problem text are carried out here and two of the additional problems in 7) are addressed.

The collision problem is my interest, so I have been working on the same topic in both the project work and thesis work. Most background theories, which have been described in the project thesis, will not be repeated again herein. Long time was spent on the modeling of the platform. But it is an interesting, challenging and rewarding task.

I learnt a lot during the period of both the master project and master thesis. I believe all of these will be a great fortune for me in my future work. I have been as a student for almost 20 years and now final graduation is coming. I have been loving to be a student and now nostalgia drifts in the air. After coming to Norway, I realize the academic pleasure, which I actually never felt in deep before. This owns to all the professors who have lectured to me in these two years. Listening to these lectures is becoming a kind of enjoyment. Herein I would like to thank my supervisor Prof. Jørgen Amdahl especially. To be precise, the course Buckling and Collapse of Marine Structures aroused my deeper interest to my major thoroughly. That is why I chose my supervisor and topic with no hesitation. I believe interest is the best teacher.

During the thesis work, I have been discussed with various persons and they offered great help. Herein I would like to thank my Master Thesis advisor Prof. Jørgen Amdahl for the guidance and understanding, Ragnar Thunes (SEVAN) for the data support, Martin Storheim and Ekaterina Kim for help with FE modeling in MSC Patran, as well as the LS-DYNA configuration and modeling, Jan Børge Sætre for the selfless help regarding the serious problem I met in LS-DYNA, and a special thank to Stud. Martin Slagstad who always took time to help me whenever I needed.

Meilin Ma

Tyholt, Trondheim

July 25, 2014

Table of Contents

List of Figures

List of Tables

Nomenclature

Variable	Unit	Description
E_k	J	Kinetic energy
m_s	kg	Mass of striking ship
a_s	kg	Added mass of striking ship
E_s	J	Strain energy
v_s	m/s	Impact speed of the striking ship
v_i	m/s	Velocity of the platform
m_i	kg	Mass of the platform
J	$kg \cdot m^2$	Mass moment of inertia of installation (including added mass) with respect to effective pivot point
z	m	distance from pivot point to point of contact
M	-	Diagonal mass matrix
P^n	N	External and body force loads
a^n	m/s^2	Acceleration
F^n	N	Stress divergence vector
H^n	N	Hourglass resistance
u	m	Global nodal displacement vector
v	m/s	Nodal velocity vector
L_s	m	Characteristic element length
c	m/s	Sound speed in the material
ρ	kg/m^3	Density of the material

E	Pa	Young's modulus
β_o	-	Parameter deciding element type
A_s	m^2	Area
$L_1 - L_4$	m	Length of the sides defining the shell elements
V_n	m^3	Volume of virtual neck
l_e	m	Element length
t	m	Element thickness
V_r	m^3	Volume outside the instability
V_{el}	m^3	Total element volume
ε_n	-	Strain of virtual neck
ε_r	-	Strain outside the instability
ε_{cr}	-	Critical strain
σ_y	Pa	Yield stress
ε_{plat}	-	Plateu strain
K	-	Strength coefficient
σ	Pa	Stress
G_{ij}	-	Incremental displacement gradient
ε_{ij}	-	Incremental strain tensor
σ_{ij}	-	Incremental stress tensor
ω_{ij}	-	Incremental spin tensor
ε	-	Strain
P	kg·m/s	Momentum

E_p	J	Potential energy
α	rad	Waterline angle
β	rad	Frame angle
β'	rad	Normal frame angle
γ	rad	Sheer angle
n	-	Strain hardening exponent
υ	-	Possion ratio
$E_{dissipated}$	J	Total dissipated energy
v_a	m/s	Velocity after impact of object a under body frame of object a
v_b	m/s	Velocity after impact of object b under body frame of object b
E_0	J	Kinetic energy of striking body before impact
ρ_0	-	Energy ratio between dissipated energy and kinetic energy
I_i	m^4	Moment of inertia of spar around horizontal axis including added inertia
ω	rad/s	Rotational velocity
R	m	Distance of platform center of gravity to point of impact
a, b	-	Coefficient
K_0	J	Energy before impact
K_1	J	Energy after impact
E_a	J	Difference between K_0 and K_1
ρ_a	m	Radius of gyration of the spar

Chapter 1 Introduction and Scope

Floating production storage and offloading units (FPSO), is becoming more popular in the oil and gas industry [1]. Shuttle tankers have to be used in tandem offloading. Normally there are two popular methods of the mooring, using hawsers and Dynamic Positioning (DP). DP requires the cargo to be off loaded through floating hoses. For the Sevan concept the base case offloading scenario is with a shuttle tanker on DP, while no hawser, and in addition the offloading hose is not a floating hose. The use of tankers for offshore loading implies risk for various types of collision.

Tanker platform collisions are of public interest due to the high impact oil leakage might have on local communities and the environment. This may be due to human error, machinery failure on approach, or due to a mooring or Dynamic Positioning (DP) failure during offloading operations. Herein the collision of shuttle tanker with FPSO during offloading is focused on.

The Sevan Stabilized Platform (SSP) is a certain kind of platform with a circular shape. The special nature of SSP in terms of shape makes the platform have the same roll and pitch motions and the same surge and sway motions. The hydrodynamical resistance will also be the same no matter which direction the wave comes from. The SSP has all the advantages of a normal vessel, for example big deck load, large deck, and large storage capacity, but allows better motion behavior. This type of FPSO has an advanced feature in some degree. In this thesis, the impact between the Sevan FPSO SSP300 and the shuttle tankers is considered.

Platform-shuttle tanker collision can be subdivided into inner collision mechanics and outer collision dynamics. The inner collision mechanics is a crash problem governed by buckling, yielding and rupture of materials or assemblies. Outer collision dynamics is the global motion of the two bodies considered as rigid bodies under collision forces and hydrodynamic pressure forces.

The SSP300 platform was analysed for ship impacts in 2005 by means of simplified, plastic analysis [2]. This thesis work will expand and contribute more advanced analysis based on the non-linear finite element method.

Scope

This thesis mainly focuses on the integrated Nonlinear Finite Element Method (NLFEM) analysis, which takes consideration of both the inner and outer mechanics. NLFEM gives an authentic simulation of the reality. Different scenarios are chosen to perform the analysis. Internal mechanics are also particularly considered. Simplified methods are compared with NLFEM results to assess its suitability.

NLFEA models are established for the SSP300 platform and the shuttle tanker. Two main tools, MSC PATRAN and LS-DYNA, are utilized to do modeling and analyzing.

Chapter 2 Overview of Basic Principles

The principles behind ship collision analysis and design are described in detail in NORSOK STANDARD N-004 [3] and DNV-RP-C204 [4]. It can be seen that in the collision analysis, we commonly consider the followings.

2.1 General Description on the Collision

To put it simply, the essence of collision is an energy conversion process. During the process, there will be conversion between kinetic energy and potential energy, also the energy dissipation. Dissipation of energy depends on the relative strength between the FPSO and the shuttle tanker. The kinetic energy equation is shown below.

$$E_k = \frac{1}{2}(m_s + a_s)\cdot v_s^{\,2} \tag{1}$$

The ship kinetic energy depends on the ship mass, which includes the hydrodynamic added mass and the ship speed at the moment of impact. It is proportional to first power of the mass and second power of the speed. The velocity has a greater affect on the kinetic energy.

After the collision, some of the kinetic energy will remain while some of it will be dissipated as strain energy by the installation and the ship. The amount of the dissipated energy differs with the type of the installations.

Commonly, there are three different kinds of installations [3]:

(1) Compliant installations: it can be assumed that the installation and the ship have the same speed after impact. The dissipated strain energy can be calculated by:

$$E_s = \frac{1}{2}(m_s + a_s)\cdot v_s^{\,2}\,\frac{\left(1-\frac{v_i}{v_s}\right)^2}{1+\frac{m_s+a_s}{m_i+a_i}} \tag{2}$$

(2) Fixed installations: it can be assumed that all the kinetic energy is dissipated as strain energy.

$$E_s = \frac{1}{2}(m_s + a_s)\cdot v_s^{\,2} \tag{3}$$

(3) Articulated columns: the dissipated strain energy will decease compared to fixed installations, which is due to the impact of the “articulated support”.

$$E_s = \frac{1}{2}(m_s + a_s) \cdot \frac{\left(1 - \frac{v_i}{v_s}\right)^2}{1 + \frac{m_s z^2}{J}} \tag{4}$$

m_s - ship mass

a_s - ship added mass

v_s - impact speed

m_i - mass of installation

a_i - added mass of installation

v_i - velocity of installation

J - mass moment of inertia of installation (including added mass) with respect to effective pivot point

z - distance from pivot point to point of contact

2.2 Design Principles

With respect to the distribution of strain energy dissipation there are distinguished regions between strength, ductility and shared-energy designs. The illustration showing the relationship between these are shown in Figure 2.1 [3].

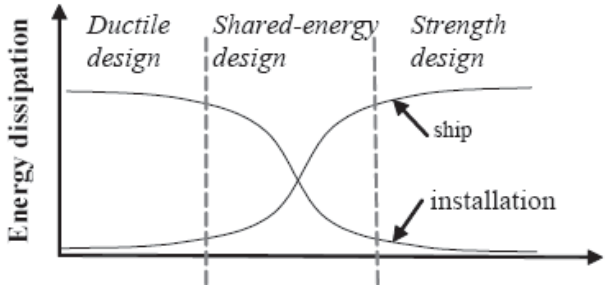

Figure 2.1 Energy Dissipation for Strength, Ductile and Shared-energy Design

The design principles mainly depend on the relative strength between the impact structures. If the installation strength is smaller than the ship strength, more energy will be dissipated by the installation. The strength assessment of the installation becomes more important and must be modified to a ductile design; However, if the installation strength is larger than the ship

strength, more energy will be dissipated by the ship. The strength assessment of the ship becomes more important and must be modified to strength design; if the strength difference between the two is not big, it indicates that both of them will contribute significantly to the energy dissipation, thus the shared-energy design is optimum.

2.3 Impact Caused Deformation

In the collision study, the strain exceeds elastic stage in the stress-strain curve. Plastic regime has to be focused on. That is, when the deformation of either the installation or the ship or both is large. This explains why non-linear finite element analysis has to be performed in the collision problem. There will also be large plastic strains and significant structural damage. So the force-deformation relationship (curve) is an important feature in the collision analysis. Commonly, the deformation will increase non-linearly as the force becomes large. When the force reaches a certain large enough value, the structure may fracture or be damaged. The curve will fall suddenly as the stress is reduced via the failure. The total dissipated energy by the ship and the platform could be estimated from the curve, which is the total area under the force-displacement curve.

But in the NORSOK standard N-004, there is a limitation when establishing the force-deformation curve. When establishing the curve of one side in the collision, it is assumed that the other side is totally rigid and has no deformation. In reality, both will be deformed. However, this will not have much influence especially in the ductile design and the strength design.

In the NORSOK standard, some other information regarding the principles behind ship collision are given. For example, the effect of force contact area, denting, stiffeners, the strength of connections and the adjacent structure and buckling, etc. Due to the scope of this work, the NORSOK standard will not be further discussed.

Chapter 3 Theory in LS-DYNA

The information in this chapter is mainly found from the LS-DYNA Theory Manual [5]. Some simple descriptions of the relevant topics for this study are listed.

3.1 Time Integration

LS-DYNA uses the explicit central difference scheme to integrate the equations of motion. The semi-discrete equation of motion in time is presented in Eq. (5).

$$Ma^n = p^n - F^n + H^n \tag{5}$$

Where M is the diagonal mass matrix, p^n accounts for the external and body force loads, F^n is the stress divergence vector and H^n is the hourglass resistance.

To advance in time the central difference time integration is applied.

$$a^n = M^{-1}\left(p^n - F^n + H^n\right) \tag{6}$$

$$v^{n+\frac{1}{2}} = v^{n-\frac{1}{2}} + a^n \Delta t^n \tag{7}$$

$$u^{n+1} = u^n + v^{n+\frac{1}{2}} \Delta t^{n+\frac{1}{2}} \tag{8}$$

$$\Delta t^{n+\frac{1}{2}} = \frac{\Delta t^n + \Delta t^{n+1}}{2} \tag{9}$$

Where u is the global nodal displacement vector and v is the nodal velocity vector. The geometry is updated by adding the displacement increments to the initial geometry:

$$x^{n+1} = x^0 + u^{n+1} \tag{10}$$

The sequential process each time integration loop represents is presented in Figure 3.1

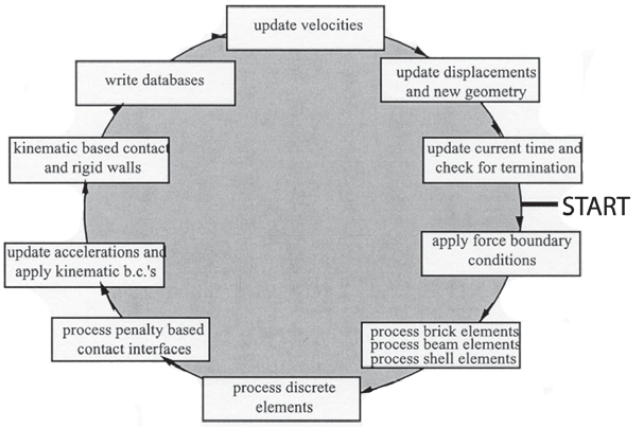

Figure 3.1 Time Integration Loop in LS-DYNA from [5]

3.2 Time Step Size

An explicit dynamic FEA solver is only conditionally stable. To ensure stability a requirement is put on the time step size in the analysis so that each time step is lower than the critical time step for the model. The critical time step is governed by several parameters. To fulfill the conditions for stability the time step needs to be smaller than the time a pressure wave uses to pass through the element. If this was not the case, uncontrolled pressure waves could pass through the model and the results would at best be inaccurate. Another important factor regarding time step size is contact between bodies, as this requires a low time step to be stable [6].

In LS-DYNA the next time step ensuring a stable solution is found by cycling through all the elements and checking heir minimum time step size from the respective equations. A safety factor of 0.9 is then applied to the smallest step size found to ensure that the critical time step size is not violated. The time step factors for shell element types used herein is presented below.

For shell elements the critical time step is given by Eq.(11).

$$\Delta t_e = \frac{L_s}{c} \tag{11}$$

Where L_s is the characteristic element length and c is the sound speed in the material, given by

$$c = \sqrt{\frac{E}{\rho\left(1-\nu^2\right)}} \tag{12}$$

The characteristic element length can be defined in three different ways:

- The default option: calculate L_s based on the length of the element sides.

- A conservative option: calculate L_s based on the diagonals of the element that gives a larger characteristic length, thus smaller time steps.
- A non conservative option: gives a larger time step size, which is frequently used when small triangular shell elements are needed.

For simplicity, the default option is used to calculate L_s. The time step is then given by Eq. (13).

$$L_s = \frac{(1-\beta_0)A_s}{\max(L_1, L_2, L_3, (1-\beta_0)L_4)} \tag{13}$$

Where $\beta_0 = 0$ for quadrilateral and 1 for triangular shell elements, A_s is the area, and $L_i, (i = 1..4)$ is the length of the sides defining the shell elements.

3.3 Material Models

There are approximately 300 material types in LS-DYNA. In the LS-DYNA Keyword User's Manual, all these materials and input values are described in detail [7]. Proper materials that should be used in this project have to be chosen carefully. In this analysis, we will use two of these materials, which are rigid and user defined elastoplastic materials with a fracture criterion.

MAT_RIGID

This is material type 20. The rigid material model *MAT_RIGID* is used in the pure ductile and strength design analysis where certain parts of the structure are assumed to be rigid.

It is always very convenient to turn a structure or some parts of the structure into a rigid part. In practical engineering, a deformable body or part is often approximated as a rigid body, which is a very effective method and could make the analysis much easier. In most cases, the error of this method is very small. The elements associated to this material will not deform during the process. Modulus of elasticity, Poisson ratio and density are defined for the rigid material in order to get the sliding effect in the contact simulation correct towards the non-rigid elements.

MAT_USER_DEFINED with fracture criterion

This kind of material used is a material model developed in house by Alsos [8], from which the following information can be studied in further detail. The material model contains a fracture criterion that is element size dependent. The material uses a modified power law hardening as a basis, and applies a criterion to the maximum allowable plastic strain in an element. As the element size is reduced, the strain in the elements in a hot spot zone (e.g.

close to a stiffener) will increase rapidly. To get a more accurate representation of the element fracture, small elements are needed. However, small elements in an explicit analysis are unfavorable due to critical time step considerations.

For offshore structures this can pose a serious problem for several reasons. The classification societies often only specify a lower requirement on the material used in structure building. This implies that the as built material properties can be tougher than the original, giving a stronger structure. The sheer size of the structure will furthermore result in an analysis with a coarse mesh due to computational limitations. Coarse meshes will not capture the strain concentrations typically seen in offshore structures. This is especially apparent close to crack tips, at structural intersections or in the post necking zone in sheet metal. The problems are further amplified by the fact that shell elements are especially sensitive to mesh scale effects. These factors are generally not compatible with a complex damage model required to predict fracture.

Failure mechanisms such as local necking typically takes place in narrow bands as wide as the shell thickness. With a mesh size 5-10 times the shell thickness the elements are too large to detect these local instabilities. As a remedy for these problems, mesh scaling of the rupture criterion based on the equivalent strain is applied in the material model. If this is not done, the FE analysis would often yield to ductile results. Figure 3.2 shows the scaling function together with calibrated results obtained from [9].

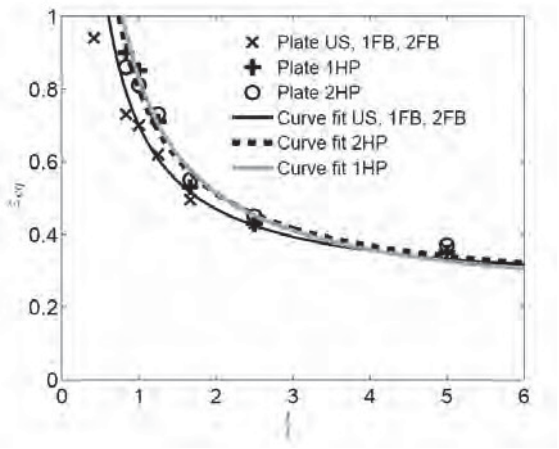

Figure 3.2 Mesh Scaling of Fracture Criterion from [9]

Assuming that the localized mechanisms appear parallel to the element side, the average equivalent strain at fracture for various element sizes can be formulated in terms of Eq. (14). Here the width of the virtual neck is assumed to be as wide as the element thickness giving a neck volume of $V_n = t^2 l_e$ where l_e is the element length and t is the element thickness. The volume of the remainder of the element is $V_r = V_{el} - V_n = t l_e^{\,2} - t^2 l_e$. Inserting this into Eq. (14) gives Eq. (15). Eq. (15) is used as a basis for the plastic strain rupture criterion.

$$\varepsilon_{cr} = \frac{\varepsilon_r V_r + \varepsilon_n V_n}{V_{el}} \tag{14}$$

$$\varepsilon_{cr} = \varepsilon_r + (\varepsilon_n - \varepsilon_r)\frac{t}{l_e} \tag{15}$$

Where V_{el} is the total element volume, V_n is the volume of virtual neck, V_r is the volume outside the instability, ε_n is strain of virtual neck and ε_r is the strain outside the instability. The relationship between these variables is illustrated in Figure 3.3.

It should be noted that correcting the failure level as a function of element size can be dangerous. This is because it is not guaranteed that local deformation mechanisms take place before fracture. Applying mesh scaling of the fracture criterion should therefore be made with caution, but for offshore structures it is generally acceptable to use [9].

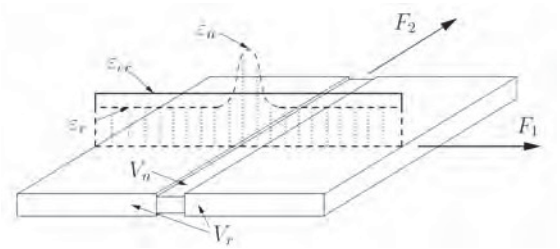

Figure 3.3 Element Necking Model by [9]

The nominal stress-strain relationship is represented by a modified power law formulation which includes the plateau strain (Eq.16). The strain ε_0 describes an expression which allows the plateau and power law expression to intersect at $(\varepsilon_{plat}, \sigma_y)$ as shown in Eq. (17).

$$\sigma_{eq} = \begin{cases} \sigma_y & if \varepsilon_{eq} \le \varepsilon_{plat} \\ K(\varepsilon_{eq} + \varepsilon_0)^n & otherwise \end{cases} \tag{16}$$

$$\varepsilon_0 = \left(\frac{\sigma_y}{k}\right)^{\frac{1}{n}} - \varepsilon_{plat} \tag{17}$$

3.4 Element Models

Here in this thesis, the main element models used are Hughes-Liu Shell Elements, which will be discussed briefly. Other details can be found in [5].

The Hughes-Liu shell element formulation is the default shell element in LS-DYNA. The element formulation has some desirable qualities:

- It is incrementally objective, allowing for the treatment of finite strains
- It is simple, which translates into computational efficiency and robustness
- It includes finite transverse shear strains

The element is described by a reference surface that can be chosen as either the mid surface or either of the shell outer surfaces. Originally developed based on a standard 8-nodes brick element, it defines a nodal fiber at each corner which represents the brick element's two nodes in the thickness direction. These nodal fibers are used to describe the rotation of the nodes. It uses an isoparametric representation in which the same parameters are used to describe the reference surface, nodal fibers as well as the shell element displacements.

The incremental strain tensor is calculated from the incremental displacement gradient G_{ij}, and is then expressed as in Eq. (19). In a similar manner the spin tensor is found in Eq. (20). The stresses are updated incrementally in the local element coordinate system (Eq.21) and rotated back to the global system by Eq. (22).

$$G_{ij} = \frac{\partial \Delta u_i}{\partial y_j} \tag{18}$$

$$\Delta \varepsilon_{ij} = \frac{1}{2}\left(G_{ij} + G_{ji}\right) \tag{19}$$

$$\Delta \omega_{ij} = \frac{1}{2}\left(G_{ij} - G_{ji}\right) \tag{20}$$

$$\sigma_{ij}^{l^{n+1}} = \underline{\sigma}_{ij}^{l^{n+1}} + \Delta \sigma_{ij}^{l^{n+1/2}} \tag{21}$$

$$\sigma_{ij}^{n+1} = q_{ki} \sigma_{kn}^{l^{n+1}} q_{nj} \tag{22}$$

Chapter 4 Impact Scenarios Discussion

It is hard to predict how a shuttle tanker will collide with the FPSO. Actually the impact direction with the critical condition is most concerned. In order to find this, several possible impact scenarios are assumed.

Each impact scenarios has different load conditions, different impact direction and different initial velocities. Moreover, the location of the impact will also have an effect. In this Chapter, several possible main scenarios are discussed in the first three sections. Afterwards, a summary of chosen scenarios are discussed.

4.1 Impact Locations

4.1.1 Impact Locations on Tanker

Different impact locations will cause different energy dissipation amount due to the strength difference.

A: bow impact (with headings consideration)

- Head on: This is a specific impact heading. It is supposed that in head on impact, there will be the more energy dissipation as strain energy compared to the collision with a glancing angle, which is to be checked later in the finite element analysis and simple method.

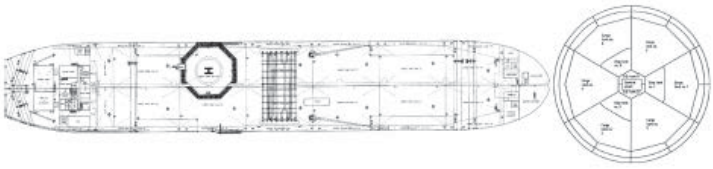

Figure 4.1 Head on collision_Mid Tank [10]

- Glancing angle: But in more general condition, there will be an angle when the tanker approaches the FPSO. In reality, the glancing angle will be different. Figure 4.2 shows a smaller glancing angle and Figure 4.3 shows a larger one.

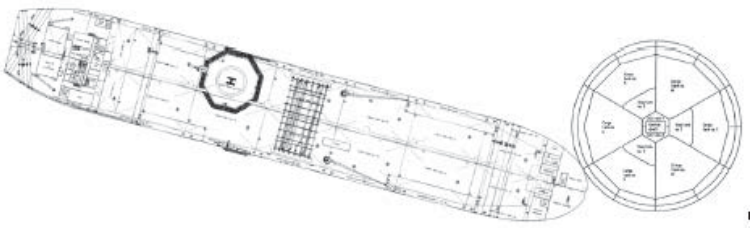

Figure 4.2 Glancing Collision 1 [10]

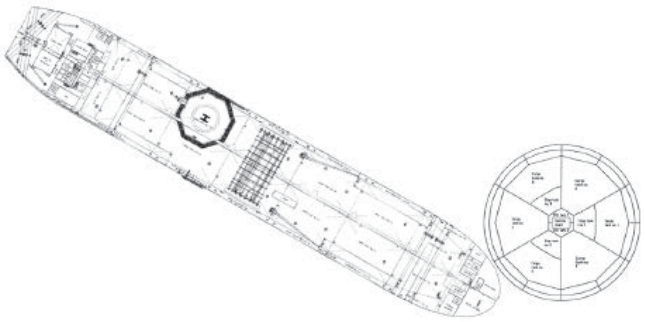

Figure 4.3 Glancing Collision 2 [10]

In a collision with the tanker bow for this case, different parts could be impacted. For example, either the bow or the forecastle deck or both would be contacted, which depends upon the dimensions and geometry of the two structures. Furthermore, the draught variations of the FPSO and the shuttle tanker, the sea state at the operation environment, and the motion between each other are important.

B: side impact

C: stern impact

Due to the focus, side impact and stern impact will not be discussed in detailed here.

4.1.2 Impact Locations on Platform

- Between transverse bulkheads
- On transverse bulkhead

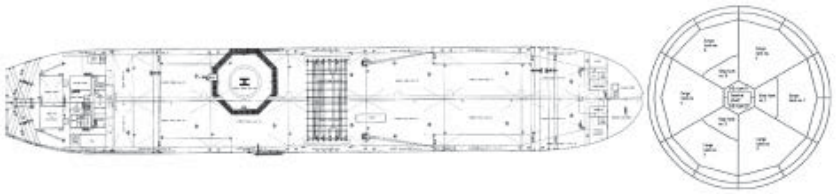

Figure 4.4 Head on Collision_Mid Tank [10]

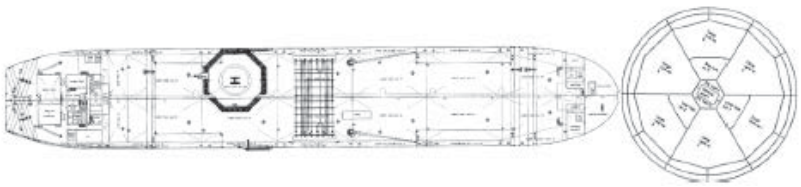

Figure 4.5 Head on Collision_Transverse Bulkhead [10]

Different impact locations on the platform, which is shown in Figure 4.4 and Figure 4.5, will affect the energy dissipation absolutely, but in the simple external mechanics method, no difference due to this effect can be shown.

4.2 Impact Elevations

- Shuttle tanker in ballast, FPSO in full load conditions
- Shuttle tanker in full load, FPSO in ballast conditions

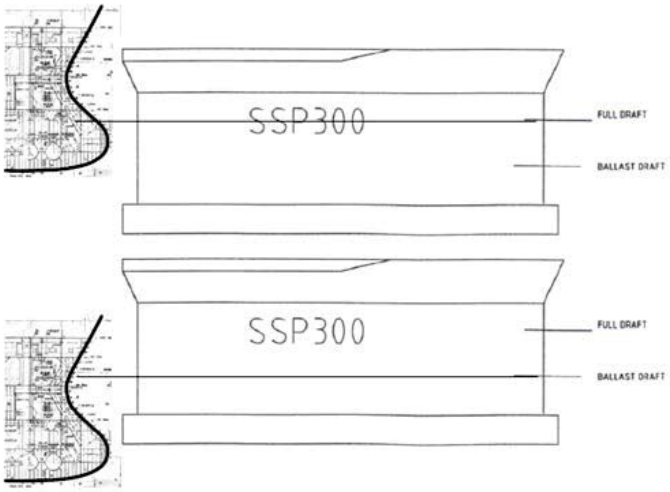

Figure 4.6 Collision Scenarios with Different Impact Elevation [10]

It is considered that in the approach phase is the most critical scenarios with respect to collision. In this condition, the SSP300 will be in fully loaded condition, while the shuttle tanker will be in ballast condition or partly ballast condition.

This could be explained by Eq. (23) and the Figure 4.7.

$$E_s = \frac{1}{2}\left(m_s + a_s\right)\cdot v_s^{\,2}\,\frac{1}{1+\dfrac{m_s + a_s}{m_i + a_i}} \tag{23}$$

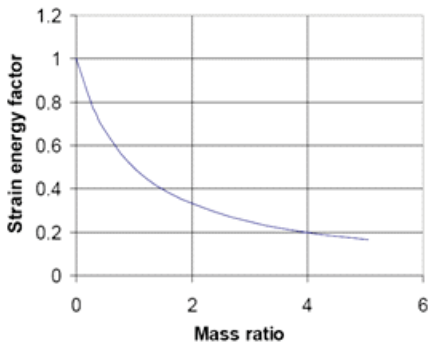

Figure 4.7 Fraction of Kinetic Energy Absorbed versus Mass Ratio

The mass ratio is $(m_s + a_s)/(m_i + a_i)$. The smaller the total mass of the tanker is, the more energy will be dissipated as strain energy. Besides these two ultimate loading conditions, there are also conditions between these two ones.

4.3 Impact Scenarios

For the impact locations, only bow impacts are considered. Two impact directions are chosen, one is head on collision which is considered to be the critical situation for the platform, and the other one with the glancing angle is a more realistic case. A glancing angle 30 degrees is chosen for the analysis. The impact location on the platform is not considered separately due to the limitations of the model.

Two impact speeds, 2m/s and 4m/s, are chosen as the initial impact speed. The speeds of the striking shuttle tanker will decrease after the impact begins, while the speed of the platform will increase. It is assumed that the damage of the two bodies will be larger with the increase of the initial impact speed.

Regarding the impact elevations, shuttle tanker in ballast condition and the platform in full load condition is mainly discussed in this report. There are several reasons for this. During the shuttle tanker offloading process, this elevation condition is the most common one. This condition is the critical condition. Another reason is the model limitation. The double bottom of the platform is not modeled in detail. If the shuttle tanker is in full load condition and the platform is in ballast, the tanker will impact on the double bottom. This will result in a error. However, besides this main elevation scenario, a different impact elevation is also chosen as a comparison in order to study if different impact elevations will have an effect on the results. It is assumed that the tanker will not impact on the double bottom during the collision.

Chapter 5 Collision Mechanics

A ship collision is a multi-physical and highly coupled process. However, in ALS, the analysis of collision may conveniently be split into two uncoupled processes: namely, internal mechanics and external mechanics, see [11]. Both mechanics are considered in this work. For internal mechanics, NEFEA is performed. For external mechanics, several simplified methods are utilized, which is Liu's method and the two methods described in Chapter 10. In this chapter, theories behind the two mechanics are described.

5.1 Internal Mechanics

Internal mechanics is related to the structural response and damage in collisions. It concerned with how the strain energy is dissipated in the striking and struck objects. It also involves the assessment of the structural resistance during large deformations. The change of the structures near the colliding points after the energy absorption is crucial. In this process, the analysis of force-deformation relationship is very important.

In a normal collision problem, the primary energy absorbing mechanisms of the structures are

- Membrane deformation of shell plating and attached stiffeners
- Folding or crushing of transverse frames and longitudinal stringers
- Folding, cutting and crushing of horizontal decks
- Cutting or crushing of ship bottoms
- Crushing of bulkheads

This conclusion is obtained from full-scale ship accidents and model experiments [12]. There are various methods available when dealing with the problem of internal mechanics [13]. Experiments are considered the most straightforward method to investigate the impact process and observe the structural behavior. Plenty of experiments are conducted during the 20th century. The results are widely considered as the most convincing means for understanding the local and global structural behavior, verification of numerical simulations and theoretical formulations. Experiments are also very often carried out to shed light on the internal mechanics of ship collision and grounding. NLFEA is considered the most powerful tool for analyzing structural problems, and is often regarded as "numerical experiments". Several commercial finite element software programs are available and capable of analyzing impact problems, such as LS-DYNA that is used in our case. Simplified analytical methods based on plastic mechanism analysis were introduced to the naval architecture industry in the 1960s. These methods are characterized by capturing the basic structural deformation mechanism with little modeling efforts. In other words, the failure mechanism is considered to be known prior to analysis which implies extensive fundamental research work on the mechanism analysis. Simplified methods are recognized as the best at balancing modeling difficulty with prediction accuracy.

The main features of different methods are summarized in Table 5.1.

Table 5.1 Main Features of the Methods for Internal Mechanics

	Modeling effort	Calculation effort	Result	Accuracy
Statistical/empirical method	very few	very few, hand calculation	energy	reasonable
Simplified analytical method	few	few, hand calculation	energy, load	good
Non-linear finite element method	considerable	considerable, expensive commercial FE software package	energy, load, stress	satisfactory if properly modeled
Experimental method	moderate to extensive	intensive data collection and processing	energy, load, stress	most convincing

In summary, empirical methods are not robust because they are usually concluded from historical data or extrapolated from experimental results. Compared to other methods, they provide little information on impact loads. Full or large scale experiments are costly and intensive for the ship industry. NLFEA, though successfully applied in many situations, is not practical due to the cost constraints and high level of expertise. Concerning the large amount of potential accident scenarios to be evaluated in a realistic or rational design procedure against collision or grounding, simplified analytical method is considered as the most suitable method for evaluation the ship structural performance for the moment.

However, the limitations of simplified methods should not be disregarded. The limitations may typically be specific failure modes, shape of indenter, structural arrangements, welding failure and fracture. If the assumptions made in the theoretical model do not comply with actual structural response, the predicted energy dissipation may become erroneous.

5.2 External Mechanics

5.2.1 Basic Theory

External mechanics is concerned with the rigid body motions of the colliding ships. We have to take both the installations and the ship as a whole. Simply put, the essence of collision is an energy conversion process. During the process, there will be conversion between kinetic energy and potential energy, with additional loses to energy dissipation. Dissipation more depends on the relative strength between the FPSO and the shuttle tanker.

Collisions must obey energy and momentum conservations. The basic formulas are:

(1) Energy conservation

$$E_{p1} + E_{k1} = E_{k2} + E_{p2} \tag{24}$$

$$E_{k,before} = E_{k,after} + E_{dissipated} \tag{25}$$

(2) Momentum conservation

$$p = p' \tag{26}$$

$$m_1 v_1 + m_2 v_2 = m_1 v_1' + m_2 v_2' \tag{27}$$

p and p' represents the total momentum before and after the impact. The kinetic energy is:

$$E_k = \frac{1}{2}(m_s + a_s) \cdot v_s^2 \tag{28}$$

We can see from the formula that the ship kinetic energy depends on the ship mass, which includes the hydrodynamic added mass and the ship speed at the moment of impact. And it is proportional to first power of the mass and second power of the speed. So in my opinion the speed has a greater affect.

After the collision, some of the kinetic energy will be remained while some of it will be dissipated as strain energy by the installation and the ship. The amount of the dissipated energy differs as the type of the installations is different.

In the external mechanics, the effect of the surrounding water is taken into account, which means the added mass should be accounted for. Through the two conservation equations, the dissipated energy could be calculated.

5.2.2 Brief Introduction of Liu's Method

In this thesis, Liu's method is used to perform a reliable simplified analysis of the impact problem. This method is a new three dimensional analytical solution, which is developed by Liu and Amdahl (2010) [14]. This fully 3D solution to the ship collision problem is proposed based on Stronge [15] and Pedersen and Zhang's work [11]. The two dimension (2D) case can be treated as a special case. The vertical geometry shape is taken into account. The main point of this approach is that all equations are formulated in a local coordinate system, which allows the dissipated energy along each axis in the local coordinate system to be obtained in a closed form.

Stronge has done a comprehensive research work on the impact theory [15]. The local coordinate system is established to derive the equations of motion. The origin of the coordinate system is set to the collision point. It is assumed that the surface of at least one of

the two impact bodies has a continuous curvature at the collision point, so there is a common tangent plane that constrains the collision point. Then two of the local coordinate system axes are at the tangent plane and the other one is normal to this plane. All the calculations in the Stronge theory are performed in this local coordinate system. It should be noted that the Stronge theory is based on two assumptions. One is that the impact duration is short and the impact force is large, so all external forces are neglected. The other is that the deformations are limited to a small area within the contact surface. Stronge theory successfully investigates the external mechanics of ship collision.

Besides Stronge theory, a new formulation of the external mechanics of ship collision has been developed [14]. This new method describes the impact mechanics of ship collision in three dimensions and two coordinate systems are used during the derivation of equations, namely the global and the local coordinate system. The local system is established similarly as it is described in the Stronge theory.

In this new method, the transformation between the local and the global coordinate system is important. Thus, the definition of hull angles is important in the transformation process. The corresponding angles are defined by DNV as follows:

- α : waterline angle
- β : frame angle
- β' : normal frame angle
- γ : sheer angle

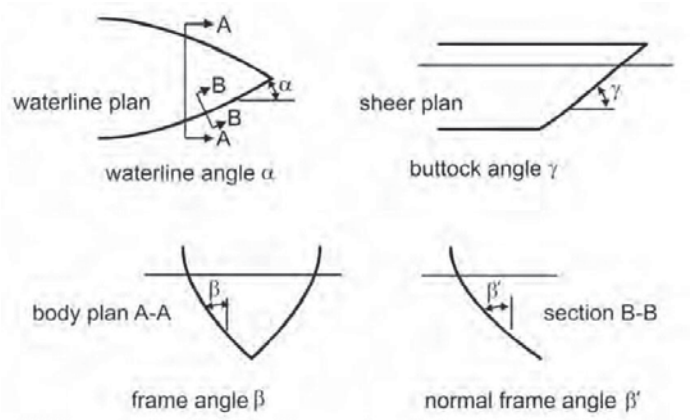

Figure 5.1 The Definition of Hull Angles, DNV (2009)

Liu developed a calculation code from Stronge theory and the new formulation in Matlab, which considers the components in all 6 DOFs and gives an effective way to investigate the external mechanics. A fully 3D solution to the ship collision problem is considered and the two dimension (2D) case can be treated as a special case. Those angle parameters in Figure

5.1 are also inputs in the Matlab program.

5.2.3 Input of Liu' Method

A MATLAB program is utilized to perform the external mechanics analysis. Due to the complex nature of 3D collisions, it is almost impossible to perform a manual calculation. In this program, an existing Stronge 3D MATLAB program is used as a subroutine [16]. It is a MATLAB function file for the 3D external mechanics, which is quoted in the main program. The main function for this program is to calculate dissipated energy and the velocity after impact. Through this Stronge 3D program, it is simpler to perform the 3D external mechanics analysis. A MATLAB program is used to do the analysis. The MATLAB code is attached in the Appendix C.

Besides the main principle dimensions, the hydrodynamic coefficients of the two structures are also necessary inputs to perform the external mechanics analysis. With respect to hydrodynamic coefficients to be used in the external mechanics analysis, there are some assumptions.

The added mass is be considered in six degrees of freedom. The added mass is frequency dependent and different in different motions. For the SSP300, the added mass is considered almost equal to the displaced mass except for the surge direction, which is in the range of 70-120% of the mass; for the Shuttle tanker: the added mass in yaw direction is assumed to be the same as in the sway direction; the added mass in pitch direction is assumed to be the same as in the heave direction.

Moreover, the radius of gyration about the y-axis and z-axis is assumed to be the same, which is larger than the one about the x-axis. The other assumptions in details are shown in the following table.

Table 5.2 Hydrodynamic Coefficients

	Added mass in 6DOF (in %)					
FPSO	surge	sway	heave	roll	pitch	yaw
	70%	100%	100%	100%	100%	100%
Shuttle tanker	surge	sway	heave	roll	pitch	yaw
	5%	100%	100%	10%	100%	100%
	Radius of gyration about three axes					
FPSO	About x		About y		About z	
	19 [m]		19 [m]		28 [m]	
Shuttle tanker	About x		About y		About z	
	0.35* tanker breadth		0.35*tanker length		0.35*tanker length	

Other inputs, for example the hull angles and the collision points are shown in the Matlab code in Appendix C.

Chapter 6 Structural Configuration Description

In order to establish the detailed finite element models of the shuttle tanker and the Sevan SSP300, it is of importance to clarify the structural configurations of the two structures. The parts that contribute to the resistance of the structures during the impact must be determined.

6.1 Structural Configuration of the Sevan SSP300 Platform

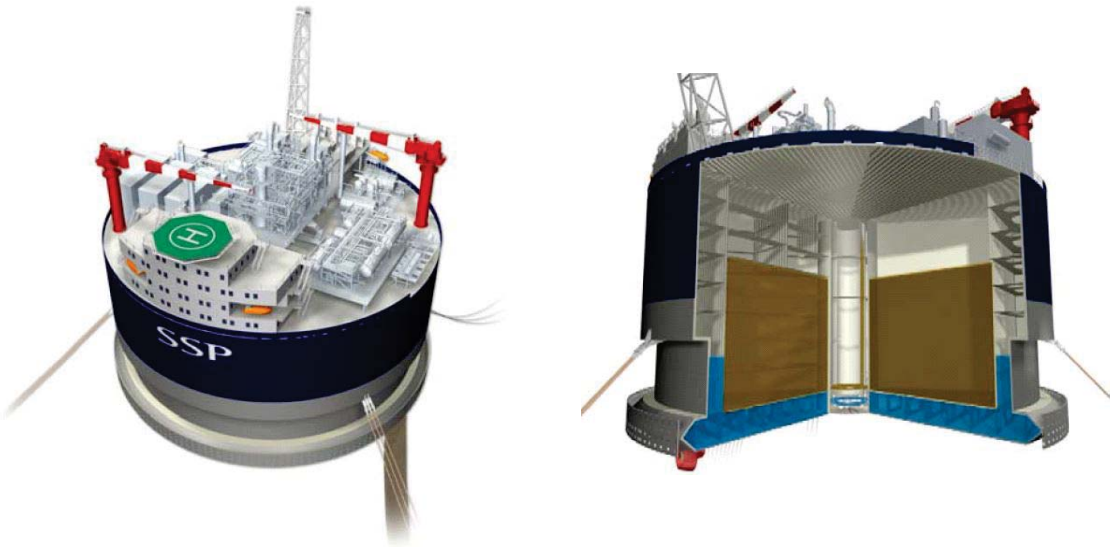

Figure 6.1 The SSP Concept [17]

Figure 6.1 give the general structural description of the Sevan SSP platform. A general impression can be obtained form these two figures because the SSP (Sevan Stabilized Platform) is a certain kind of platform with a circular shape and similar interior structure. In this report, the SSP300 is analyzed and the structural configuration is slightly different form what is shown in Figure 6.1. Figure 6.2 shows the sketch of the SSP-300 platform. The offloading tanker will operate from the left side of the platform in Figure 6.2, where the collision point is located. The plate thickness around the collision area is 18mm. While the plate thickness of the lower part of the outer hull side and the box section side is 20mm.

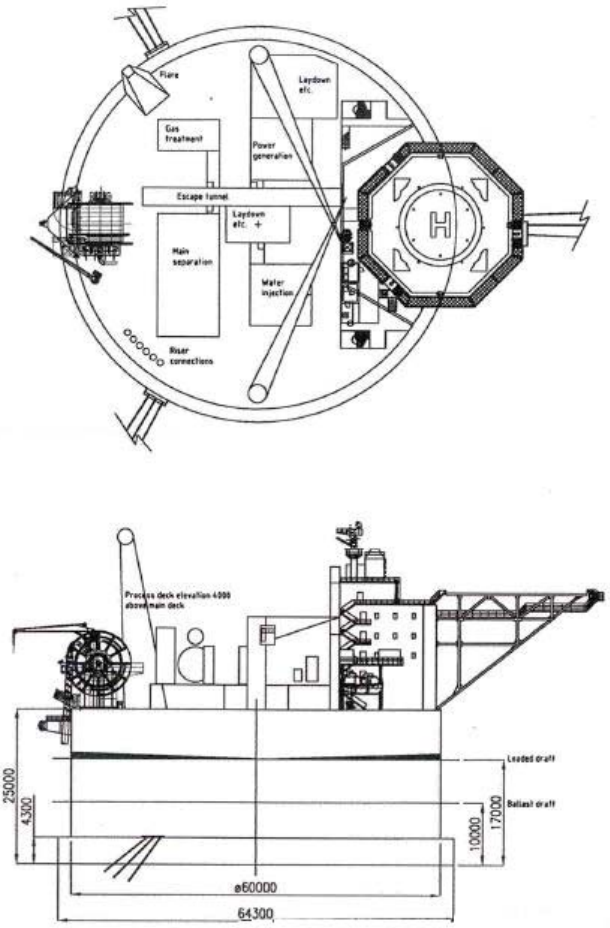

Figure 6.2 Structure Profile of Sevan SSP300

Table 6.1 Principal Dimensions for SSP300 FPSO

Length O.A.	65.15m
Length B.P.	60m
Depth Moulded	27m
Draft Ballast	13m
Draft Scantling	18.2m
Draft full loaded	17m
Double Bottom	2.5m

The Sevan SSP300 platform is a mono-hull with circular shape, depending on the same stability principles as a ship-shaped vessel. The SSP300 refers to one SSP hull size, capable of storing 300,000 barrels of cargo. An important feature of SSP300 is that the platform is wider than the vertical height, with an operational draft that is typically less than one third of its diameter.

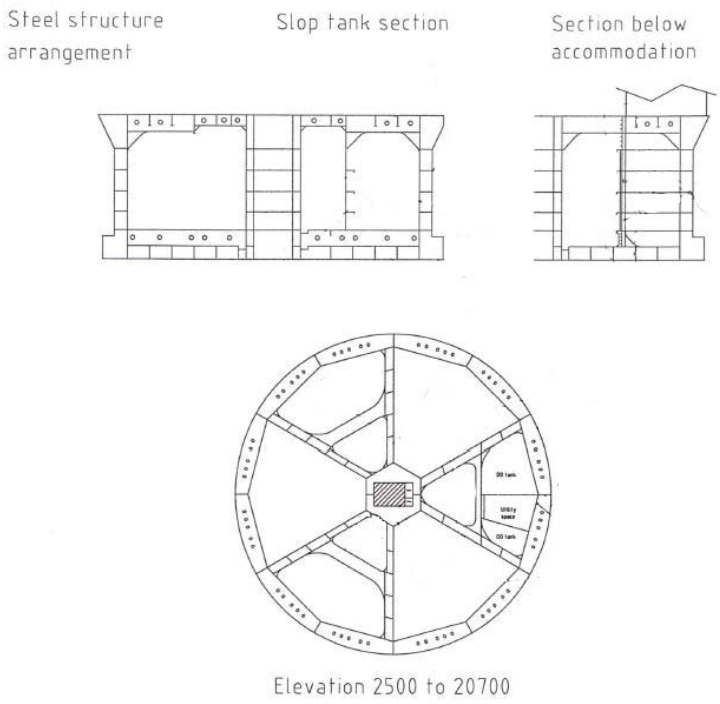

Figure 6.3 Various Section of Sevan SSP300

The Sevan SSP300 has a hull diameter of 60 meters and the total height of 27 meters. It has six cargo tanks, three slop tanks and twelve ballast tanks. Its highly symmetrical shape gives a good stress distribution throughout the hull, which prevents fatigue stress concentration to some extent. The cylindrical shape gives much lower moments that is imposed on the structure, which could also reduces fatigue stress levels, load concentration, as well as sagging and hogging.

From vertical sight of view, the platform can be divided into three parts, the upper conical part, the main hull part and the double bottom part. The platform also has double sides in the main hull part. Both the double bottom and the double sides are important to the safety features.

The double sides constitute the ballast tanks. These not only allow for segregated ballast, but also offer structural strengthening. The double sides provide horizontal stiffness in combination with the central shaft, to which they are linked via vertical bulkheads and horizontal stiffener elements. Vertical bulb steels are arranged on both outer hull plating and the inner side, with a distance of around 714 millimeters. NV32 Bulb 340×12 and NV32 Bulb 370×15 are used here. Generally, the thickness of the inner side plate is smaller than that of the outer hull plate, which varies from 12mm to 18mm.

The upper deck and the double bottom work as the radial beams, which improve vertical and horizontal stiffness. The deck will sustain not only the force from impact, but also the force from the superstructures. So there are intensive stiffeners and beams on it in order to make it strong enough.

The stiffeners on the main deck are combinations of bulb steels (NV32 Bulb 300×12) and flat bars (NV32 Flat bar 300×12), while on the bottom are combinations of T-stiffeners (NV32 T400×12/150×20) and flat bars (NV32 Flat bar 400×15). Radioactive arrangements of

stiffeners are similar on the main deck and on the bottom, which are shown in Figure 6.4. The distance between the frames and stiffeners are also shown in these figures.

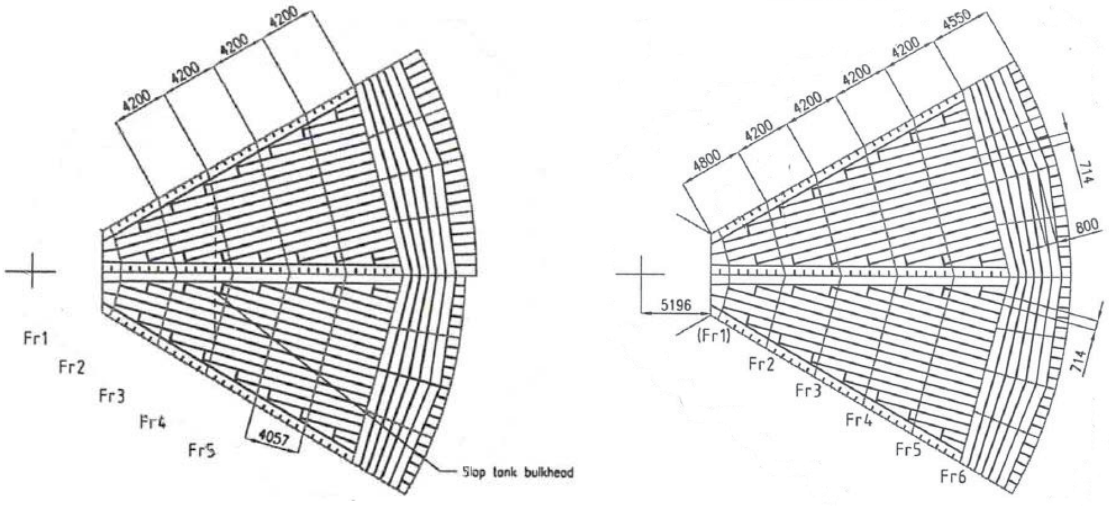

(a) Deck Stiffeners (b) Bottom Stiffeners

Figure 6.4 Stiffener Arrangement on Deck and Bottom

Besides stiffeners, there are also beam structures on the deck to strengthen it. For example there is a radial deck beam on tank centerline section and also on the sections every 7.5 deg in tank, shown in Figure 6.4 (a). Transverse deck beams and deck frames also exist on the deck. The deck frames are denoted as Fr1, Fr2, etc. in Figure 6.4 (a). The heights of the beams are 2000mm as shown in Figure 6.5. All these beams and stiffeners constitute a robust deck structure.

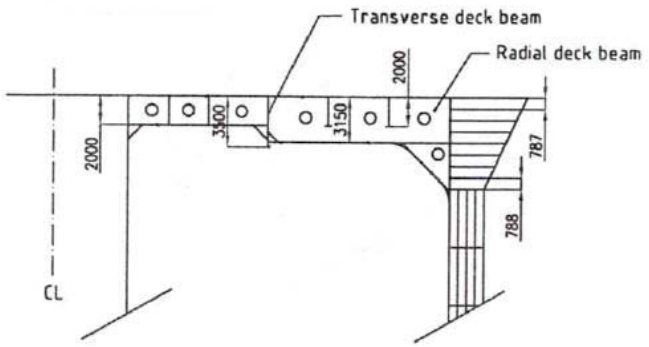

Figure 6.5 Section in Centerline of Tank without Slop Tank

Similar beam and frame arrangements on the bottom are shown in Figure 6.4 (b). An isometric view of double bottom section is shown in Figure 6.6. Box sections exist in the double bottom.

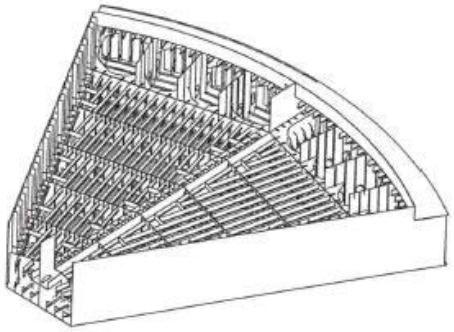

Figure 6.6 Double Bottom Section Profile

Besides the deck, the double bottom and double sides stated above, there are also structure components inside the platform that is of crucial importance to the energy dissipation.

Horizontal frames are arranged in every second tank section. These frames exist on five elevations, which are elevation 5.5 meters, 8.9 meters, 12.7 meters, 16.7 meters and 20.7 meters. There are flat bars on each frame. The size of the flat bar is FB120×12 and FB200×15. The horizontal frames together with all these stiffeners offer a robust resistance against the tanker impact.

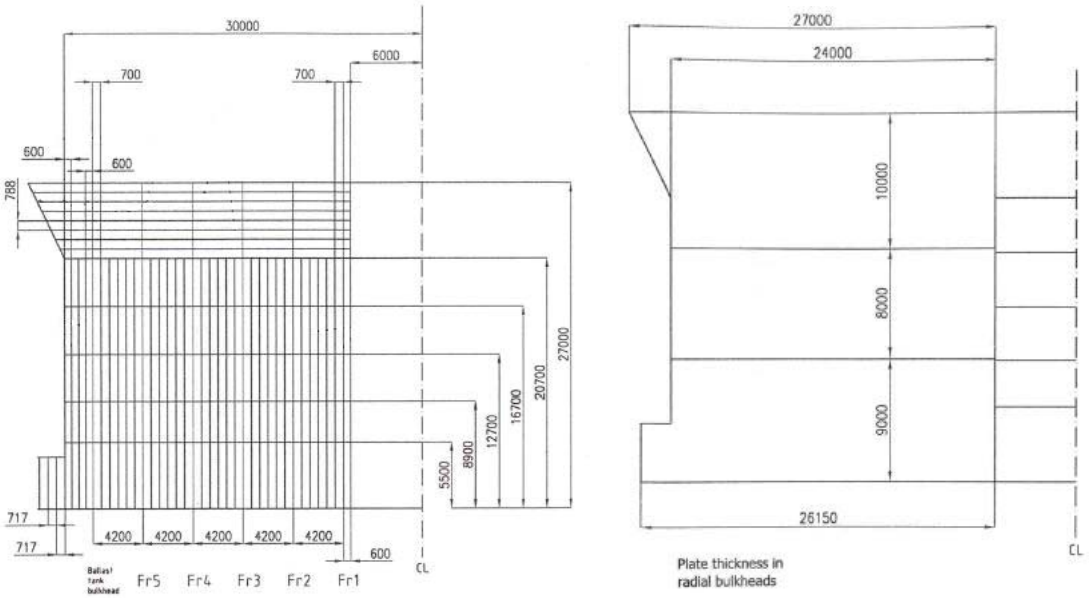

(a) Stiffener Arrangement (b) Plate Thickness

Figure 6.7 Radial Bulkhead Profile

In the radial direction, the six radial bulkheads between cargo tanks are very important components, which are shown in Figure 6.7. Figure 6.7 (a) shows the stiffener construction on the bulkheads and Figure 6.7 (b) shows the plate thickness on the bulkheads. The thickness of the plates varies in the vertical direction as illustrated in Figure 6.7 (b). The thicknesses are 12mm, 15mm, and 18mm, respectively, from top to bottom. The bulkheads of the tanks are

only reinforced at every other tank. This is because any of the two adjacent tanks share one common bulkhead. This fact contributes to the symmetry feature and the overall weight of the platform.

On the bulkheads are there vertical bulb steels between the bottom to elevation 20.7 meters. From elevation 20.7 meters to the main deck, horizontal bulb steels with a distance of 787.5 millimeters exist. The bulb steel size is NV32 Bulb 340×12. The most important structures on the radial bulkheads are the vertical frames in section with slop tank. The width of the frame is 1000mm from elevation 16.7m to elevation 25m, while from elevation 5.5m to elevation 16.7m, the width is 1200mm. The thicknesses of these frames are mainly 15mm. These frames are arranged every 4.2 meters. There are also radial bulkheads dividing ballast tanks, which are located between each main radial bulkhead. Stiffener arrangement and stiffener size on these bulkheads are the same as those on the bulkheads between cargo tanks.

However, it is worth mentioning that the platform will be impacted on the side where the shuttle tanker operates during offloading, so this part of the platform resists more impact energy than the other parts. As a result, only a small part of the platform near the collision point is affected. In this thesis, only one-sixth of the platform is modeled in detail, while for the rest part only a coarse model is used. The coarse part plays a role of the boundary condition for the detailed part in a way. A coarse model is also established for the double bottom part.

Many other structural details, such as brackets and man holes are not critically important, this will not be considered.

6.2 Structural Configuration of the Shuttle Tanker

A 147 500 dwt. Samsung shuttle tanker is chosen as the striking ship against the Sevan SSP300 platform herein.

Figure 6.8 147 500 dwt. Samsung Shuttle Tanker [18]

Table 6.2 Principal Dimensions for Shuttle Tanker

Length O.A.	278m
Length P.P.	262m
Length Scantling	259m
Breadth Moulded	46m
Depth Moulded	26.6m
Draft Scantling	17m
Draft Design	15.85m
Double Side	2.55m
Double Bottom	2.8m

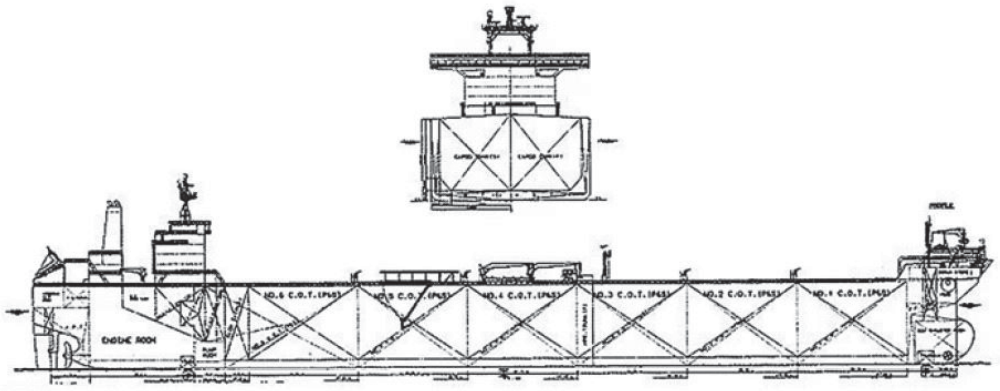

Figure 6.9 Profile of Shuttle Tanker

The whole shuttle tanker structural configuration description is divided into two parts. One part is the first 20 meters of bow section, where the detailed modeling is performed. The other part is the rest of the ship, which is of less importance for the impact problem, so only coarse model is established in this part. The structural configuration is also described respectively.

First is the coarse part. The outer plate thickness varies from 17mm to 23mm. In the longitudinal direction, there is a longitudinal bulkhead that locates in the centerline of the ship. The ship has double bottom. The inner bottom is on elevation of 3791mm with a deck plate thickness of 15mm. There are also decks on other three levels. They are elevation 8250mm, elevation 13050mm and elevation 17870mm. The deck thickness on elevation 13050mm is 13.5mm, while the other two is both 12mm. Besides these, upper deck and forecastle deck also exist. There are stiffeners and frames on all these decks, which are not described in detailed here because it is not important to the impact analysis.

In the transverse direction, there are seven transverse bulkheads in the main hull part and one transverse bulkhead in the stern part. They are arranged in uniform spacing, which are around 30m and 40m.

The first 20 meters of the ship is relatively more important in a collision scenario. The bow stem reaches 4.5 meter ahead of the bulb. In this part, all the large structural components are defined, for example the six decks and the centerline longitudinal bulkheads. There are girders in the double bottom with a distance of 3.2m. The deck locations are the same as those in the coarse part. There are also several minor plates, e.g. chain locker rooms etc. The transverse frames are also added. The smaller frames are arranged every 800mm, while the large frames are every 3200mm.

Stiffeners are located on decks, frames and bulkheads. For example, the upper deck longitudinal stiffener spacing is 820mm. The stiffeners are angle bars with size of 200×90×9\14. On the deck, the stiffener configuration varied in the shuttle tanker between longitudinal and transverse stiffening. But the transverse stiffening is replaced by longitudinal stiffening here due to simplifications. There is also diagonal stiffening in the fore part.

The plate thicknesses of the outer shells vary from the mid to the side. The plate thicknesses in the mid part are generally larger than the side part. The stiffeners on the outer shell are mainly flat bars and angle bars.

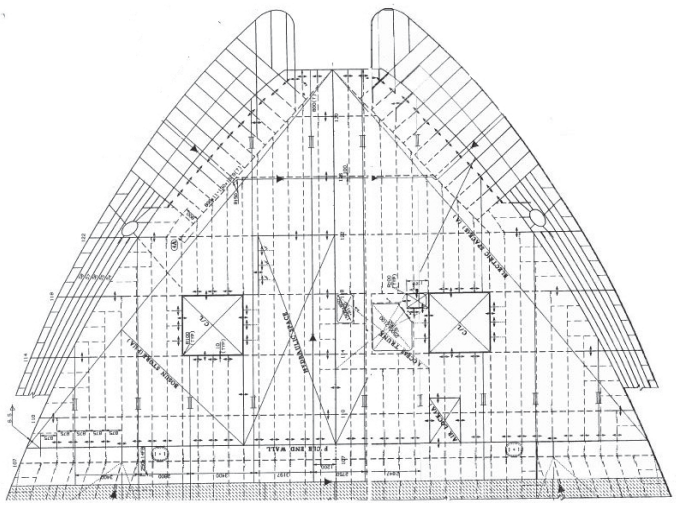

Figure 6.10 Profile of Tanker Upper Deck

The bow thruster tunnel is included. The shuttle tanker is equipped with a retractable azimuth thruster and a bow thruster in the bow. The thrusters will not be included in the model, but all the stiffening in the vicinity of the bow thruster tunnel is kept intact. A large room is located over the bow thruster tunnel and further back to accommodate these thrusters.

The No.3 Stringer Deck is cut to accommodate the bow thruster room with a 4.8m wide and 9m long opening. This deck is placed in the mid section of the bulbous bow, see Figure 6.11. The bow thruster room will thus weaken the bulbous bow significantly, as one of its main supports is weakened severely. On the structural drawings of the shuttle tanker the internal arrangement of the bow thruster room is not presented in great detail. The room is thus left

open with no installed machinery. The inclusion of the room itself weakens the bow, but the lack of internal components in this room will increase this weakening severely as the room is allowed to fully collapse instead of obtaining internal contact with the installed machinery.

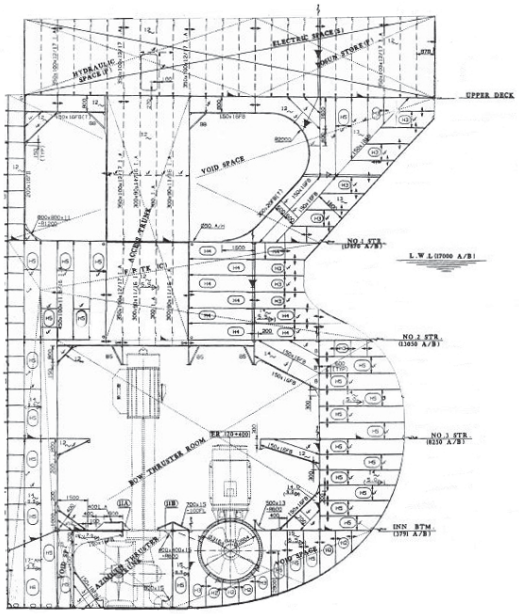

Figure 6.11 Profile of the Tanker Center Line Section

Other details which are less important will not be specified here.

Chapter 7 FEA Modeling

7.1 Software

The FEA modeling herein is executed with the use of MSC.Patran, which is an extremely powerful and user friendly software for modeling. It is very convenient to construct the model. It contains many advanced meshing tools, which allows not only the meshing of complex parts, but also to generate fine mesh. There are many options for the analysis code so that it can be regarded as a pre processor for different solver, for example ANSYS and MSC.Nastran. Here it is used as a pre processor to the NLFEA code LS-DYNA. The two applications were preferable due to the in house expertise at NTNU. MSC.Patran has the superiority of the convenience and flexibility. Not only the large amount of intelligence modeling tools it contains, but also the various modeling methods. LS-DYNA is quite an efficient explicit NLFEA solver.

7.2 SSP300 FPSO

The SSP300 FPSO is regarded as the struck object in this damage assessment problem, while a Samsung shuttle tanker is chosen as the striking object. The shuttle tanker model is given in this case, so the main task is the modeling of the SSP300 FPSO. A complete set of structural drawings for this FPSO is available. The general arrangement is taken as the main reference when doing the modeling. However, due to the complexity of the FPSO, different kinds of simplifications are applied to simplify the modeling and meshing processes. The basis for the simplification is that there should not be significant effect on the strain energy dissipation of the platform.

The scope of the modeling is limited into 70000 millimeters in MSC.Patran. The platform can be divided into three parts in the vertical direction, the upper conical section, the middle main hull section and the lower box section. There are three slop tank, six cargo tank and twelve ballast tank totally. Five horizontal frames exist in order to strength the structure. All these main parts including some other details have to be modeled in order to give a full description of the FPSO when doing the finite element analysis.

7.3 SSP300 FPSO Model

The geometry modeling and the meshing of the whole FPSO are tough processes because of two reasons, which are the large amount of geometries and finite elements involved and the lack of experience in using MSC.Patran. It takes more than eight weeks to finish the whole FPSO model.

7.3.1 Geometry Modeling

As there is no need to analyze all the details of the platform, different simplifications are used during the geometry modeling. Some components which have nonsignificant effect on damage assessment are omitted, such as the equipment and the accommodation above the deck. Also the parts far away from the collision point can be simplified.

Figure 7.1 Sketch of SSP300

The sketch above indicates that the conical section of the platform is asymmetric. However, the modeling of the conical section and the deck are considered to be symmetric. The principal dimensions during the modeling are shown in Table 7.1.

Table 7.1 Principal Dimensions in FPSO Model

	Diameter (m)	Vertical Height (m)
Conical Section	66	6.3
Main Hull	60	16.4
Box Section	64.3	4.3

The platform is divided into two parts. One-sixth of the whole structure near the collision point is modeled in detail. There is no slop tank in this part. The remaining section is modeled coarsely. Minor simplifications allow symmetry to be used, which will reduce the workload in some extent.

The first step during the FPSO modeling is to generate the geometry lines that represent the shape of the whole structure. Curves have to be used to define the surfaces representing all the shells, as well as all the stiffeners. Since all the parts of the structure are in regular shape, all the surfaces are smooth enough without any imperfections.

All the main structure components are included in the detailed part, such as the hull plating, the ballast tank, radial bulkheads, the five horizontal frames, as well as the vertical frames every 4200mm on the main radial bulkheads between cargo tanks, but only two of them nearest to the collision point are modeled. The brackets on all the frames are included without any radian, which means that all the brackets are considered as triangles.

There are some special simplifications on the structural components that have to be mentioned. For example, the typical section on elevation 23850mm in Figure 7.2 (a) is simplified modeled as what is shown in Figure 7.2 (b).

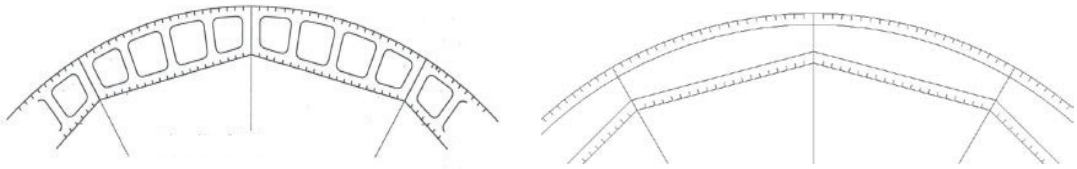

(a) In real case (b) In model

Figure 7.2 Elevation 23850mm of the Platform

Another simplification is the stiffeners on the horizontal frames, where there are quite complex arrangements. For simplification, the stiffeners are arranged every two outer hull stiffeners, which is illustrated in Figure 7.3. This means that the horizontal frame stiffener distance is twice of the outer hull vertical stiffener distance. This will not cause significant effects on the analysis.

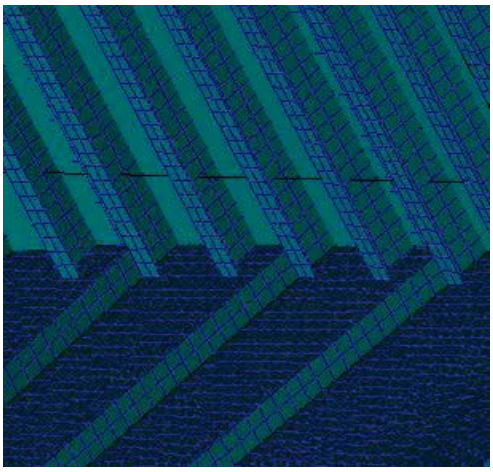

Figure 7.3 Stiffeners on Horizontal Frames and Outer Hull

Modeling of the stiffeners is tedious. The stiffeners are only modeled in the detailed part. There are three kinds of stiffeners involved in the modeling process, which are flat bar, T-stiffener, and bulb, whose dimensions are T400×12/150×20, NV Flat bar 120×12, NV Flat bar 200×15, respectively. The bulb is modeled as the L-stiffener. The principle is to make the height of the web, the thickness and the area the same.

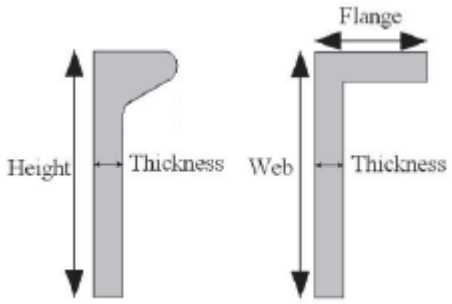

Figure 7.4 Bulbous Profile and L-stiffener Profile

The dimension comparison of the bulb steel and L-stiffener is shown in Table 7.2.

Table 7.2 Dimensions of the L-stiffener

	Area (mm^2)		Web Height (mm)	Flange Height (mm)	Thickness (mm)
Bulb 300×12	4973	Corresponding L-stiffener dimensions	300	126	12
Bulb 340×12	5884		340	162	12
Bulb 370×15	7710		370	159	15

Stiffeners are mostly executed by breaking the surfaces along the line where stiffeners exist. Then there will be a line between the two surfaces, which is also the edge of the surfaces. This curve can be extruded a certain distance along the direction that is normal to the surface, so that a new surface is generated. This surface performs as the basis of the stiffener web. In a similar way the top curve of the surface can also be extruded to form the stiffener flange basis.

There is another method to generate the stiffener, which is creating the finite elements of the stiffeners directly without making geometries as the basis. To be specific, meshing the surfaces first and sweeping the element edges on the lines where stiffeners exist along the normal direction to the surface. This method is the main one that is used in the stiffener modeling process.

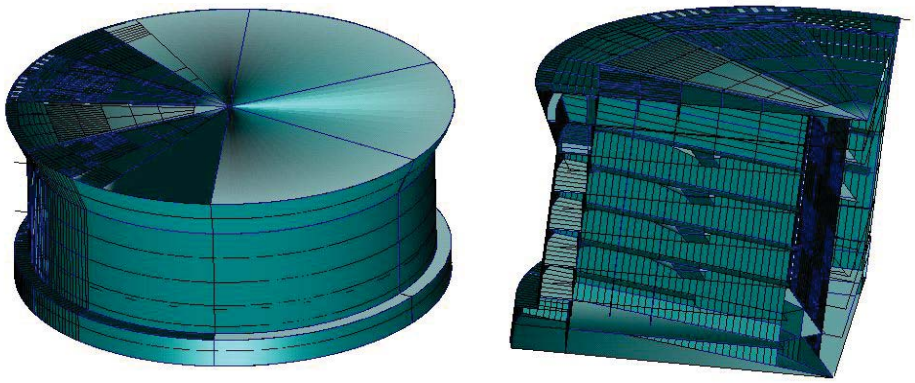

(a) Whole model (b) Detailed part

Figure 7.5 SSP-300 Platform Model

Another important simplification related to the detailed part is that for all the stiffeners, such as the stiffeners on the deck, on the radial bulkheads and the horizontal frames, only those within the range of around 15-meter distance from the outermost hull plate are included. This is because these stiffeners are nearer to the collision point and the collision will have serious impact on the structures within this range. Conversely, which can be also confirmed from the results afterwards, the farther structure components out of this range receive negligible influence. So this simplification is deemed insignificant in terms of strain energy absorption.

The section outside the collision zone is performed without much detailed modeling. Many of the structure components such as frames, stiffeners and other insignificant sections are discarded. Only the hull plating and the main radial bulkheads between cargo tanks are included.

Details that are excluded from the model include manholes, detailed geometry of corners and cutouts, contents of double bottom etc. These simplifications are of small importance compared to the rest part of the model and will not have significant influences on the results. But other techniques are used to counteract the simplifications, for example modifying the material properties of the coarse part. This will be illustrated in more details in the following material part. In a word, special care has to be taken if the simplification is expected not to have a moderate contribution to the energy absorption.

7.3.2 Meshing

Meshing is quite important for the accuracy of the finite element results. The results depend strongly on the mesh used, as this limits the detail of the geometry and mechanisms involved in the collision analysis. 4-mode shell elements were used as the main element category. 3-node shell elements are also used to avoid very small 4-node elements. Torgeir Moan reports that the use of 3-node shell elements should be minimized, as these elements yield less accurate results than the 4-node elements [19]. 3-node elements were thus used more at the places where it is difficult to model the geometry properly, or when creating extra nodes such that different structural components could be thoroughly connected where needed. For

example in some places with gradually varied geometry or some places with sharp corners.

During meshing, it is important to minimize the use of small elements also, as very small elements may cause very small time step. This is due to limitations in LS-DYNA analysis, the critical time step should not be very small. The critical time step is 1.98E-06s, which is in a reasonable range.

Hagbart S. Alsos shows a convergence study on the mesh of a grounding structure, which is similar as the collision analysis essentially [9]. It is found that the element length is better to be between 5 and 10 times larger than the plate thickness in order to give a good physical modeling and a good representation of the shell folding during the large deformations. The plate thicknesses in the platform vary from 12mm to 20mm, so a mesh size of around 100mm is adopted for the entire model. However, few small elements also exist. The smallest element is around 60mm, which is in a controllable range and will not lead to very small time steps. In total, the number of elements in the platform is around 810 000. This is a large model, but will allow large deformations to be modeled with good accuracy.

The mesh type mainly used in the platform model is Isomesh. The Paver and Hybrid mesh type is also used on the fan-shaped and triangular surfaces, or in the area of transition from detailed mesh to coarse mesh. The mesh size is around 1m in the coarse model part, which will increase the calculation efficiency. As for the meshing of stiffeners, also shell elements are used rather than bar elements. This is because shell elements are allowed buckling of the stiffeners themselves, so that buckling of the stiffeners can be reflected.

The connections of nodes are the most important. It must be ensured that geometry is connected at all the nodes, so that the transfer of forces in each connection is modeled properly. Figure 7.6 illustrates the type of connections made.

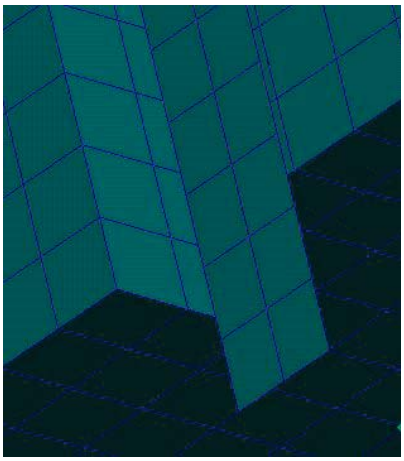

Figure 7.6 Stiffener Connection

The connections of the L-stiffener are special. All the nodes at the web of the stiffener are connected towards the deck, whereas the flange of the stiffener is not connected. So when there is deformation for the stiffeners, the flange can move freely, which is representative of actual behaviour.

The tool *verify free edges* in Patran can check if all the structural elements are properly

connected. By using this, all the unconnected edges are shown, and the nodes which need modification can easily be identified and corrected. Throughout the platform structure modeling this technic is adopted constantly to ensure that the structural elements are properly connected.

7.3.3 Material

Only one kind of material is used in the platform model. However, for the detailed part and the coarse part, different material property values are used. MAT_USER_DEFINED_MATERIAL is used. From the structural drawing the material specifications are not specified. Due to the loading nature, a fracture model is important in the analysis for the platform model. So fracture criterion is included in the material parameters.

There are many simplifications in the coarse part of the model, so the total mass will be a lot smaller than the real platform structure and the center of mass will deviate from the real one. Methods have to be taken to adjust the total mass and the mass of center of the model. The density of the detailed part has to be fixed to the real density. Therefore changing the density of the coarse part can realize this goal. Three different kinds of densities are utilized to achieve this goal. This way, the rotational inertia would also be close to the real one.

Another change to the coarse part is that the Young's Modulus is increased to make up the strength loss due to the simplifications. According to the supervisor's advice, the Young's Modulus is increased to 1.3 times of the original one. Specified values are shown in Table 7.4.

7.3.4 Element Properties

Element property groups were created according to structural element group and thickness. Each group of structural elements had the necessary number of thickness groups to model the thicknesses as on the structural drawings. Actually all the properties setting are accomplished in LS PREPOST. In Patran, only dummy properties are given. The property group itself contains only description of the material used and the thickness of the shell elements. After defining the properties in advance in Patran, LS-DYNA sorts the model based on the element property groups. Therefore, a good group definition saves time during post processing.

7.4 Shuttle Tanker Model

The whole shuttle tanker model is an existing one, so the process of modeling is not described herein. Even though, some modifications are made to the shuttle tanker. The unit of the given tanker model is in meters, while the unit of the platform is in millimeters. Therefore, units of the tanker are transformed from meter to millimeter. In the head on collision, only the tanker bow is used as the striking body. So the main hull part of the shuttle tanker is omitted. There is a rigid back for the bow. The density of the rigid back is adjusted to obtain an accurate total mass of the real tanker. Herein added mass is included which will be discussed in more detail

later in Section 7.6.3.

In the impact with a glancing angle, a more accurate model is used. The main hull outer shell is retained, but the detailed structures in the main hull are still omitted, for example the horizontal decks and transverse bulkheads. This way, the total mass of the tanker is assigned to the hull structure evenly, thus the center of mass and rotational inertial will be in the correct range.

Two different materials are used in the shuttle tanker model. MAT_RIGID and MAT_USER_DEFINED_MATERIAL are used for the rigid back and the bow part, respectively. For the impact with glancing angle, rigid material is used on the main hull, so that no deformation is allowed in the main hull. A fracture criterion is also included in the material. In the rigid part, the density is scaled so that the desired mass of the striking ship is obtained. The specified values of the material properties are presented later in Section 7.6.4.

7.5 Collision Setup

- **Boundary Conditions**

The boundary conditions used vary depending on analysis type. Both the integrated analysis and the internal mechanics analysis are performed. For the integrated analysis, no boundary conditions are used. Both the platform and the tanker are allowed to move freely. This is more representative of reality.

When running the internal mechanics analysis, the tanker is still moving freely as the striking body. The platform is set to be fixed spatially. This is achieved by fixing all the nodes in the coarse part of the platform. All these nodes are fixed in all six degrees of freedom. If just few nodes are fixed, there will be large force concentration at the fixed nodes. This way, the force is distributed to all these nodes and will not have large force concentration.

- **Contact**

The contact is defined by specifying the contact between striking and the struck bodies. In LS PREPOST, AUTOMATIC_SURFACE_TO_SURFACE contact is set. This will distinguish between the master part and slave part. In our case, the striking shuttle tanker is regarded as the master part and the struck platform is regarded as the slave part. This kind of contact is an automatically updating surface to surface penalty algorithm, also with static and dynamic friction coefficients of 0.15. Two contact sets are made, one for bulb vs. platform vertical main hull, and one for stem vs. main hull in the conical part.

With the two contact sets, the energy dissipation, as well as the force-displacement relationship, can be distinguished between the two collision zones.

- **Initial Velocity**

Two kinds of initial velocities for the striking tanker are used herein, both for the head on collision and the collision with glancing angle. One is 2m/s and the other is 4m/s. The velocity is set by giving all the nodes in the tanker an initial velocity.

As the kinetic energies in the collision scenario increases, it becomes more important to have a model that can represent the inertia effect of both the striking and struck ship properly. According to NORSOK [3], a NLFEA analysis needs to include or assess all the important effects like mass, hydrodynamic added mass and remaining kinetic energy after collision. This is automatically included in the inertia controlled model. This is considered in the impact with glancing angle, but not considered in the head on collision because of the limiting time. Though there will be no large difference, this is still an area that can be improved in the future.

7.6 Analysis Overview

7.6.1 Software

LS-PrePost is an advanced pre and post-processor that is delivered by LS-DYNA. This is to define the material properties and add the boundary conditions. LS-DYNA is utilized only as a calculator to run the analysis. The result of the analysis could be shown also in LS-PrePost.

In order to solve the non linear problems, we can perform both static analysis and dynamic analysis. Moreover, many NLFEM softwares are created, such as ABAQUS and LS-DYNA. In the collision problems, LS-DYNA is used partly because this program is efficient at solving transient dynamic problems, for example the high velocity and short duration analysis such as colllision.

7.6.2 Consistent Units in LS-PrePost/LS-DYNA

The units which are used in LS-PrePost/LS-DYNA must be defined. There is a definition of a consistent system of units required for LS-DYNA:

- 1 force unit = 1 mass unit * 1 acceleration unit
- 1 acceleration unit = 1 length unit / (1 time unit)^2
- 1 density unit = 1 mass unit / (1 length unit)^3

So a set of units according to this is given out in Table 7.3. The density, Young's modulus and gravitational constant are given as a point of reference.

Table 7.3 Consistent Units of Variables Used in LS-DYNA

Mass	Length	Time	Force	Stress	Energy	Density	Young's Modulus	Gravity
ton	mm	s	N	MPa	N-mm	ton/mm^3	MPa	mm/s^2

7.6.3 Dynamic Mass

This is an inertial controlled analysis, so the mass of the striking and struck bodies are important. In the worst case the struck body is in fully loaded condition and the striking body in ballast. The striking body will hit the platform as the structurally worst location, causing rupture of the hull below the waterline and possible serious flooding. The added mass is then an important consideration.

The displacement of the platform is 51 185 tonnes in full loaded condition. The added mass coefficient in full loaded condition is assumed to be around 100%. So the total displacement which includes the added mass is assumed to be 100 000 tonnes. The mass is added by adjusting the density of the coarse part.

The displacement of the tanker in ballast condition is 90 000 tonnes. The added mass coefficient for this is assumed to be 10%. Thus the total mass is 99 000 tonnes. It is found that the total mass of the platform and the tanker is almost the same. The mass is added by adjusting the density of the rigid back or the rigid hull.

7.6.4 Material

In this section the specified values of the material properties are given, which is shown in Table 7.4. All the materials used have Possion ratio $\nu = 0.3$. For all material, except the rigid material, the shear modulus is taken as 79615.4 MPa, while the bulk modulus is taken as 172.5 GPa. Strain hardening is also considered. The strain hardening formula is $\sigma = K\varepsilon^n$. σ represents the applied stress on the material. ε is the strain. K is the strength coefficient. n is strain hardening exponent. E represents the Young's Modulus. σ_y is the yield stress. ρ is the density of the material. ε_{cr} is the critical strain.

Table 7.4 Material Properties

		$\rho\,[kg/m^3]$	$\sigma_y\,[MPa]$	$E\,[GPa]$	n [-]	$K\,[MPa]$	ε_{cr} [-]
Buoy	Detailed	7850	275	207	0.24	740	0.71
	Coarse	1.9E+5	275	269.1	0.24	740	0.71
Tanker	Bow	7830	235	207	0.24	670	0.71
	Rigid	*Scaled	/	207	/	/	/

The density of the rigid part of the tanker is a scaled one. The value is different in head on collision and collision with glancing angle, because in glancing angle collision the whole main hull is used.

Chapter 8 FEM Results-Integrated Analysis

In this chapter only one impact elevation, shuttle tanker in ballast and platform in full load conditions, is considered due to model limitations. The double bottom of the platform is not modeled in detail. It is unwise to perform the simulation that may impact on the double bottom. So the condition that the platform in ballast and the tanker in full load condition is not considered here. This choice is relatively reasonable as the impact elevation chosen here is the most common scenario. Different impact headings and different impact velocities are proposed.

Output from the NLFEA is enormous, and the results from on analysis can be utilized in many different ways to study the different aspects in the collision scenario. Herein a small selection of data is presented by which some of the aspects can be presented. The most important output is the contact force between the structures, and the energy dissipation. The simplified method is also used, comparing it with the NLFEM to evaluate the accuracy of the simplified methods. Sequential cut profiles of the collision progress are also presented to give a 2D representation of the collision event.

In this chapter, integrated analysis is performed, which means that the analysis is not split into external mechanics and internal mechanics. The split analysis will be discussed in Chapter 9.

8.1 Head On Impact

For both 2m/s and 4m/s cases, there are two collision points, one is on the main hull of the platform and the other is in the junction of the deck and the conical outer shell. The low part impacts a little earlier than the up part.

8.1.1 Impact Velocity of 2m/s

First an initial velocity of 2m/s is chosen, with the termination time of 4s. In this impact problem, only the bow is utilized as the striking part instead of the whole ship. Though the total mass of the bow is the same as the whole ship, the rotational inertia is different. It results in a larger rotation in the tanker bow than in the real case, shown in Figure 8.1.

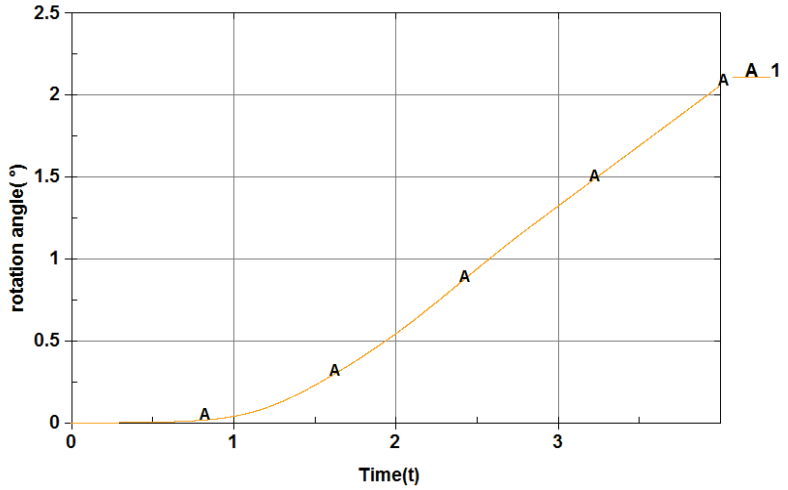

(a) Tanker

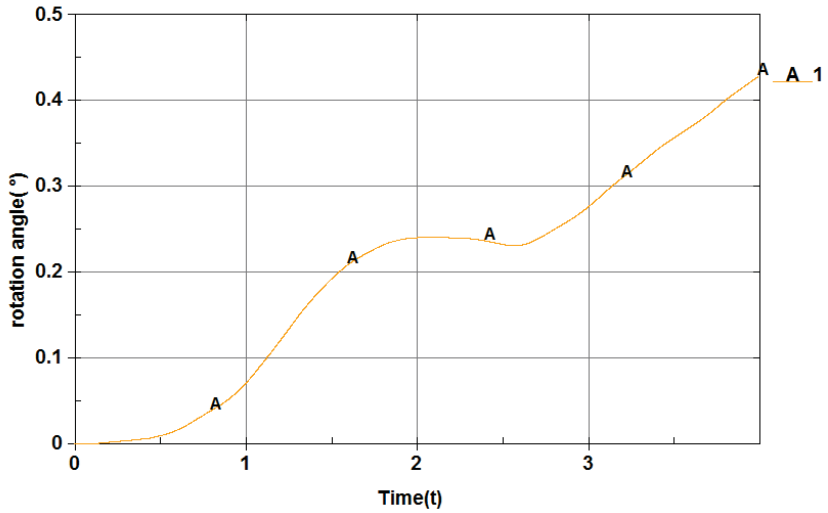

(b) Platform

Figure 8.1 Rigid Body Rotation Angle_Head on_2m/s

The bow only rotates approximately 2 degrees in 4s. While in the first 2 seconds, it rotates only for 0.5 degrees. The rotation angle is relatively small and will not have great effect on the energy dissipation, especially for the first two seconds. The platform rotation is even much less. So there will be no much difference when using a bow as the striking body.

It can be read from Figure 8.14 (a) that the largest deformation of the lower part of the platform is around 2.1m. The deformation along a cut through the centerline of the bow and the platform is presented in Figure 8.2 for the first 2.1m of deformation in the lower part of the platform. Four stages are chosen. 0m, 0.7m, 1.4m, 2.1m are the deformation in the main hull of the platform.

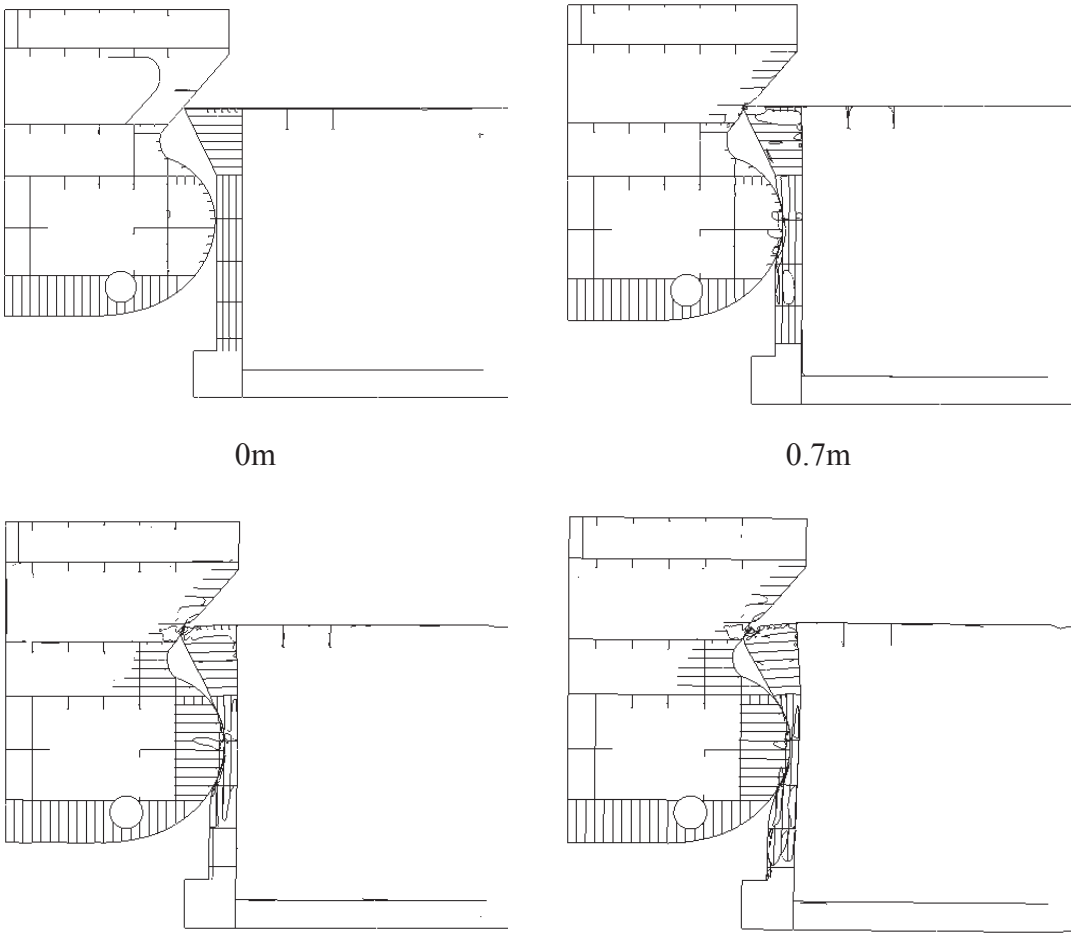

Figure 8.2 Deformation Sequence_Head on_2m/s

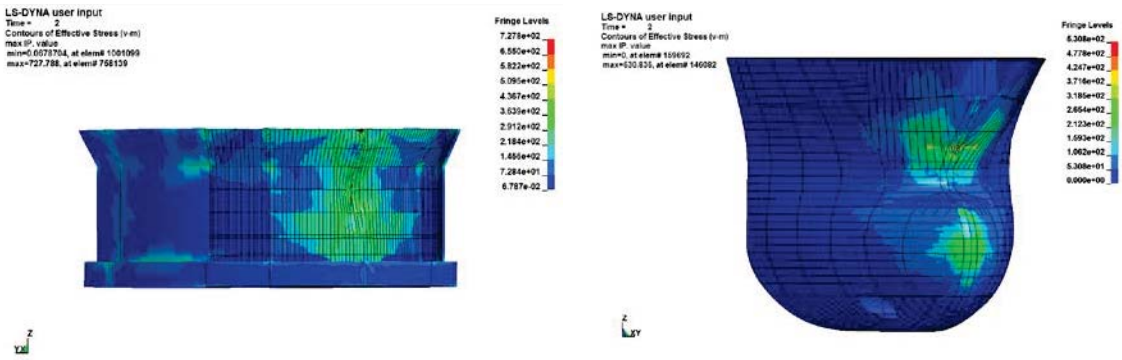

Figure 8.3 Von-Mises Stress Contours_Head on_2m/s

It can be seen in Figure 8.2 and Figure 8.3 that the platform deforms much more than the tanker. Especially for the bulbous of the tanker, the deformation is little. While the upper part of the tanker bow deforms a little more due to the sharp intersection of the platform deck and conical part. When the crush is severe, the coarse part will be affected. This will be a shortcoming of the model. However, only very little energy is dissipated by the coarse part, there will be no big influence to the results.

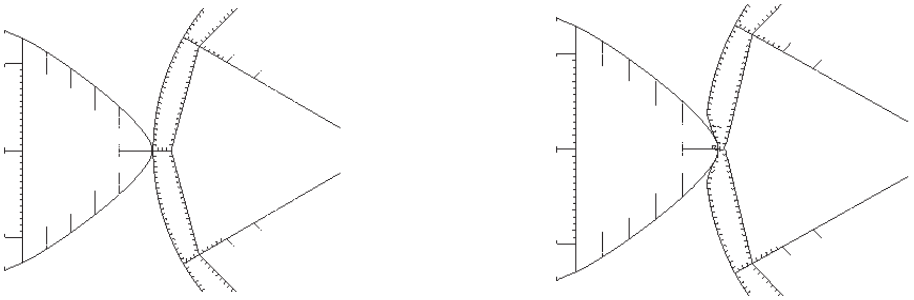

Figure 8.4 Platform Main Hull Deformation_Head on_2m/s

Figure 8.4 shows a horizontal cut in the middle of the bulb during crushing. The deformation in the platform is really large. It is clearly shown from the figures that the platform fails mostly by bending of the hull, the deck and the hull stiffeners. The bulkhead between the ballast tankers are also damaged a lot.

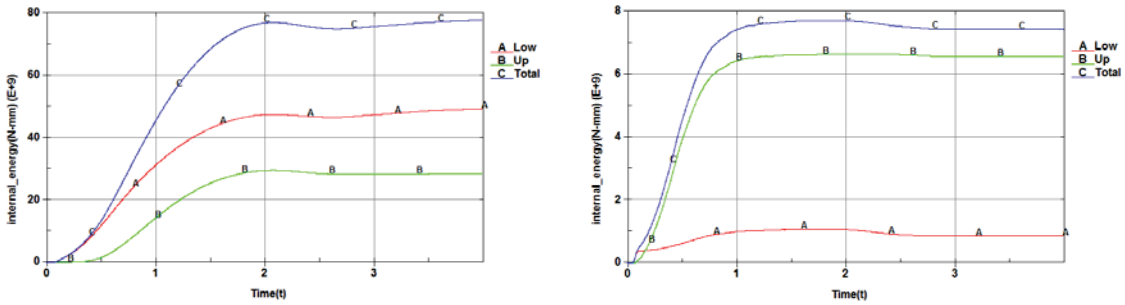

(a) Platform (b) Tanker

Figure 8.5 Dissipated Energy vs. Time_Head on_2m/s

The energy-time curve diagrams are presented in Figure 8.5. From the diagrams it is evident that the platform dissipates almost ten times more energy than the tanker. Specifically, the platform dissipates around 91.1% of the total energy, while the tanker only dissipates 8.9% of it. For the platform, the lower part dissipates more energy, that is up to 62.8% of the energy dissipated by the whole platform. While for the tanker, the upper part dissipates much more, which is 85.5%. The bulbous bow of the tanker is rather strong in this case. In the very beginning of the impact, the low part of the tanker absorbs almost all the energy, but soon the up part energy absorption exceeds and becomes much more than the low part.

The tanker energy dissipation stops at around 1s and the platform at around 2s. Therefore after 2s, the two structures will stop the relative motion and move in the same velocity. After 2 seconds of crushing the total energy absorption is almost 90MJ. This matches the fact that a 99000 tonne ship hitting a platform with an initial velocity of 2m/s and coming to a same relatively small velocity after impact.

- Cracks on the platform

Figure 8.6 shows the cracks on the platform. The two pictures show the first crack and the largest crack, respectively. The first crack occurs at around 0.36s. It can be read from the deformation-time curve that the deformation at the collision point is around 0.5m at 0.36s, while the largest deformation at the same point is around 2,1m. The largest rupture takes place close to the horizontal frames

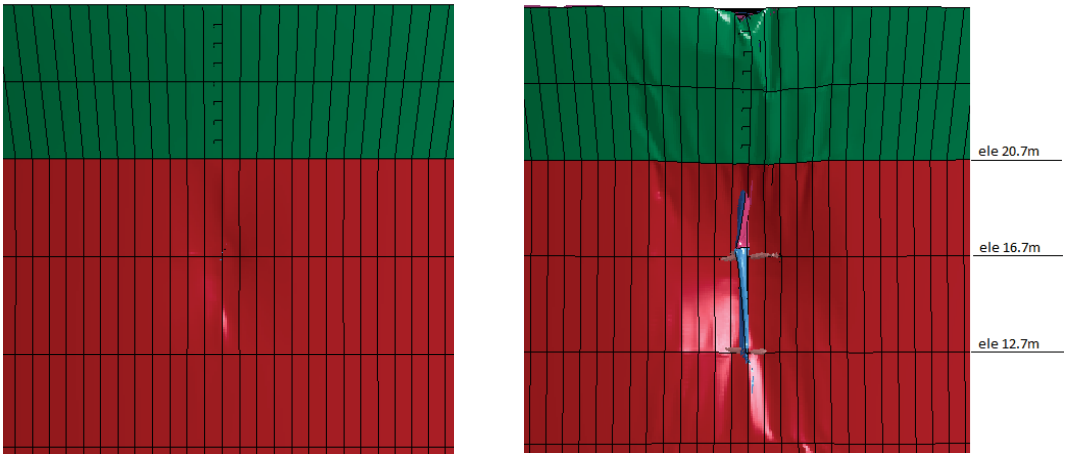

(a) First crack (b) Largest crack

Figure 8.6 Cracks on the Platform_Head on_2m/s

On elevation around 18.5m where the upmost of crack is located, only the vertical centerline bulkhead impales the outer shell, so the crack is relatively narrow with a width of around 0.5m. On elevation 16.7m, the crack almost has the largest width of around 2.5m. The length of the crack is approximately 8m, from elevation 10.5m to elevation 18.5m. The draught of the platform in full load condition is 17m, which is higher than 10.5m, thus there will be flooding.

There is also crack on the upper conical part. The size of the crack is around 2.8m in the circumferential direction and 0.6m in the vertical direction.

8.1.2 Impact Velocity of 4m/s

An initial velocity of 2m/s is then chosen, with the termination time of 5s.

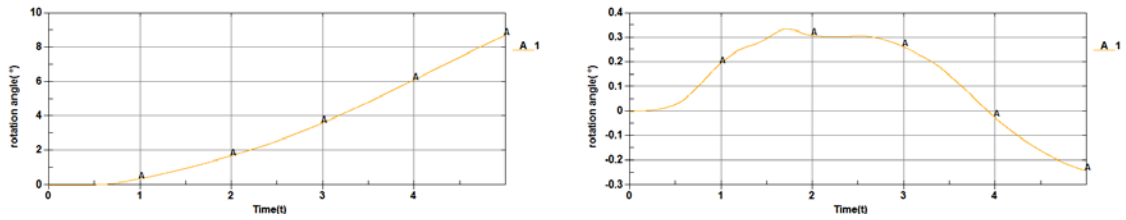

(a) Tanker (b) Platform

Figure 8.7 Rigid Body Rotation Angle_Head on_4m/s

Figure 8.7 shows that the tanker rotation angle is larger than that of 2m/s impact velocity. From 0s to 3s, the angle increased by less than 4 degrees, but in the last two seconds, the angle increased by almost 5 degrees. So in the first three seconds, the results are regarded as reasonable.

For the platform, the angle is considered positive when it rotates clockwise and negative when it rotates anticlockwise. It can be read from Figure 8.7 that the platform rotates clockwise at the beginning of the impact. When it comes to 2.5s, it begins to restore to the original place and then after about 4s, the platform will have a negative rotation angle. This is probably due to the large deformation in the main hull of the platform. Overall, the platform rotation angle is quite small, even small than that of 2m/s impact velocity case.

The deformation along a cut through the centerline of the bow and the platform is presented in Figure 8.8 for the first 7.5m of deformation in the lower part of the platform. This 7.5m is also the largest deformation in the corresponding location. 0m, 2.5m, 5.0m, 7.5m are the deformation in the main hull of the platform.

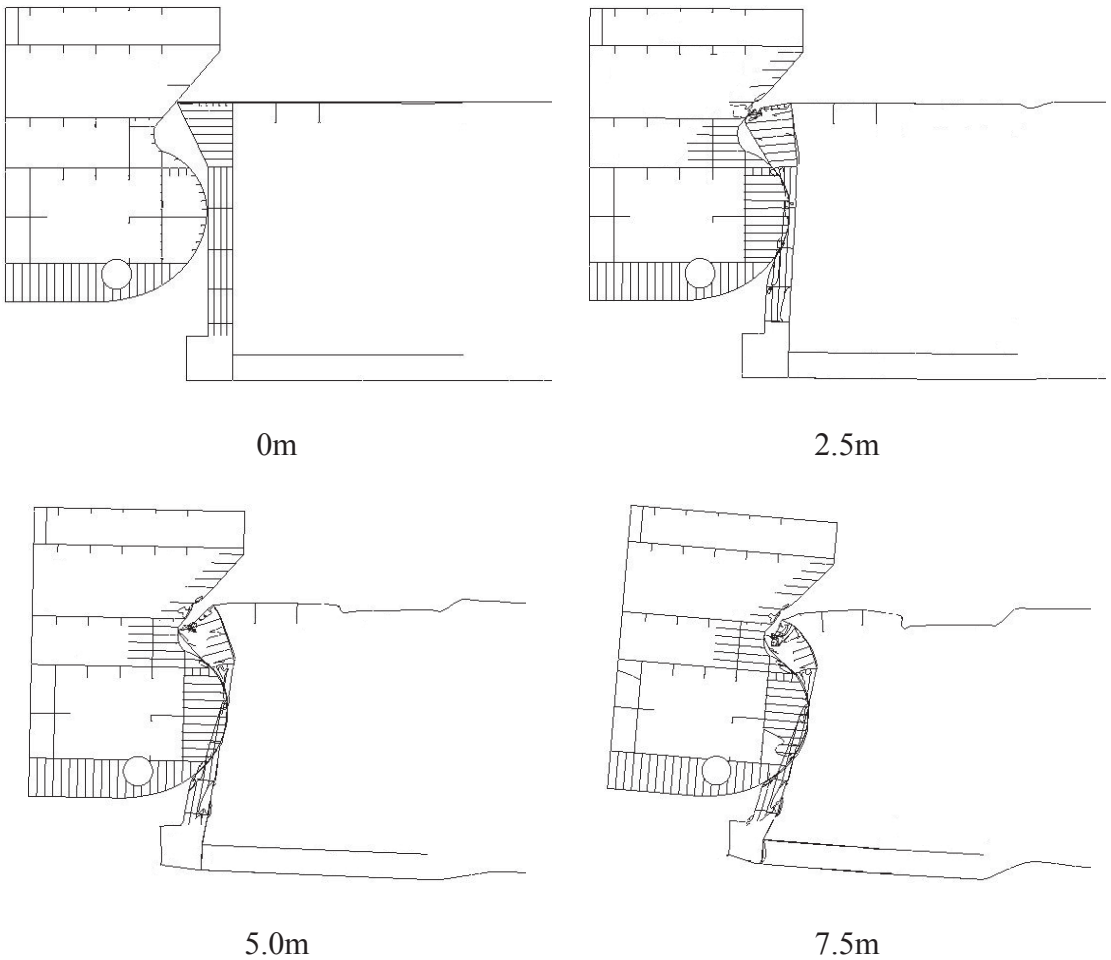

Figure 8.8 Deformation Sequence_Head on_4m/s

Figure 8.9 shows a horizontal cut in the middle of the bulb during crushing. Obviously, the deformation is much more severe than that in 2m/s case. Initially the deformation is not severe and the inner sides are not influenced in great extent. This means that the side deforms

by local indentation of the side structure. In this case, the outer shell itself and the stiffeners on it, including the centerline bulkheads, will resist the impact force and dissipate most of the energy. Neither the top deck nor the double bottom is deformed.

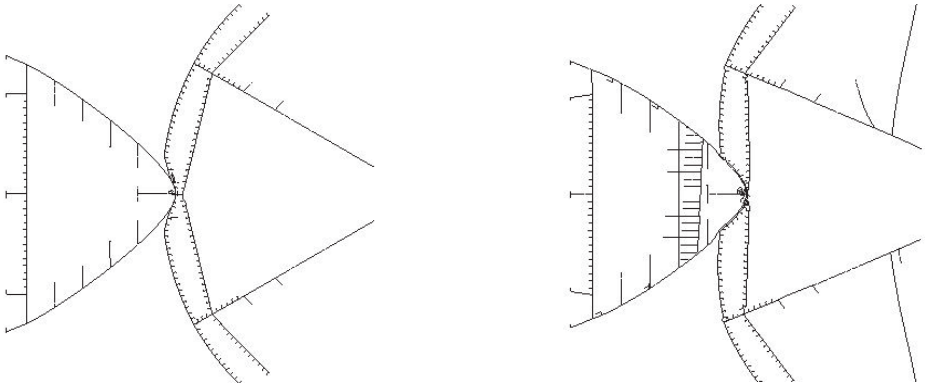

(a) (b)

Figure 8.9 Platform Main Hull Deformation_Head on_4m/s

As the deformation continues the double side is crushed. At the same time the top deck and the double bottom begins to fold. The upper part of the side is weakened by the top deck severely, but the membrane forces from the surrounding side plating still holds it in place. It can be seen from the last picture in Figure 8.8 and the second picture in Figure 8.9 that the centerline bulkhead between the ballast tanks are severely folded, so the support from this almost disappears. While for the deck and the double bottom, the support is weakened due to the deformation, but still exists. Figure 8.10 shows the energy dissipation of different parts on the platform and the tanker.

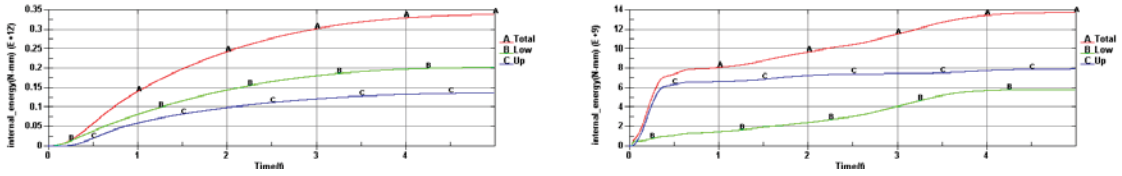

(a) Platform (b) Tanker

Figure 8.10 Dissipated Energy vs. Time_Head on_4m/s

The energy dissipation in this case of 4m/s is much larger than that of 2m/s. This is because the penetration in the same time is larger and the deformed structure components become more. Therefore more energy is dissipated as strain energy.

The stress contours are attached in the DVD in Appendix D.

- Cracks on the platform

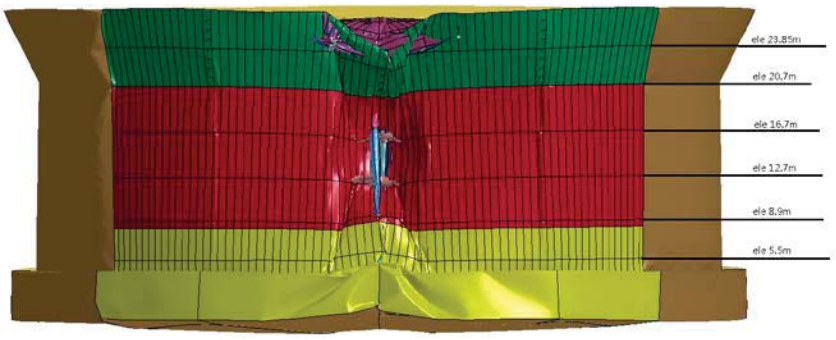

Figure 8.11 Cracks on the Platform_Head on_4m/s

Figure 8.11 shows severe damage on the platform and the ruptures for both collision positions are large. Not only ruptures but also large depressions exist in the main hull. The length of the crack on the main hull is around 10 meters, while the widest part is around 5m. The crack position is lower compared with the cracks of the 2m/s case. This may due to the rotation of the tanker. The depression size is around 10.7m wide and 11.8m long.

There are also cracks on the up conical part. Both the outer shell in the conical part and the upper deck fold downwards. The failure mode is no long the cracking of the commissure between the deck and the upper part shell, which is the failure mode in the 2m/s case. The deck and the stiffeners on the deck impale the shell from two sides as shown in Figure 8.11. So the crack is on the shell in this case. The total damaged size is almost 13.5m in the circumferential direction

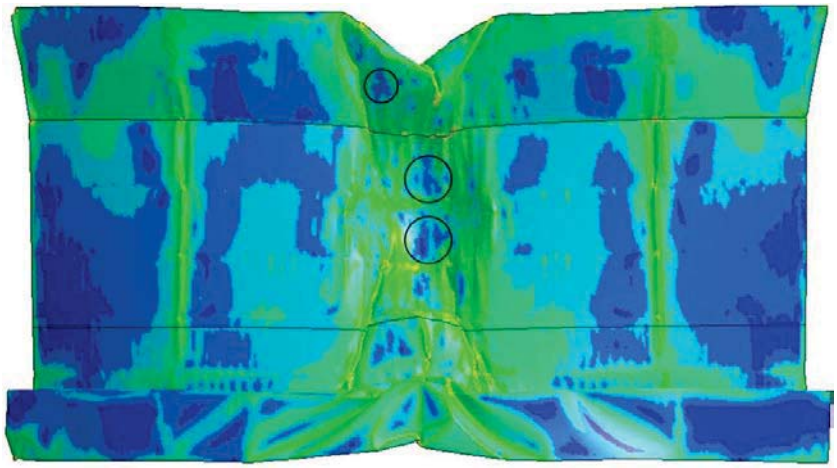

Figure 8.12 Outer Shell Stress Contour_Head on_4m/s

Figure 8.12 shows the Von-Mises stress contour of the outer shell in the detailed modeled part. In Figure 8.12 there are some points that deserve to be mentioned. First are the two places with lower stresses that are marked with circles in the figure. The reason for the low stresses may be due to the total failure of the shell. In areas where fracture has occurred, the stress is relieved. The places where the horizontal frames and the drapes are located give larger stresses, sometimes stress concentration.

8.1.3 Comparison Between 2m/s Case and 4m/s Case

- Energy Comparison

For both cases, initially the system has kinetic energy for the striking ship only. When they start to impact with each other, both striking and struck bodies have kinetic energy. The striking ship will still have a higher velocity than the struck ship. As the analysis continues, the two ships would eventually have the same velocity.

Figure 8.13 show the kinetic, internal and sliding energies vs. time for both case. The change in kinetic energy represents the total change in velocity for the model. The internal energy is the energy absorbed by strain dissipation. Sliding energy is the energy dissipated due to the friction between the two contact faces. There is sliding energy in this case because the friction coefficient is set to be 0.15. But it is seen from the figure that the sliding energy is very small compared to the internal energy. The largest frictional energy is only 1.3MJ for the 2m/s case and 5.3MJ for the 4m/s case. Table 8.1 shows the energy comparison between 2m/s and 4m/s head on collision cases.

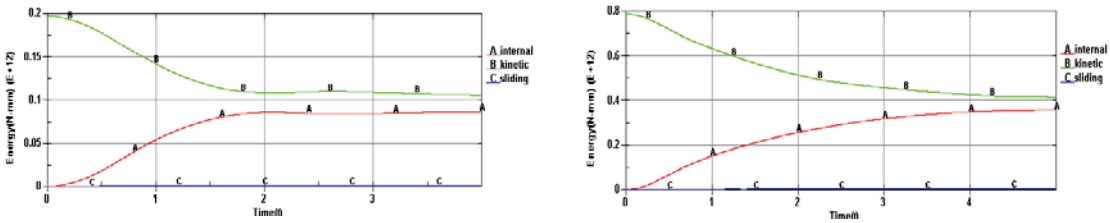

(a) 2m/s (b) 4m/s

Figure 8.13 External vs. Internal Energy_Head on

Table 8.1 Energy Comparison Between 2m/s and 4m/s Cases_Head on

Case 1	Total 2m/s	85.6 MJ	Platform	78 MJ *91.1%*	Up	29 MJ *37.2%*
					Low	49 MJ *62.8%*
			Tanker	7.6 MJ *8.9%*	Up	6.5 MJ *85.5%*
					Low	1.1 MJ *14.5%*
Case 2	Total 4m/s	353.8 MJ	Platform	340 MJ *96.1%*	Up	137 MJ *40.3%*
					Low	203 MJ *59.7%*
			Tanker	13.8 MJ *3.9%*	Up	8.0 MJ *58.0%*
					Low	5.8 MJ *42.0%*

It can be read from Table 8.1 that the total dissipated energy in case 2 is almost four times of case 1. It is consistent with the fact that the kinetic energy of the striking tanker in case 2 is

four times of case 1 and almost all the kinetic energy is dissipated as strain energy at the end of the impact. For both cases, the platform absorbs much more energy than the tanker. Moreover, more energy dissipated in the lower part of the buoy than the upper part, while more energy dissipated in the upper part of the tanker than the lower part.

It is noteworthy that the energy dissipation difference between the two structures is larger in case 2. However, the difference between the low and up part of each structure is larger in case 1. For example the difference between the up and low part of the tanker in case 1 is 71%, while the corresponding difference in case 2 is only 16%. The reasons for these may be that the larger impact velocity amplifies the strength difference between the platform and the tanker. But for each structure, the balance between the up and low part is better due to the larger impact intensity.

- Force-displacement curve comparison

It has to be mentioned that the forces and displacements in force-displacement curves in this section are all the components in the tanker heading x-direction. Because the x-direction components are the main components that are analyzed in the head on collision case. The displacements in these curves are the deformations at the four contact points. This means that they are all relative displacements, subtracting the rigid body motion of the platform and the tanker.

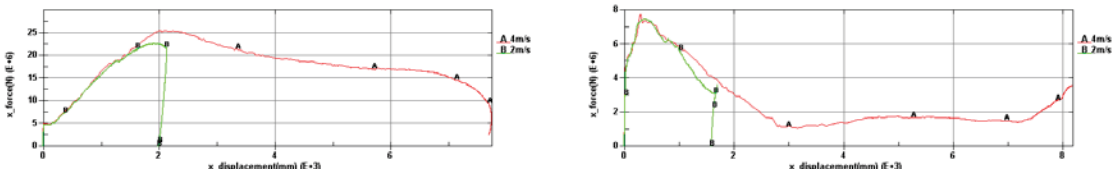

(a) Low (b) Up

Figure 8.14 Force-displacement Relationship for Platform_Head on

In order to interpret more phenomena, the deformation choice mechanism has to be explained here. In LS-DYNA, the deformation of the structures is represented by the displacement of certain points. In more detail, a certain point, called the ‘study point’, near the collision point is chosen to represent the displacement of the contact part. Another point, called the ‘reference point’, is chosen on the rigid back of the tanker bow or the mid line of the platform to represent the displacement of the rigid body. This reference point is on the same elevation as the study point. Therefore, the deformation of the structures is obtained by making subtraction of the study point displacement and the reference point displacement. To determine the force, RCFORCE is used in LS-DYNA, which is the contact force rather than the nodal force.

Normally, there are some reasons for an increase of the forces in the force-displacement curve. For example, when the structure deforms, the affected area will increase and may spread to very strong components which can give large resistance. The membrane stresses due to the deformation can also lead to the increase of forces. Another possibility is related to the relative strength of the two colliding bodies. Often the stronger of the ship and platform will

experience less damage and the softer side experiences more damage. As the softer structure deforms, the impact force is distributed over a larger contact area. Accordingly, the resistance of the strong structure increases. If the force decreases, the most possible reason is the failure of structure components. If the forces decrease rapidly to zero, it means that the two colliding bodies separate from each other. The change of force may also due to the rotation of the two bodies.

Figure 8.14 shows that for both low and up part, the two curves from the two cases fit quite well in the early stages until they separate apart. It is reasonable because the forces ought to be the same with the same penetration. The deformation for 4m/s case is much larger. The contact force of the low part is much larger than the up part. In the beginning of these curves, there is an increase in the tail of the red line in plot (b), which may due to the rotation of the structures. The deformation of the 4m/s case is much larger than that of 2m/s case. Figure 8.15 is the force-displacement curve for the tanker in head on collision case.

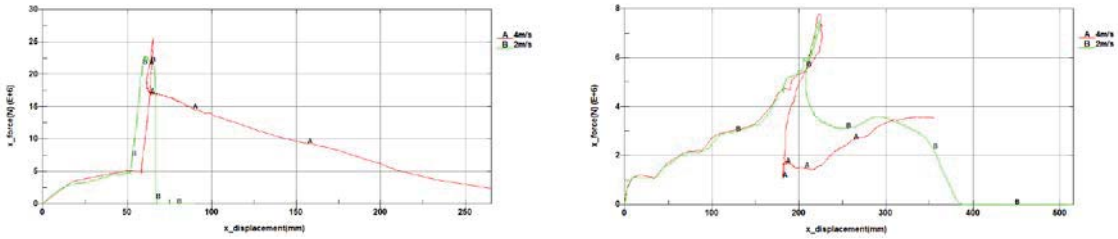

(a) Low (b) Up

Figure 8.15 Force-displacement Relationship for Tanker_Head on

In Figure 8.15 (a), the force increases gradually at first and after about 56mm of deformation the force increases rapidly. By checking the animation from D3plot, it is found that this is due to the horizontal stiffener and horizontal deck, which is shown in Figure 8.16.

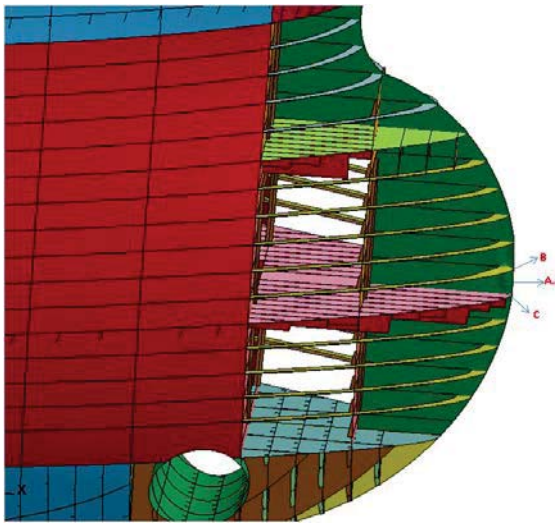

Figure 8.16 Tanker Bow Profile_Head on

It can be read from the animation that point A, which locates between the horizontal stiffener

at point B and the horizontal deck at point C, is the first point of collision. Point A is also the study point. The displacement for the low part of the tanker is very small. At the beginning when the displacement is tiny, only the central bulkhead and the outer shell offer resistance. As the impact continues, the affected area increases to point B and C. The stiffener and the deck will also resist the impact. Especially for the deck, it is a strong component and can give large resistance. So the force will increase rapidly at the corresponding displacement.

Figure 8.15 (b) shows a rapid drop at the deformation 224.8mm. It regains resistance when the force drops down to 1MN. This implies that this phenomenon is not due to the separation of the two bodies. After checking the D3plot, nothing related to the reason of this is found. The displacement is so small that it is not easy to find the difference visually. According to the theory, it is believed that the rapid drop is due to the collapse of the structure components. Actually a milder drop is expected. The sharp drop shown in Figure 8.15 (b) may be because of the choice of the study point and the reference point. After all, the displacement of a certain point can not fully represent the deformation of the whole colliding part.

8.2 Impact with Glancing Angle 30°

In collision with a glancing angle 30°, two impact velocities are chosen, 2m/s and 4m/s. Due to the limitations of the detailed mesh, the two impact points on the platform are still set more or less in the middle section of the detailed part. Therefore the locations of the two collision points are closed with those in head on collisions.

The main difference between the head on collision and the 30° glancing angle collision is that there are force and displacement components in y-direction for the later case.

In the beginning of the study, only the bow of the tanker is used as the striking part. Though the total mass of the bow is the same as the tanker, the rotational inertial is less than the whole tanker. Therefore theoretically, a problem may occur, which is the increased pitch and yaw rotation of the tanker bow. However, after simulating the 2m/s case with only the bow, the results show that the yaw motion of the bow is tiny. The pitch rotation of the bow is a little larger when coming to the later stage of the impact, which is similar to what is shown in the head on collision.

In order to produce better results, the whole tanker with the correct mass, center of gravity and rotational inertial is used as the striking body. The results show little difference from the earlier trial with only the bow, especially for the early stage of the impact because the rotation is not obvious then. Only slight differences occur when the impact becomes severe. It is interesting to see that when only using the bow, the rotation of the tanker is dominant and there is almost no rotation for the platform. While if the whole tanker is taken, the rotation of the platform is a little larger and there is less rotation for the tanker.

Though the results show little difference, the case with the whole tanker as the striking part is still utilized here. This is believed to give a more accurate result.

8.2.1 Impact Velocity of 2m/s

First an initial velocity of 2m/s is chosen, with the termination time of 4s. Figure 8.18 and Figure 8.19 show the vertical sections and horizontal sections during the impact. Figure 8.17 is the relationship curve between the x-direction deformation at the low collision point on the platform and time. It can be read from this curve that the deformation in the x direction reaches the largest value at around 2s. Therefore two time points are chosen for the impact profile.

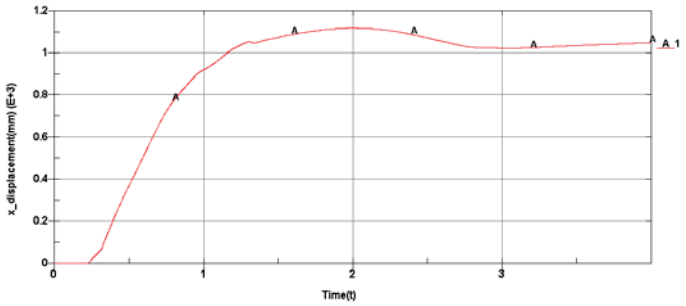

Figure 8.17 Platform Low Point Deformation_Glancing Angle_2m/s

One of them is at the time 0.45s when the impact is not serious. The corresponding deformation is only 0.3m. The other one is at the time with the largest deformation, here the time 2s is chosen. The corresponding deformation is around 1.1m.

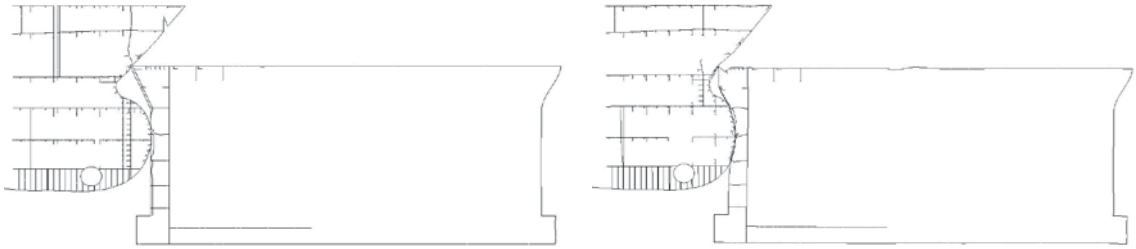

(a) 0.3m (b) 1.1m

Figure 8.18 Vertical Section_Glancing Angle_2m/s

The deformation in the platform is more concerned in our case. The low collision point on the platform and the central line of the platform can constitute a plane. The section shown in Figure 8.18 is made from this plane. For the section in Figure 8.19, the same collision point on the platform is chosen as a reference point and then a horizontal cut is made according to this point. This cutting method will clearly show the deformation on the platform, especially at the low collision point.

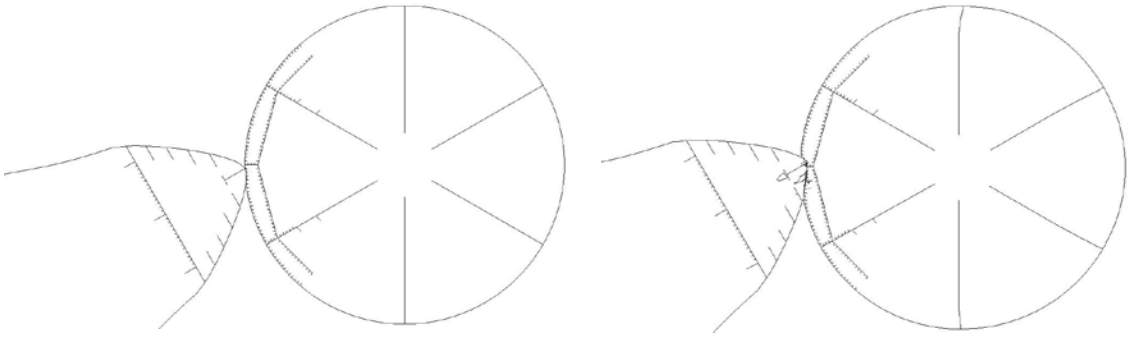

(a) 0.3m (b) 1.1m

Figure 8.19 Horizontal Section_Glancing Angle_2m/s

Figure 8.19 highlights that when the impact is not that serious, only the double side and the horizontal frame of the platform around the collision point are deformed. The deck and the central line bulkhead do not fold. The deformation on the bulbous is tiny, only little deformation is visible at the up conical part of the tanker bow. When the impact becomes much more serious when the time goes on, the impact area becomes much larger. The central line bulkhead and more horizontal frames on the platform are affected. The deck folds seriously. It can also be observed that the stiffeners on the bulbous of the tanker also begin to deform. All of these will yield a higher contact force.

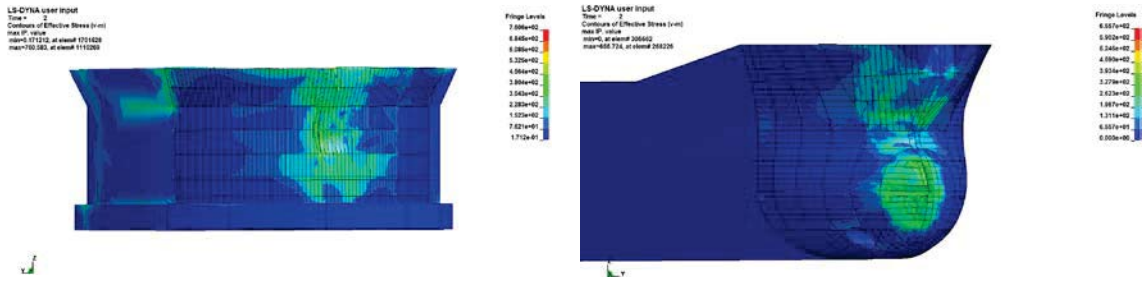

(a) Platform (b) Tanker

Figure 8.20 Von-Mises Stress Contours_Glancing Angle_2m/s

It is noticed that the impact area becomes larger than the head on collision case. This may due to the geometry of the bow and the force components in the y-direction. Another feature during the glancing angle impact is that there will be relative movement along the tangent plane of the two bodies, which will also increase the contact area.

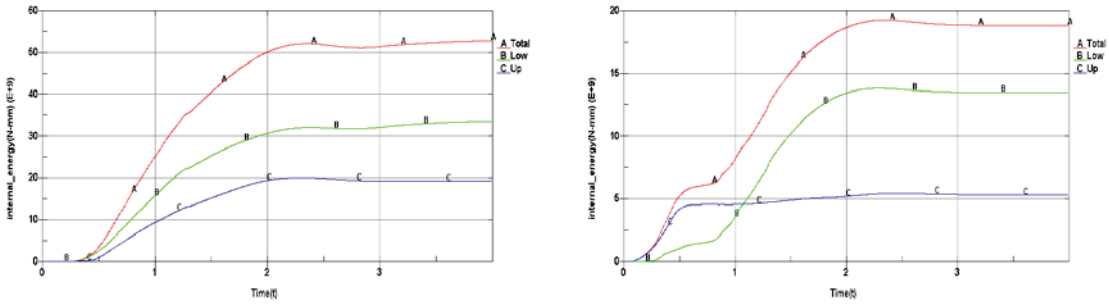

(a) Platform (b) Tanker

Figure 8.21 Dissipated Energy vs. Time_Glancing Angle_2m/s

The energy dissipation is different from the head on collision case. The energy dissipation amount for the platform and the tanker does not differ that much. The tanker dissipated more energy compared to the head on collision. This difference is probably due to the existence of the central line bulkhead. When it is head on collision, the collision point is in the vertical central line of the tanker, so not only the shell and the stiffeners will resist the impact, also the bulkhead makes contribution. Therefore, the structure around the collision points is robust with little deformation. While for the collision with glancing angle, the collision points deviate from the central position, so there is no contribution from the bulkheads. The tanker is easier to deform in this case.

For the platform, the energy dissipation distribution is similar to head on collisions. The low part absorbs more energy than the up part. For the tanker, it differs a lot from the head on collision case, the low part absorbs more energy as a whole. However, before 1.1s, the up part absorbs more energy than the low part. At around 2s, the two bodies reach the same velocity and stop the relative movement. This means that in the first half of the impact process, buckling of the upper structure components is dominant. As time goes on, the situation will be inversed. Figure 8.22 shows the initial crack on the platform for the 2m/s case in glancing angle collision.

- Cracks on the platform

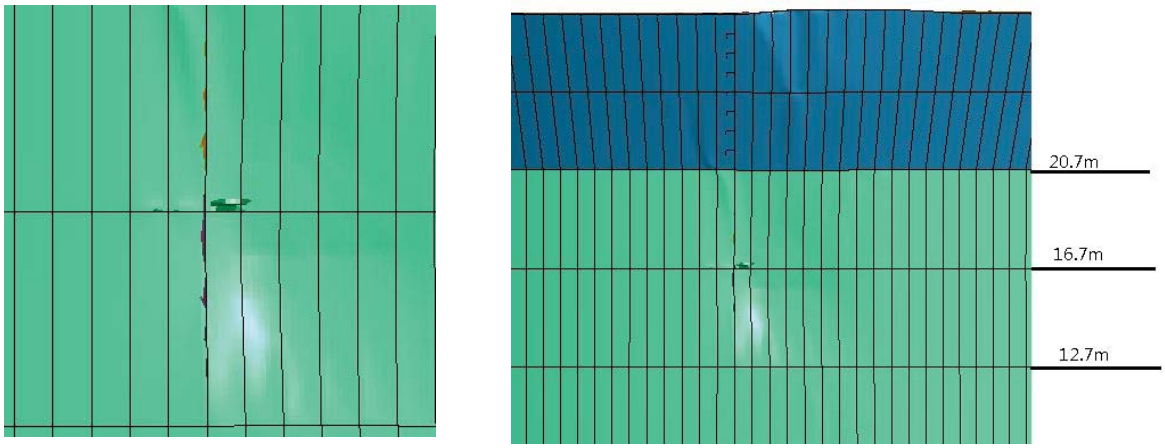

(a) Details (b) Overview

Figure 8.22 Initial Crack on Platform_Glancing Angle_2m/s

Figure 8.22 shows the crack in the early stage. The first crack appears at elevation of 16.7m, where the horizontal frame closest to the collision point is located. In the vertical perspective, the cracks will begin from the central line due to the existence of the central line bulkhead. The crack will grow as the impact goes on.

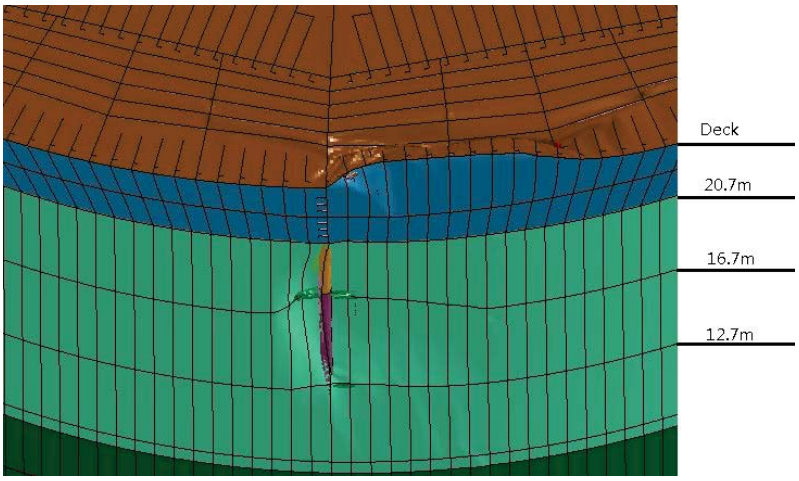

Figure 8.23 Largest Crack on Platform_Glancing Angle_2m/s

Figure 8.23 shows the largest crack. It is obvious that there is large crack on the main hull, while there is almost no crack on the deck and up shell. The shells fold seriously with no deformation at the up part, which is different from the head on collision. The widest part of the crack on the main hull is at elevation 16.7m, with the width around 2.8m. The crack spreads from elevation 12.7m to elevation 20.7m, with a length of 8m. The size of the crack on the main hull is almost the same with that in head on collision case. The crack will allow water to enter and cause flooding.

8.2.2 Impact Velocity of 4m/s

Then an initial velocity of 4m/s is chosen, with the termination time of 5s. The deformation on the low part of the buoy is also taken as a reference. The buoy low part deformations 0.32m and 3.96m are chosen to show the cut plot.

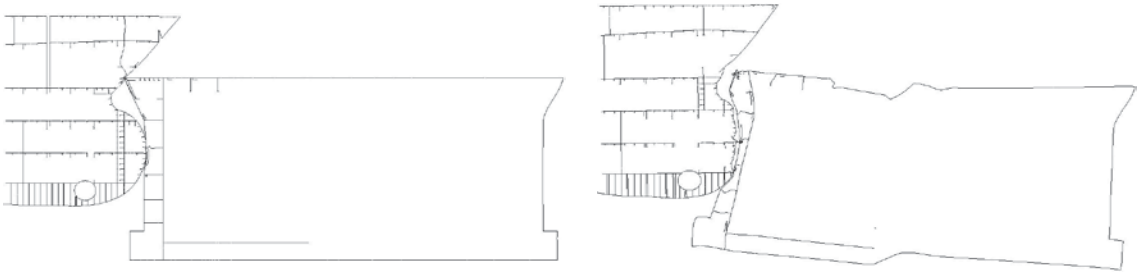

(a) Vertical_0.32m (b) Vertical_3.96m

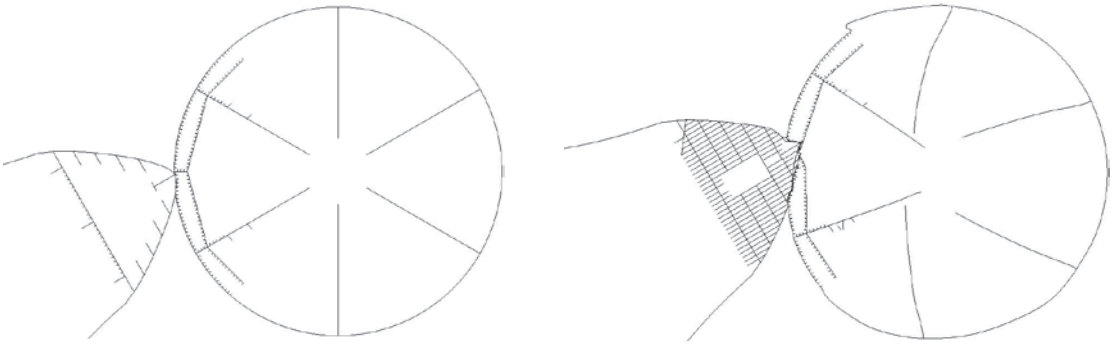

(c) Horizontal_0.32m (d) Horizontal_3.96m

Figure 8.24 Section Profile_Glancing Angle_4m/s

The (b) profiles show almost the largest deformation. It is interesting to note that the tanker bow also has large deformation. The side structures of the platform are damaged a lot. When the penetration is small, buckling of the outer shell and the corresponding stiffeners is the main failure mode. If the platform is more penetrated, buckling of the horizontal frames, inner side and the corresponding stiffeners would be an accessorial failure mode, yielding a much higher contact force.

It can be also read from (b) profiles that the structure fold along the boundary of the detailed modeled part and the coarse part. Therefore, when the deformation is large, the coarse part will be affected. This will cause inaccuracy. However, this inaccuracy is considered to be small and can be disregarded, especially when the deformation has not become so large. Figure 8.25 shows the Von-Mises stress contours for the 4m/s case in the glancing angle impact.

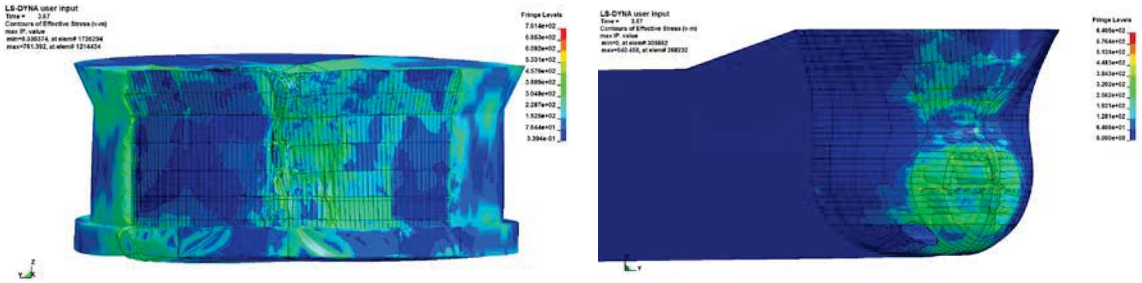

(a) Platform (b) Tanker

Figure 8.25 Von-Mises Stress Contours_Glancing Angle_4m/s

The affected areas are much larger in the platform. There is stress concentration along the boundaries between the detailed part and coarse part. The stresses near the collision points are large. If zoomed in, it is found that stress concentrations occur at the connection of the horizontal frames nearest to the collision point and the vertical stiffeners, where there is spiral torsion. The stress is larger at the places where the horizontal frames locate.

For the tanker, the stresses are large where the horizontal decks and transverse frames locate.

In the up area, there is a horizontal shell stiffener, causing larger stress.

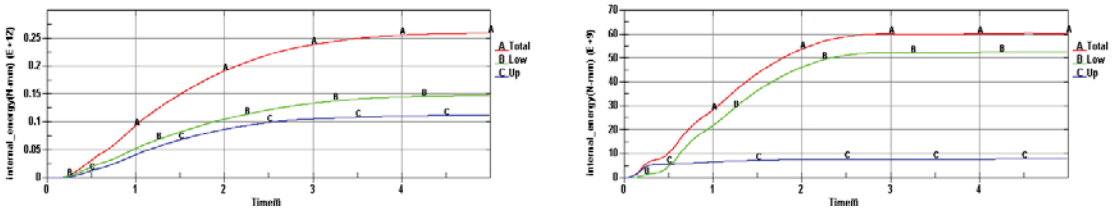

(a) Platform (b) Tanker

Figure 8.26 Dissipated Energy vs. Time_Glancing Angle_4m/s

It can be found from the figures that the energy dissipation difference between the platform and the tanker becomes larger again compared to the 2m/s case shown in Section 8.2.1. The low part of the tanker dissipated much more energy than the up part, which is quite different from the head on collision. After around 4s, the absorbed energy increment becomes tiny. It seems that the tanker will stop the energy absorption earlier than the platform. It means that in the later stage, the deformation of the platform dominates.

- Cracks on the platform

From reading D3plot in LS PREPOST, it can be found that at around 0.3s, the first crack will appear on the main hull of the platform. Figure 8.27 (a) shows the crack at 0.35s, so that the initial crack can be seen clearly. The location of the initial crack is the same as that in 2m/s case.

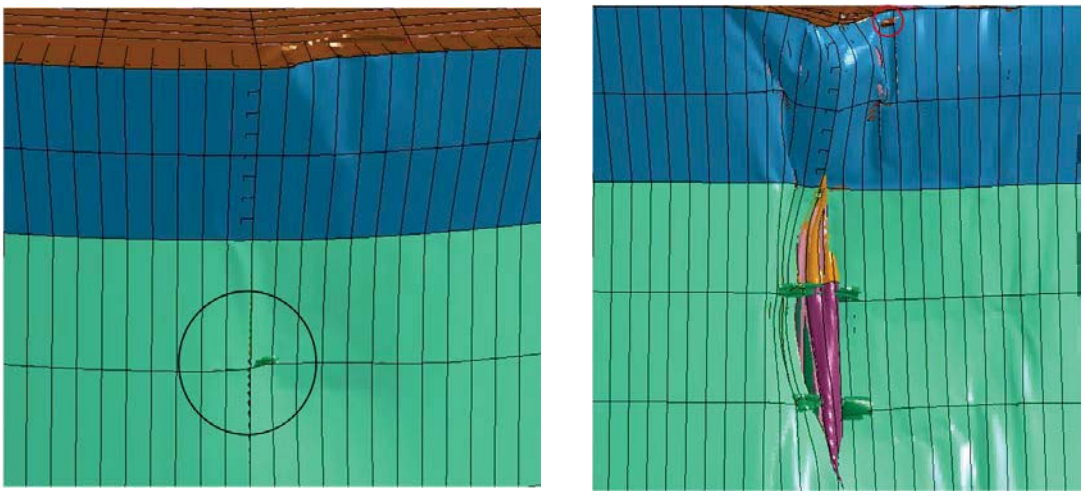

(a) Main hull (b) Up part

Figure 8.27 Initial Crack_Glancing Angle_4m/s

There is no crack on the deck and conical part of the platform at this moment. The crack on the up part will appear later than on the main hull. Figure 8.27 (b) shows the initial crack on the up part, which occurs at around 1.4s. The failure mode is the impaling of the deck into the upper hull, which is shown with red circle in the figure. The crack on the main hull is quite large by this time.

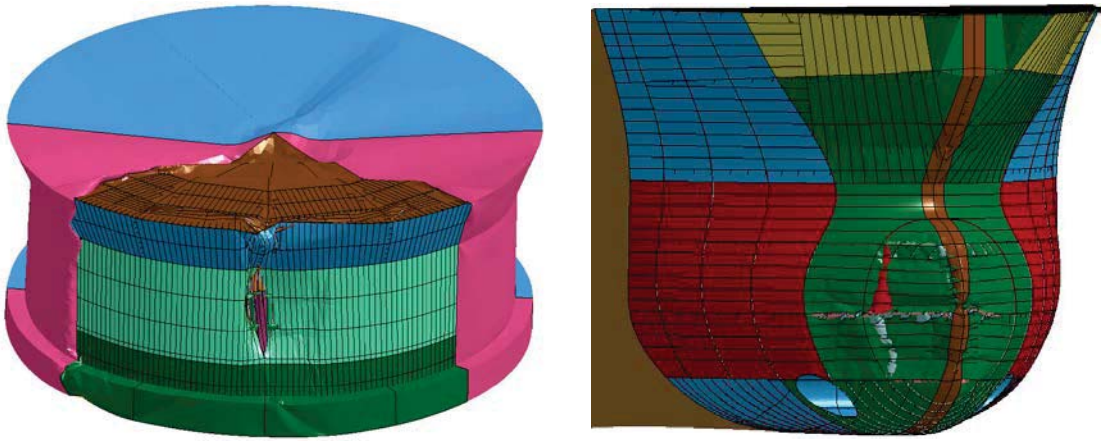

(a) Platform (b) Tanker

Figure 8.28 Largest Cracks on Both Bodies_Glancing Angle_4m/s

Figure 8.28 shows the largest crack on both bodies. The size of the crack can also be estimated visually from Figure 8.28 (a). The widest part of the crack on the platform main hull is around 5 meters and the length is around 12.5 meters. The crack on the up part of the platform is lathy with a length of 3.5 meters.

For the tanker, the outer shell of the tanker bow is impaled by the horizontal deck (as well as the stiffeners on the deck) and the transverse frame near the collision point. The largest crack is the most concerning. The vertical crack is around 10 meters long and the horizontal crack is around 20 meters long. There is almost no crack on the up part of the tanker.

8.2.3 Comparison Between 2m/s Case and 4m/s Case

- Rotation Angle

Different from the head on collision that only the pitch motion is of interest, for the impact case with glancing angle, both pitch and yaw are obvious rotational rigid body motion. Therefore the pitch and yaw motion for the tanker and the platform are considered here. Here the pitch motion is the motion around y-axis. Yaw motion is the motion around z-axis.

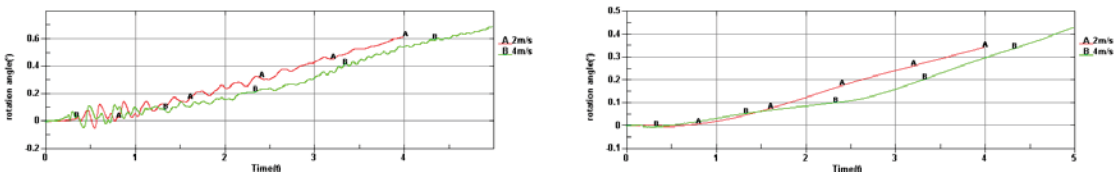

(a) Pitch (b) Yaw

Figure 8.29 Rotation Angle for the Tanker_Glancing Angle

It is interesting to find that for the tanker, when increasing the impact velocity, the rotation angle for both the pitch and the yaw will become smaller. There is fluctuation in the pitch

motion, especially in the early stage of the impact. It is important to notice that the rotation angles of the tanker are smaller than those in a head on collision. This owns to the adjustments of the tanker rotational inertia. The pitch and yaw angles in both two impact velocity cases are very small, which is less than one degree. The pitch angle is larger than the yaw angle for the tanker.

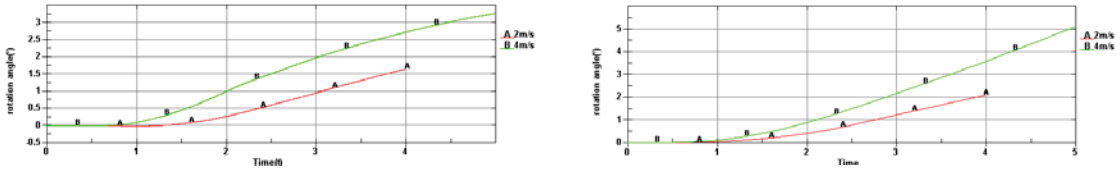

(a) Pitch (b) Yaw

Figure 8.30 Rotation Angle for the Platform_Glancing Angle

For the platform, the pitch and yaw motion angle is larger in 4m/s case, which is a reasonable result. The rotation angles of the platform are larger than those in head on collision. The yaw angle is larger than the pitch angle for the platform.

- Energy Comparison

In the case with glancing impact angle, the frictional energy is larger than the head on impact, which are 10.5MJ and 17MJ for the 2m/s case and 4m/s case respectively. For the 2m/s case, the relative motion stops at around 2s. For the 4m/s case, the two bodies almost stop relative motion at 5s. Table 8.2 shows the energy comparison between 2m/s and 4m/s cases in glancing angle impact.

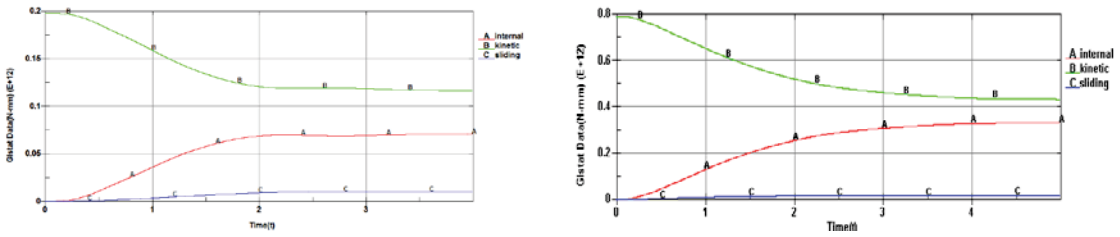

(a) 2m/s (b) 4m/s

Figure 8.31 Energy Variation_Glancing Angle

Table 8.2 Energy Comparison Between 2m/s Case and 4m/s Case_Glancing Angle

Case 1	Total 2m/s	72.9 MJ	Platform	53.7 MJ *73.7%*	Up	20.1 MJ *37.4%*
					Low	33.6 MJ *62.6%*
			Tanker	19.2 MJ *26.3%*	Up	5.4 MJ *28.1%*
					Low	13.8 MJ *71.9%*
Case 2	Total 4m/s	321.6 MJ	Platform	260.8 MJ *81.1%*	Up	112.3 MJ *43.1%*
					Low	148.5 MJ *56.9%*
			Tanker	60.8 MJ *18.9%*	Up	8.0 MJ *13.2%*
					Low	52.8 MJ *86.8%*

As a whole, the energy absorption in the glancing angle case is smaller than that in the head on collision. It is believed that more energy is dissipated by the friction in the glancing angle case. The energy absorption difference between the platform and the tanker becomes smaller compared to the head on collision, which means the tanker dissipates more energy. The platform still absorbs more energy than the tanker.

For the platform itself, the energy dissipation of the up and low part are more averaged compared to those in the head on collision. The difference between the up and low part is not big and as the impart velocity increases, the energy dissipation by the up and low part of the platform will be more averaged.

The tanker is in a different situation. The low part of the tanker will dissipate much more energy than the up part. Moreover, the difference becomes larger when the impact velocity increases. For example in Case 2, the up part of the tanker only absorbs 13.2% of the total energy absorbed by the whole tanker. This may be due to the central bulkhead described in section 8.2.1. The sliding energies that are due to the friction are 10.4 MJ and 17.0 MJ for the 2m/s case and 4m/s case, respectively.

- Force-displacement curve comparison

In this part, the force-displacement relationships for the low and up part of both the tanker and the platform are given out. This is an impact case with glancing angle of 30 degrees, the force-displacement curves are given in two directions, which is x- and y- directions in the global coordinate system. Figure 8.32 shows the coordinate system used in this section.

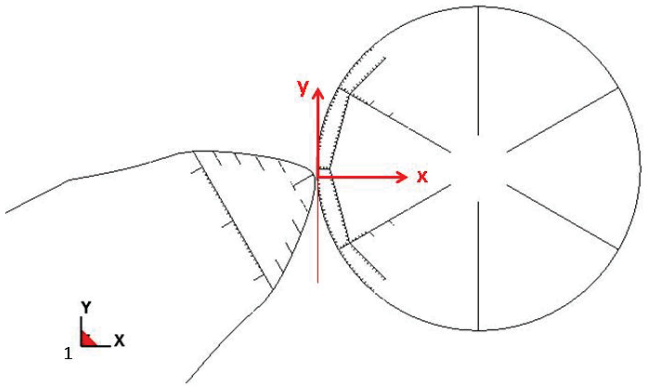

Figure 8.32 Sketch of Coordinate System_Glancing Angle

The coordinate system 1 in Figure 8.32 is the global system. It is easier to see if moving this to the collision point as shown by the red coordinate in the Figure 8.32. The y-coordinate is along the tangent plane, while x-coordinate is normal to the tangent plane. The force and displacement will be considered separately according to these two directions.

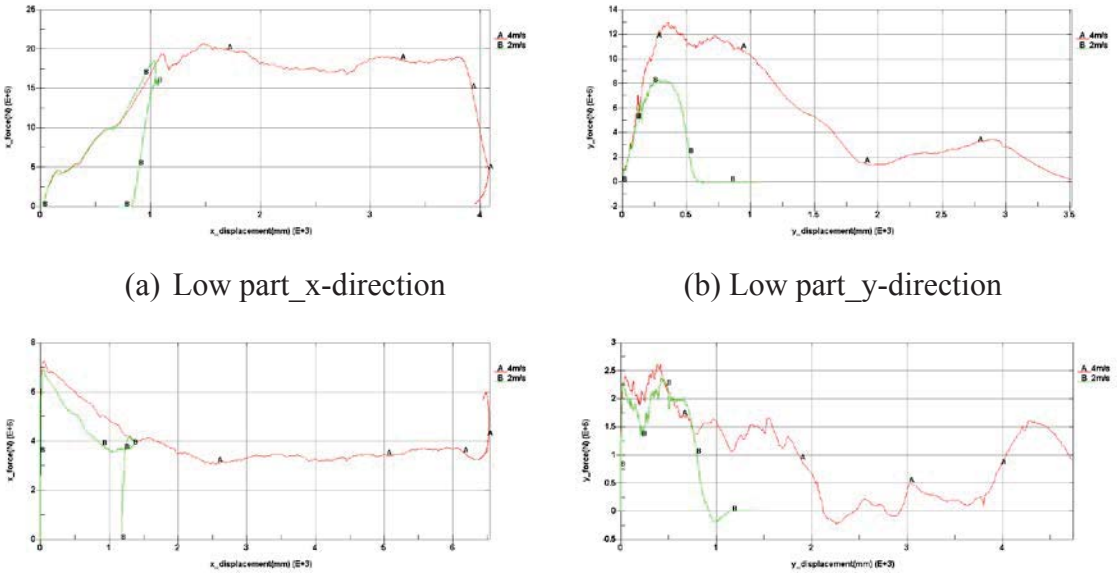

(a) Low part_x-direction (b) Low part_y-direction

(c) Up part_x-direction (d) Up part_y-direction

Figure 8.33 Force-displacement Relationship for the Platform_Glancing Angle

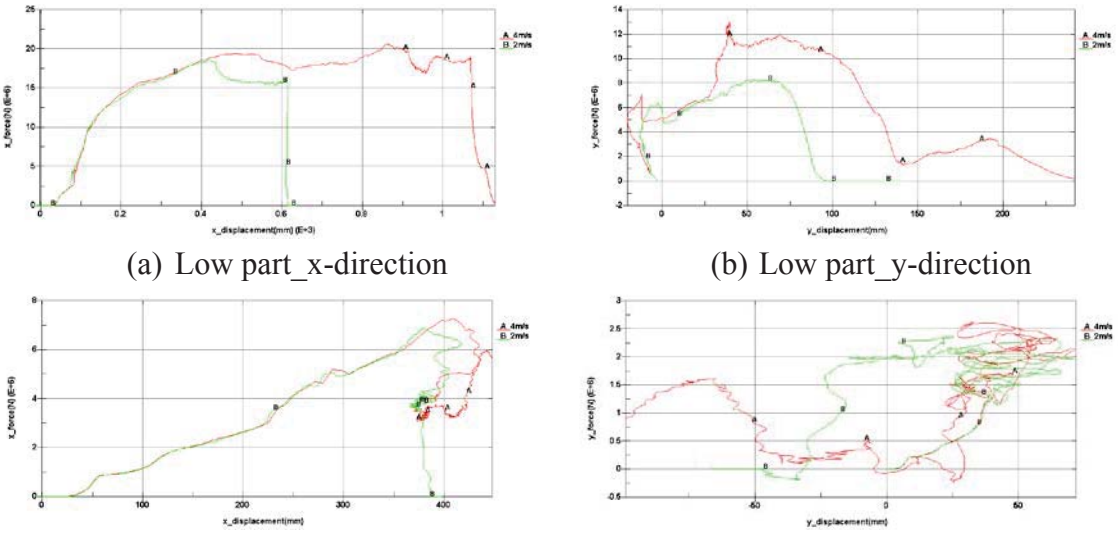

(a) Low part_x-direction (b) Low part_y-direction

(c) Up part_x-direction (d) Up part_y-direction

Figure 8.34 Force-displacement Relationsip for the Tanker_Glancing Angle

Figure 8.33 and Figure 8.34 show the force-displacement relationship for the platform and the tanker, respectively. From the overall view, the results in x-direction behave better than that in the y-direction. The red ones are the curves in the 4m/s case and the green ones are those in 2m/s case. In the initial stage, the curves in two cases coincide with each other very well, especially for the curves in x-direction. This is because in the beginning, the deformation and the force will be the same, despite of the impact velocity. For the 2m/s case, after a relatively short period, the platform and the tanker will reach the same velocity and separate from each other. Then the force goes down to zero immidiately. After this moment, the curve corresponding to the higher impact velocity will continue for a far more distance, except for

the up part of the tanker. The force-displacement in x-direction always gives better results than that in y-direction.

For the platform in Figure 8.33, the deformation is relatively large. It is seen from (a) and (c) that the force maximum value is almost the same with different velocities. The force remains constant for a period, though the deformation continues. This means that some components fail as the impact goes on. When the contact area becomes larger, more components will be affected, so that some new structure components will offer the resistance again the impact. There is an difference between the up and low part of the platform curves. For the low part, the force increases gradually with the deformation. For the up part, the force jumps to a high level suddenly when the impact begins and then decrease to a certain level. This is related to the study point chosen when measuring the deformation. Perhaps the chosen 'study point' deviates a little from the real first collision point. So there is no deformation in the very beginning of the impact, though the force exist. The force decreases gradually in the beginning in Figure 8.33 (c) because that more and more components, for example stiffeners, collapse and fail to offer resistance.

Figure 8.33 (b) and (d) shows the force-displacement relationship in y-direction. It seems that for the y-direction, the largest force for the 2m/s case is smaller than the 4m/s case, which can be seen clearly from (b). This shows for larger impact velocity, the structure components can give larger resistance in y-direction.

Figure 8.33 (c) and (d) show the deformation in the up part of the platform, it is found that after about 3.8 meters deformation in x-direction and about 6.5 meters deformation in y-direction, the forces rapidly increase. This is due to the horizontal frame at elevation 20.7m, which at this displacement becomes important to the stiffness of the up part of the platform. At this point further displacement of the corresponding point mobilizes large membrane stresses from the frame section. The effect of this is that this horizontal frame is pulled up when the analysis progresses further. Therefore the force will increase due to the existance of the membrane stresses.

For the up part of the tanker, which is shown in (c) and (d) in Figure 8.34, the force-displacement relationship in the y-direction gives no meaningful information. The phenomenon may be due to the choice of the study point and the reference point. Details regarding these two points have been described in section 8.1.3. Moreover, the possible yaw and pitch rotation of the tanker together with the instability during the impact process may also cause this phenomenon. Figure 8.34 (a) and (c) give better results. Both the forces in x-direction increase gradually from zero to a specific value, which are 18MN and 7MN, respectively.

8.3 Effective Plastic Strain

The impact with a glancing angle of 30 degrees and impact velocity of 4m/s is taken as an example to explain the effective plastic strain.

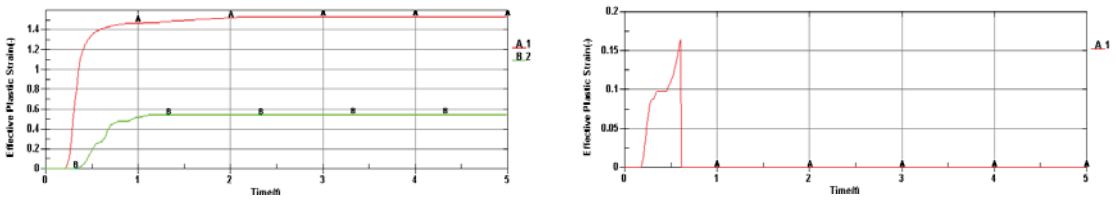

(a) (b)

Figure 8.35 Effective Plastic Strain_Glancing Angle_4m/s

In Figure 8.35 (a), Line 1 shows the strain history of the element with the largest strain. Line 2 is the strain history of an arbitrary element near the collision point. The largest strain of Line 1 exceeds the critical strain and that of Line 2 is below the critical strain. It shows that after around 1 second, the strain begins to remain unchanged. This is because that after some time, the effects on these elements stop due to the transmission of the affected area, so that the forces and deformations will be transmitted to other surrounding elements.

Figure 8.35 (b) shows the element at the rupture. At around 0.6s, it ruptures and thus the elements are deleted in LS-DYNA. Therefore there will be eroded energy. Eroded energy is the energy associated with deleted elements (internal energy) and deleted nodes (kinetic energy). Figure 8.36 shows that the eroded energy is small compared to the internal energy. Thus, the elements deleted due to fracture are few.

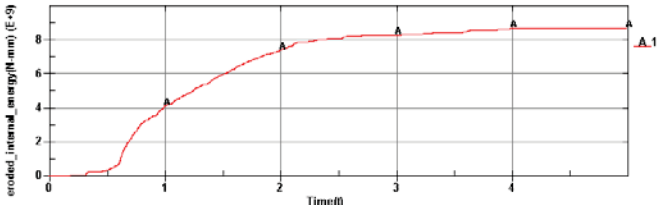

Figure 8.36 Eroded Internal Energy_Glancing Angle_4m/s

Chapter 9 FEM Results-Split Analysis

Different from Chapter 8, this chapter deals with split analysis rather than the integrated analysis. The impact problem is considered from two aspects, external mechanics and internal mechanics. These two split methods can be regarded as two simplified method to do the impact analysis. Sometimes it is not convenient and time consuming to perform the integrated analysis. It is meaningful to test if these two methods are reasonable enough to replace the full integrated analysis in some cases.

9.1 External Impact Mechanics

The results of the external mechanics analysis which is obtained from the MATLAB program are shown in Table 9.1.

Table 9.1 Results of Liu's External Mechanics Methods

		$E_{dissipated}$ (MJ)			V_a (m/s)			V_b (m/s)			E_0 (MJ)	ρ_0
		E_1	E_2	E_3	n_1	n_2	n_3	n_1	n_2	n_3		
Head on	2m/s	≈0	0	89.3	1.04	0	0	1.04	0	0	90.6	0.986
		89.3										
	4m/s	≈0	0	357.3	2.08	0	0	2.08	0	0	362.4	0.986
		357.3										
Glancing angle 30°	2m/s	0.44	0.26	81.8	1.07	-0.23	-0.03	1.00	0.41	0.05	90.6	0.911
		82.5										
	4m/s	1.76	1.06	327.4	2.15	-0.47	-0.06	2.01	0.82	0.10	362.4	0.911
		330.2										

$E_{dissipated}$ - Total dissipated energy

V_a - Velocity after impact of object a under body frame of object a

V_b - Velocity after impact of object b under body frame of object b

E_0 - Kinetic energy of striking body before impact

ρ_0 - Energy ratio between dissipated energy and kinetic energy, which is $\frac{E_{dissipated}}{E_0}$

It can be concluded from the tables that the dissipated energy will depend on impact velocity. The 4m/s case dissipated almost four times energy than the 2m/s case. For the same velocity, the energy dissipations for head on collision and the 30° glancing angle collision are slightly different. Generally speaking, the energy dissipation in the 30° angle case is smaller than that in the head on collision, which may be due to the friction. For impact with a glancing angle, the frictional energy will be larger than the head on impact. When increasing the impact velocity, the frictional energy will increase in a large extent. So the energy dissipation difference between the head on impact and the glancing angle impact is larger for the 4m/s case.

For the head on collision, the energy dissipation only has values in one direction. While the energy dissipation in the other two directions are both zero. This is consistent with the simple head on collision example in Liu's paper [16]. For the case with glancing angle, there are values in all the three directions. However, the dissipated energy in E_3 direction is still the main contribution, which is much larger than in the other two. Moreover, it is interesting to see that the energy ratio is the same when the impact directions are the same, regardless of the impact velocities.

For head on collision, the velocities after impact only have the component in the direction of impact, which is consistent with what is hypothesized. For collision with glancing angle, there is also velocity component in the other two directions. The velocity in the vertical z-direction is relatively small, which is probably due to the rotation of the tanker, is relatively small.

9.2 Internal Impact Mechanics

The internal mechanics focus on the deformation of the structure components. Anything related to the external movements should be separated out, for example the velocities of the platform and the tanker. Therefore the velocity variety of the two structures should not be concerned. In order to realize this, impact mechanics different from integrated analysis in Chapter 8 is forwarded. Firstly, the platform is set to be fixed spatially instead of the free moving platform in Chapter 8. Figure 9.1 shows the velocity variation for the tanker in the integrated analysis. Secondly, the bow will go forward with a constant speed rather than the gradually decreasing tanker velocity as shown in Figure 9.1.

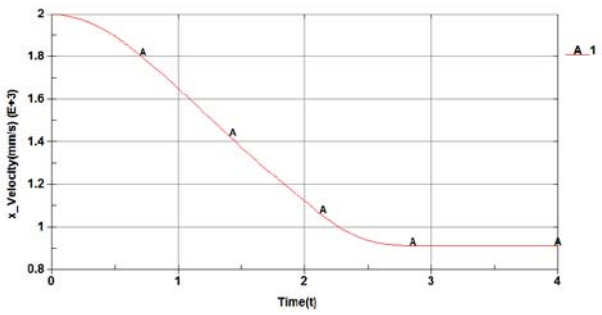

Figure 9.1 Tanker Rigid Body Velocity in x-direction_Head on_2m/s

The split analysis is also performed with two cases, heads on impact and the impact with glancing angle 30 degrees. Only the penetrations of the two bodies are interested. There is no difference whether the analysis is perform with the impact velocity 2m/s or 4m/s, provided that enough penetration is given for the analysis. For convenience, a constant velocity of 2m/s is chosen for both cases. The termination time is 4 seconds, so that the penetration is 8 meters.

9.2.1 Head On Impact

The internal energy-time relationship can be obtained herein, shown in Figure 9.2. The internal energy is regarded as the strain energy dissipated by structure components.

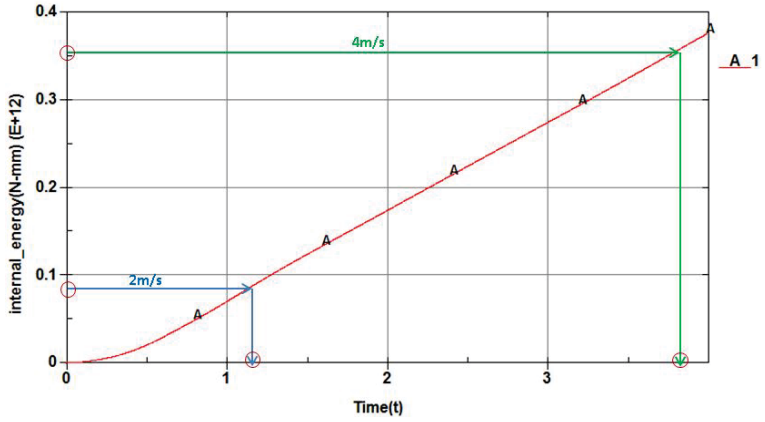

Figure 9.2 Energy-time Relationship_Head on_Internal Mechanics

The research method in this section is stated herein. From the integrated analysis in Chapter 8, the dissipated energy can be obtained for both velocity cases for integrated head on collision, which is 87.3MJ and 359.4MJ, respectively. These two values are from Figure 9.2 and then two time points corresponding to these can be obtained. The corresponding time is 1.152s and 3.833s, respectively.

The next step is to find out the corresponding deformation related to these two time points. The relative displacement-time relationships can be also obtained in the internal analysis. From the two time points, the deformation in the two velocity conditions are found, which is shown intuitively in Figure 9.3. The displacement-time relationship in the low part of the platform is used as an example in Figure 9.3.

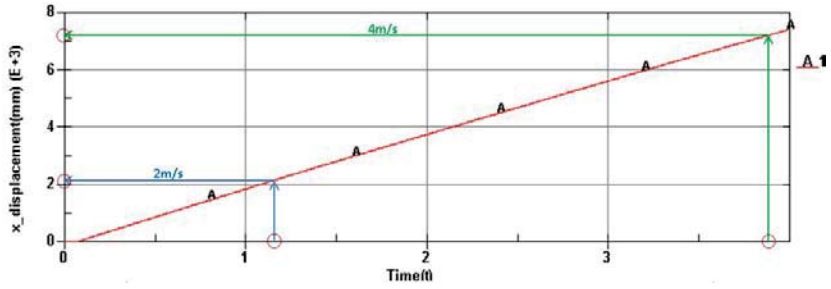

Figure 9.3 Platform Low Point Displacement_Head on_Internal Mechanics

With the similar method, the displacements results from the internal mechanics in the four points can be obtained. Comparing them with the integrated analysis results, Table 9.2 is obtained.

Table 9.2 Comparison of Internal Mechanics and Integrated Analysis_Head on

	Energy (MJ)	Time (t)		Deformation		Deviation Of Deformation
				Internal (m)	Integrated (m)	
2m/s	85.6	1.152	Platform Up	1.639	1.575	4.1%
			Platform Low	2.133	1.991	7.1%
			Tanker Up	0.191	0.172	11.0%
			Tanker Low	0.081	0.089	9.0%
4m/s	353.8	3.833	Platform Up	7.511	8.179	8.2%
			Platform Low	7.143	7.700	7.2%
			Tanker Up	0.191	0.356	*46.3%
			Tanker Low	0.141	0.266	*47.0%

The table shows that the internal impact mechanics give a better result for the velocity of 2m/s than the velocity of 4m/s, because the deviation of deformation is relatively small for the 2m/s case. This is due to that when the velocity is larger, the impact is heavier. The influence by the rigid body motion becomes more important.

In each case, the deviation of deformation for the platform is smaller than that for the tanker. This may due to the rotation of the tanker or the study point choice on the tanker. It is worth mentioning that the results for the tanker in 4m/s case, which are marked with asterisks in front, have large deviations almost up to 50%. This effect may be due to the rotation of the tanker bow. It is believed that the situation will be improved in the impact with a glancing angle, because in that case a whole tanker with a more accurate rotational inertial is used. The rotation of the tanker will be smaller and thus closer to the reality.

9.2.2 Impact With Glancing Angle 30°

Figure 8.33 and Figure 8.34 show that the displacements in y-direction seem to be always unstable. Therefore, little difference in movement pattern or in the choice of the study point will generate significant different on the displacement. The results show large difference in y-direction displacement for internal and integrated analyses. Therefore it is believed that it is meaningless to compare the y-direction results between the internal and integrated analysis.

Table 9.3 illustrates only the displacements in x-direction are shown. Similar methods as in section 9.2.1 are used to perform the comparison.

Table 9.3 Comparison of Internal Mechanics and Integrated Analysis_Glancing Angle

	Energy (MJ)	Time (t)		Deformation		Deviation Of Deformation
				Internal (m)	Integrated (m)	
2m/s	72.9	1.367	Platform Up	1.407	1.364	3.2%
			Platform Low	1.066	1.077	1.0%
			Tanker Up	0.399	0.398	0.2%
			Tanker Low	0.679	0.638	6.4%
4m/s	321.6	3.588	Platform Up	6.304	6.534	3.5%
			Platform Low	3.907	4.083	4.3%
			Tanker Up	0.390	0.448	12.9%
			Tanker Low	1.349	1.130	19.4%

Overall the results for the 2m/s case are better than the 4m/s case as in head on impact. The tanker results in 4m/s case are better than the head on collision as expected. The deviation of the internal mechanics analysis from the integrated analysis is not large. It can be concluded that the internal mechanics analysis can be used instead of the integrated analysis to some extent, especially in the case with smaller impact velocities. More accurate models will increase the veracity of the internal mechanics, for example a more accurate rotational inertial makes the results better.

Chapter 10 Simple Methods

Nowadays, advanced detailed numerical simulations can be made to assess the structure damage during collisions. However, these analysis are quite time consuming and results from these calculations depend heavily on the input and detailed model. In addition, the analysis often becomes too complicated to perform. Simple analytical methods are therefore becoming very useful.

In this chapter, two simplified methods are forwarded to calculate the dissipated energy during the collision. While other than these two methods. Liu's method based on the Stronge impact theory is also regarded as an optimized simplified method. A comparison between these three simplified methods will also be executed in this chapter.

10.1 DNV Simplified Method

The basic mechanics of ship-platform collision can be taken as an energy calculation in essence. The tanker has significant kinetic energy before the collision and moves towards the platform. The energy can be absorbed in several ways during the collision process. The most important is absorbed by strain energy dissipation. Hydrodynamic damping and acceleration of structural and hydrodynamic added mass will also change the energy. In the NORSOK requirement, all these effects are included when assessing the accident limit state.

In our case, the two collision bodies will have kinetic energy left after the impact, because they will reach the same velocities. The strain energy absorption is the main feature that considered in our case. The strain energy absorption involves large plastic strains and significant structural damage to either one or both the two collision bodies. In simple methods, the conservation of momentum and conservation of energy are the main principles.

For head on collisions closed form expressions exist for the amount of energy that has to be dissipated. Both DNV-RP-C204 and NORSOK N004-A give out the formulas for calculating the strain energy dissipations. They distinguish between fixed platforms, compliant platforms and articulated columns, so that the collision energy to be dissipated as strain energy depends on the type of installation and the purpose of the analysis. In the case which is described in this report, the platform can be considered as compliant. The formula for the compliant installation is shown in formula (3.2). In this case, the velocity of installation is zero. Therefore the formula becomes what is shown in Eq. (29).

$$E_s = \frac{1}{2}\left(m_s + a_s\right)\cdot v_s^{\,2}\,\frac{1}{1+\dfrac{m_s + a_s}{m_i + a_i}} \tag{29}$$

For a compliant installation, these expressions take into account that after a collision, ship and platform have equal velocity. The larger the weight of the platform, the higher the amount of energy that has to be dissipated. In the case in this report, the tanker is heavier than the

platform. If the added mass is taken into account, the two structures will have almost the same weight. They should have dissipated the similar amount of energy. However, from the finite element analysis, it is found that the platform dissipated much more energy than the tanker, which is thought to be from the strength differences of the two structures.

The strain energy dissipation can also be estimated from the force-deformation curves. The total area under the for-deformation curve is the total energy dissipated as strain energy.

10.2 Modified Simplified Method

A modified simplified method is forwarded by T. de Jonge and L. Laukeland in the paper Collision between a spar platform and a tanker [20]. In this paper, a problem is mentioned on the foundation of the corresponding part in DVN-RP-C204.

Both the striking and stuck parts are considered as compliant installations. Therefore, they would not lead to a fair trade-off. It is shown that the fact that a spar can rotate out of plane has a considerable effect on the amount of energy that has to be dissipated. The modified simplified method takes in the consideration of the roll motion.

The collision between a ship and a spar is considered in order to explain this method, which is as shown in Figure 10.1.

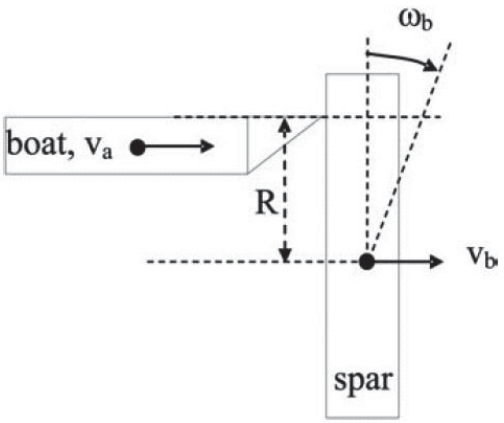

Figure 10.1 Head On Collision Between a Ship and a Spar

It is assumed that the collision is completely inelastic. The impact will cause a horizontal velocity of the spar and an angular velocity around its center of gravity. Momentum and angular momentum will be conserved during the collision. This leads to the two following equations:

$$m_s(1+a_s)v_{s0} = m_s(1+a_s)v_{s1} + m_i(1+a_i)v_{i1} \tag{30}$$

$$m_s(1+a_s)v_{s0}R = m_s(1+a_s)v_{s1}R + I_i\omega_i \tag{31}$$

The two bodies will apart from each other when the velocity at the top of the bow of the boat

and the spar at the same elevation become equal, which leads to the following condition:

$$v_{s1} = v_{i1} + R\omega_i \tag{32}$$

Solving these equations, the following expressions are obtained for the velocities after the collision:

$$v_{s1} = \left(\frac{a + bR}{1 + a + bR}\right) v_{i0} \tag{33}$$

$$v_{i1} = \left(\frac{a}{1 + a + bR}\right) v_{s0} \tag{34}$$

With: $a = \frac{m_s}{m_i}\frac{(1+a_s)}{(1+a_i)}$, $b = \frac{m_s R(1+a_s)}{I_i}$

The energy before, K_0, and after the impact, K_1, are given by the following expressions:

$$K_0 = \frac{1}{2} m_s (1 + a_s) {v_{s0}}^2 \tag{35}$$

$$K_1 = \frac{1}{2} m_s (1 + a_s) {v_{s1}}^2 + \frac{1}{2} m_i (1 + a_i) {v_{i1}}^2 + \frac{1}{2} I_i {\omega_i}^2 \tag{36}$$

The dissipated energy, E_a, is the difference between these two quantities. Inserting the expressions for velocities, it is found that:

$$E_a = K_0 - K_1 = \frac{1}{2}\left[\frac{m_s (1 + a_s) {v_{s0}}^2}{1 + \frac{m_s}{m_i}\frac{(1+a_s)}{(1+a_i)} + \frac{m_s (1+a_s) R^2}{I_i}}\right] \tag{37}$$

The last term in the denominator can be rewritten, using the radius of gyration of the spar, ρ_a, to make influences more clear:

$$\frac{m_s (1 + a_s) R^2}{I_i} = \frac{m_s}{m_i}\left(\frac{R}{\rho_a}\right)^2 (1 + a_s) \tag{38}$$

This term is in the order of one, in case that the mass of the ship is in the order of the mass of the platform and R is in the order of the radius of gyration. In that case, considerable amounts of kinetic energy will be put into pitch movement of the spar.

The expression for the energy to be dissipated described in this section has great resemblance with the specified formulas in section 10.1, which is from the DNV-RP-C204. In case that R is set to be zero, the formula reduces to the formula in section 10.1, which is the formula in DNV-RP-C204, representative for a compliant installation.

Eq. (37) gives the results of a modified simplified method for calculating the dissipated energy. Both the formulas in section 10.1 and 10.2 can only be used for the head on collision. In our case, the radius of gyration and the added mass of the platform are given. R is the distance of platform center of gravity to point of impact. This point now is how to define the point of impact.

There are two collision points during the impact process. In order to perform the simplified analysis, a certain point of impact has to be chosen. This point is chosen somewhere between the two collision point in the vertical direction. There is larger contact force and larger energy dissipation at the lower collision point, thus this compromising point should be at the place closer to the low point. Finally, the point of impact is chosen at the elevation of 19m in the vertical direction of the platform. The distance R is then decided to be 5.5 meters.

10.3 Results

The last two sections discussed the two simplified methods of calculating the dissipated energy. One is the method from DNV-RP-C204 for compliant platforms. The other one is a derivative from the corresponding formula in DNV-RP-C204, but includes effects of the roll motion. The third simplified method is Liu's Method discussed in Chapter 5, which is based on Stronge impact theory. This method takes more factors, other than the roll motion, into consideration during the collision and gives a more reliable result. All these methods can give the results of dissipated energy.

However, the first two methods can only be utilized in head on collision. For the case with glancing angles, only Liu's Method could be applied.

The results for head on collision are shown in Table 10.1 and the results for glancing angle impact are shown in Table 10.2.

Table 10.1 Dissipated Energy Comparison_Head On (MJ)

	DNV Methods	Consider the Roll Motion	Liu's Method	NLFEM
2m/s	99.5	92.0	89.3	85.6
4m/s	396	366.2	357.3	353.8

Table 10.2 Dissipated Energy Comparison_Glancing Angle (MJ)

	Liu's Method	NLFEM
2m/s	82.5	72.9
4m/s	330.2	321.6

From Table 10.1 and Table 10.2, it is interesting to realize that all the simplified methods give larger values, which is conservative. This can be explained from the following aspect. The

formula given in DNV-RP-C204 is derived from the energy conservation and momentum conservation relationship. It only takes consideration of the relative motion of the two bodies from the holistic view. The motion of the structure itself is not considered. While the second method takes the roll motion of the struck part into account. The roll motion itself will dissipate some energy. Therefore the total energy dissipated as the strain energy will be less than the first method. Similarly, the energy dissipated as strain energy in Liu's Method will be even less due to the more factors taken into consideration.

Liu's method results are the closest to the NLFEM results given in LS-DYNA, but a little larger. This is due to the existence of such as eroded energy and hourglass energy. For example, the eroded energies are 2MJ and 5.7MJ in 2m/s and 4m/s head on collision case, respectively. Hourglass energy also exists, but is not exported in head on collision case. For the case with glancing angle, the eroded energy is 2MJ and 8.2MJ, the hourglass energy is 2.2MJ and 9MJ, for the 2m/s and 4m/s case, respectively. With these energies added, the results from Liu's method are more closed to the NLFEM results. Even for the 4m/s case, the NLFEM results will exceed the results from Liu's method in the 4m/s case, so that at this time the Liu's method can not be considered as a conservative method. So it is better and safer to use Liu's method within a certain impact velocity.

In a conclusion, all the simplified methods give out conservative and relatively good results. Among these methods, Liu's method has the most comprehensive consideration and gives the best results. DNV method gives a relatively inaccurate result among these, but could still be used to estimate the dissipated energy when doing the simplified estimation.

Chapter 11 Additional Work

According to the requirements, two additional jobs are performed. One is changing the impact elevation. The other is changing the steel-steel friction coefficient. In this chapter, a short description will be made to explain these two effects and only the energy will be compared.

11.1 Impact Elevation

The relative location of the platform and the tanker in the vertical direction is changed in this section. In the original case, the tanker is ballast condition which is of the smallest draft and the platform is full loaded which is of the largest draft. In this section, in order to evaluate the effect of the loading conditions, the tanker is set to be heavier with larger draft, while the platform is lighter. However, it has to be confirmed that the tanker will not impact on the double bottom after the variation. Figure 11.1 and Figure 11.2 show the energy dissipation for different impact elevation.

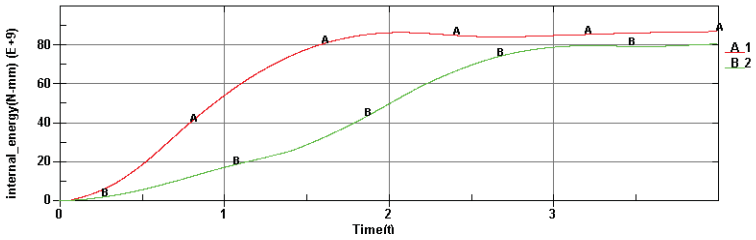

Figure 11.1 Total Energy Dissipation for Different Impact Elevation

Line 1 in Figure 11.1 and Figure 11.2 is the original loading condition and Line 2 is for the condition after changing. It is found that the original case absorbs more energy, which is consistent with what is shown in Figure 4.7. The energy dissipation will decrease if the mass ratio between the tanker and the platform increases. The tanker in ballast and platform in full loaded condition is the critical loading condition, so it is reasonable to choose this condition as the main case in the thesis.

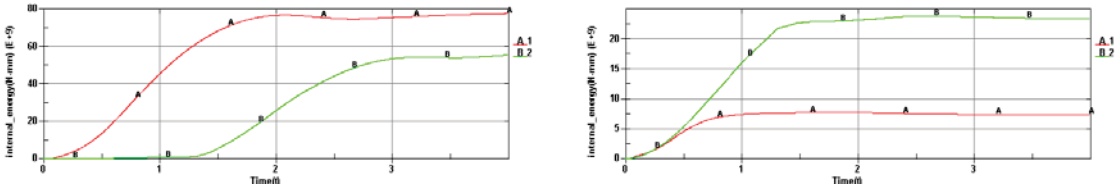

(a) Platform (b) Tanker

Figure 11.2 Energy Dissipation of Platform and Tanker for Different Impact Elevation

Figure 11.2 shows the energy dissipation of the platform and the tanker separately. The platform dissipates less energy after variation, while the tanker dissipates more.

11.2 Friction Coefficient

The original coefficient set in the contact is 0.15. In this section, the friction is increased to 0.4 without any other parameter changing. Herein the 2m/s head on collision is taken as an example. The energy dissipation plots for the buoy and the tanker are shown in Figure 11.3. It can be read from the output file that the total energy dissipation for the friction coefficient 0.4 is 84.6 MJ, which is a little smaller than that in friction coefficient 0.15 case (85.6 MJ). But the difference is not obvious. It seems that the friction coefficient will not have so much effect on the energy dissipation.

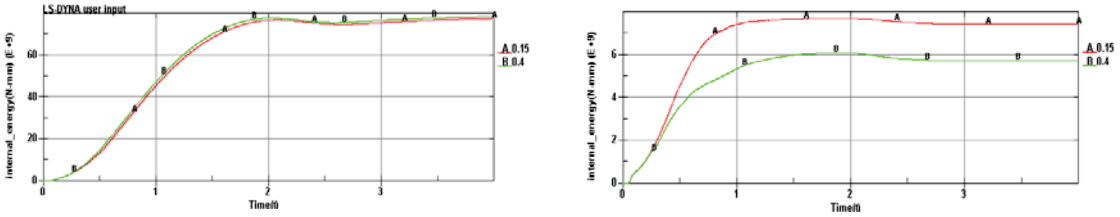

(a) Platform (b) Tanker

Figure 11.3 Energy Dissipation for Different Friction Coefficient

It is seen from the figures that the energy dissipations for both the platform and the tanker have no big difference in the two cases. But it is worth mentioning that the energy dissipation for the platform increases a little compared to the original case. This may be due to the fact that in head on collision, the friction will be not that important compared to the case with glancing angle. There is no drastic relative sliding between the two bodies. It is better to use the case with glancing angle to study the effect of the friction coefficient, which is remained as a future work due to the time limit.

It is reasonable that the energy dissipation decrease with the increase of the friction coefficient. This is because that more kinetic energy is transformed to frictional energy. The frictional energy value can be read from the output files. It is found that the frictional energy is 1.5 MJ and 2.5 MJ for the friction coefficient 0.15 and 0.4, respectively.

Chapter 12 Discussion and Conclusion

A platform model is created. This is generated by the complete set of structural drawings. A little more than one-sixth of the platform is modeled in detail and proper simplifications are made, so that the FE model is not only fine enough to capture the governing deformation mechanisms in way of the impact zone, but still meet requirements with respect to acceptable CPU consumption.

A shuttle tanker model is given. Modifications are made to get consistent units with the platform. Moreover, mass distribution is adjusted to represent the shuttle tanker in term of total mass, center of gravity and radius of gyration. Similar adjustments are also performed to the platform.

Integrated analyses are performed as the main study. Impact simulations of the platform and the tanker for the selected scenarios are conducted. Two impact velocities of the shuttle tanker, 2m/s and 4m/s, are chosen. The forward velocity is of significant importance to the collision damage. Forward speeds have positive effects, as well as some negative ones. For the disadvantages, the amount of energy to be absorbed during the collision will be increased. The rupture initiation in the stretched shells due to friction is also accelerated. For the advantages, the energy absorbed by friction is increased. Moreover, the increased velocity can decrease the energy to be absorbed by structural damage due to the increased frictional energy and the increased rigid body translational or rotational motion. In the integrated analysis, the velocity of the striking tanker changes during the impact.

Head on collision and collision with glancing angle of 30 degrees are performed in the integrated analysis. The energy dissipation in the head on collision is larger than that in the glancing angle collision, which is due to the larger frictional energy and larger rigid body rotation in the glancing angle case. Further more, the energy dissipation by the tanker and the platform is more balanced in the glancing angle collision. This may be due to the structure tanker bow.

Internal analyses are performed particularly to assess the damage on the platform and the tanker. The platform is set to be fixed spatially and the tanker impacts the platform in a constant speed. It is concluded that for all scenarios, the damage assessed from internal analysis can almost represent that from the integrated analysis well. Moreover, for cases with smaller impact velocity, the difference of the deformation between the internal analysis and integrated analysis is smaller. The results from the internal analysis are more closed to the integrated analysis if the rotational inertial is well simulated, because unrealistic rotation will cause variation of the deformation.

External mechanics analysis is performed in this thesis. Liu's method is used by performing a Matlab program. The energy dissipation and the velocity after impact can be obtain herein. It is found that the energy dissipation got from external mechanics is closed with, but a little larger than that from FEM analysis. For the same impact glancing angle with different impact velocity, the energy ratios between dissipated energy and kinetic energy are the same. While

for the head on collision, more energy is dissipated as strain energy, which is consistent with the results from FEA.

Simplified methods are used to assess the energy dissipated as strain energy. The Liu's method is regarded as one of the simplified methods. The other two are method from DNV rules and a modified DNV method. All these three methods can well evaluate the energy dissipation. Among these, Liu's method is the most accurate one due to more considerations included. Method from DNV rules is the relatively inaccurate one. The modified DNV method is better than that from DNV rules because it considers the effect of roll motion.

Relative impact elevation is changed in the additional work. The draft of the tanker is increased, while the draft of the platform is decreased. The energy dissipation is decreased after variation. This is consistent with what is shown in Figure 4.7. The mass ratio of the tanker and the platform increased, so that there will be less energy dissipation.

Friction coefficient is changed in the additional work. Though the total energy dissipation decreases due to the increasing frictional energy, the difference is small. Even for the platform, there is tiny increase in the energy dissipation after increasing the friction coefficient from 0.15 to 0.4.

Chapter 13 Further Work

- Increase the Young's modulus of the platform

It is obviously seen from the results that the tanker is much stronger than the platform, because in head on collision, the tanker absorbs little energy. The Young's modulus is 275 MPa currently, which can be increased to 315 MPa. So the resistance against deformation of the platform will be increased and the energy dissipations of the two bodies are expected to be more balanced.

- Utilize the entire tanker instead of the bow for head on collision

In this thesis, only the bow is chosen as striking body the head on collision. There is no modification against the rotational inertia. Therefore the rotation of the tanker bow is believed to be larger than expected in reality. In impact with glancing angle, the entire tanker is used so the inertial is in reasonable range.

- Utilize the impact with glancing angle case to evaluate the effect of the friction coefficient

In head on collision, the relative sliding between the two bodies is not obvious. If a glancing angle exists, there will be much more frictional energy, thus the comparison results will be more obvious and objective.

- More parameter studies can be performed

Varying the added mass coefficients or the fracture strain is a good choice if time permits.

- Mesh improvement on platform model to reduce computational time
- Model the double bottom in details to perform the case of tanker in full loaded and platform in ballast condition
- Test platform model with other bows

References

[1] A.Smedal and K.yvertsen. The SSP-300: An alternative to the oil industry. 2005.

[2] Jørgen Amdahl. SSP300 – Resistance to shuttle tanker collision. Simplified methods. 2005.

[3] NORSOK. Norsok standard N-004 design of steel structures. Appendix a: Design against accidental actions. In NORSOK Standard N-004 Design of Steel Structures. Norwegian Technology Standards Institution, 2004.

[4] DNV. Recommended practice-dnv-rp-c204. In DVN-RP. DNV, 2004.

[5] LS-DYNA Theory Manual. 2006.

[6] Martin Storheim. Analysis of structural damage of tankers subjected to collision. Master Thesis. 2008.

[7] LS-DYNA Keyword User's Manual. 2007.

[8] Hagbart S Alsos, Jørgen Amdahl, and Odd s. Hopperstad. On the resistance to penetration of stiffened plates. Part ii, numerical analysis. Part of PhD Thesis, 2008.

[9] Hagbart S. Alsos. Ship Grounding: Analysis of Ductile Fracture, Bottom Damage and Hull Girder Response. PhD thesis, NTNU, 2008.

[10] Sevan Marine ASA, Draft Master thesis 2013/2014, 2013.

[11] P. Terndrup Pedersen, Shengming Zhang. On impact mechanics in ship collisions. 1998.

[12] Shengming Zhang. The mechanics of ship collisions. 1999.

[13] Lin Hong and Jørgen Amdahl. Strength Design of FPSOs against Supply Vessel Bow Collision. PhD thesis, NTNU, 2007.

[14] Zhenhui Liu and Jørgen Amdahl. A new formulation of the impact mechanics of ship collisions and its application to a ship-iceberg collision, 2010.

[15] Stronge, W.J. Impact mechanics. Cambridge, Cambridge University Press, 2004.

[16] Zhenhui Liu. Analytical and numerical analysis of iceberg collisions with ship structures. Chapter 2: External Mechanics. Part of PhD Thesis, 2011.

[17] A.Smedal and K.yvertsen. The SSP-300: An alternative to the oil industry. 2005.

[18] Samsung Heavy Industries, *https://www.shi.samsung.co.kr/eng/default.aspx.*

[19] Torgeir Moan. TMR4190-Finite Element Modelling and Analysis of Marine Structures. Institutt for Marin Teknikk, 2003.

[20] T. de Jonge and L. Laukeland. Collision Between a Spar platform and a Tanker, 2013.

Appendix

A. Deformation Plots

A.1 Head on Collision_2m/s

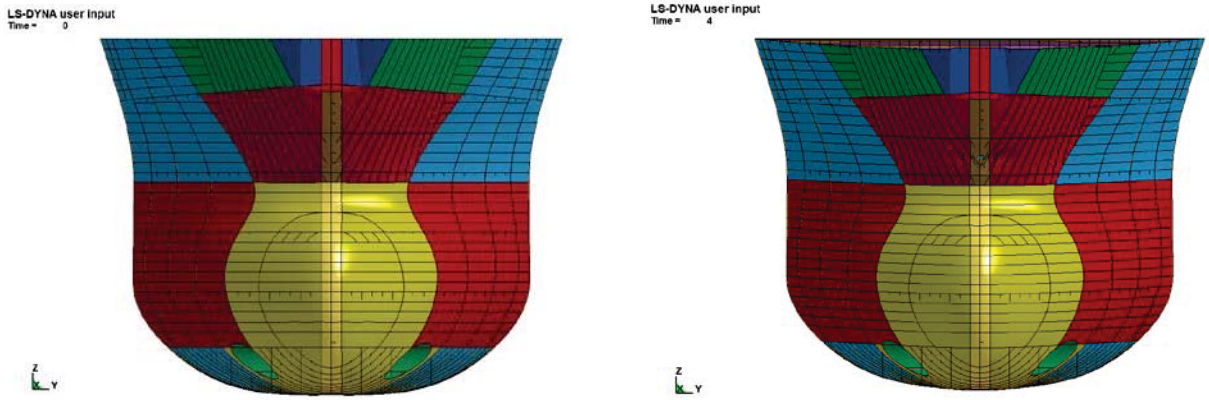

Figure A.1 Deformation of Tanker_Head on_2m/s

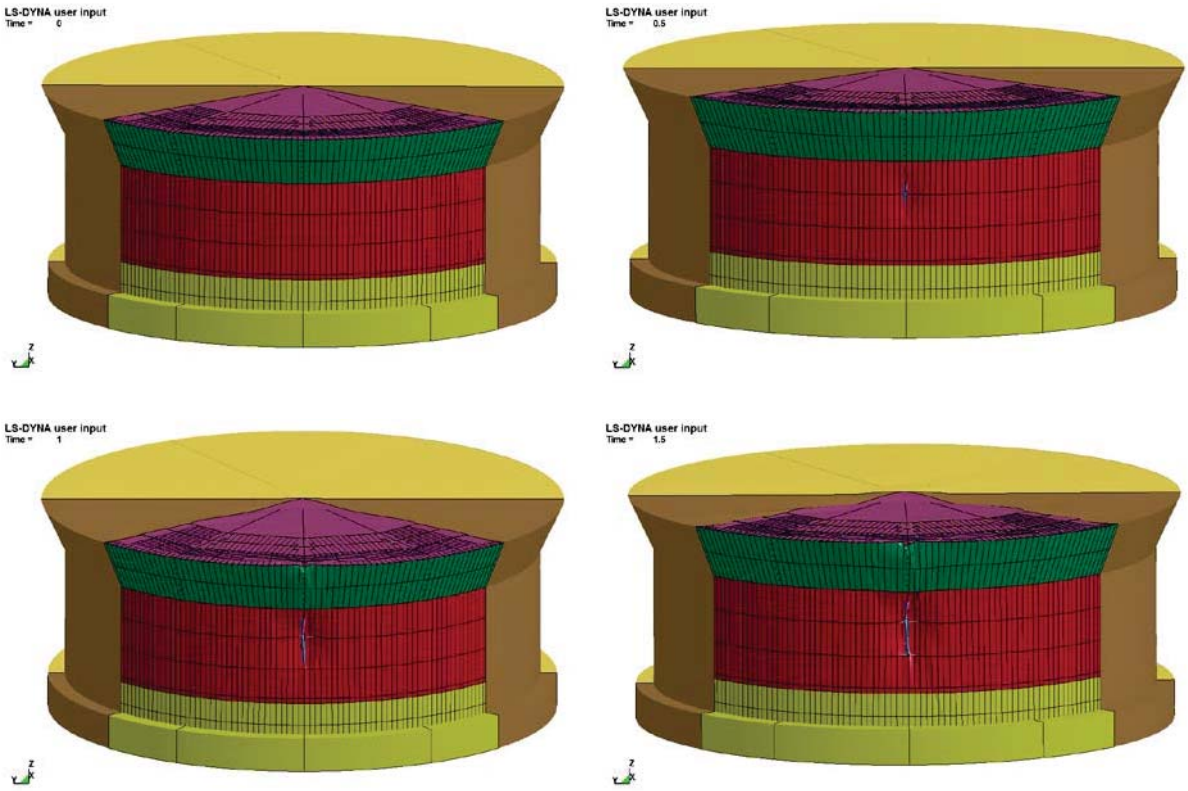

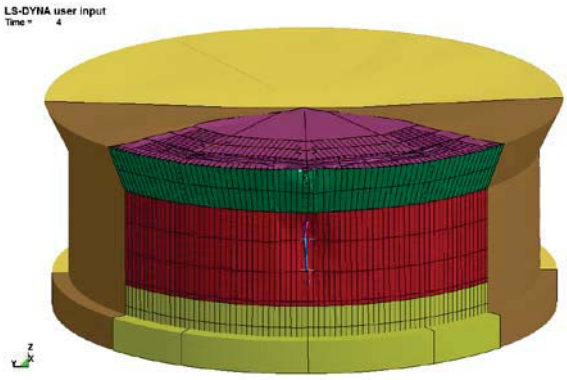

Figure A.2 Deformation of Platform_Head on_2m/s

A.2 30° Glancing Angle Collision_2m/s

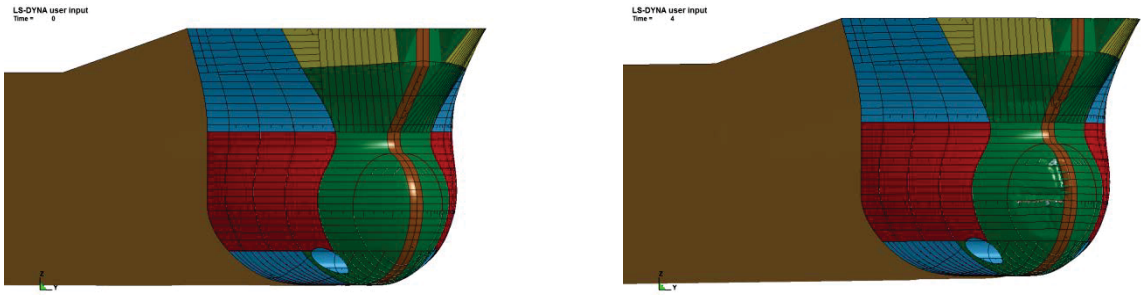

Figure A.3 Deformation of Tanker_Glancing Angle_2m/s

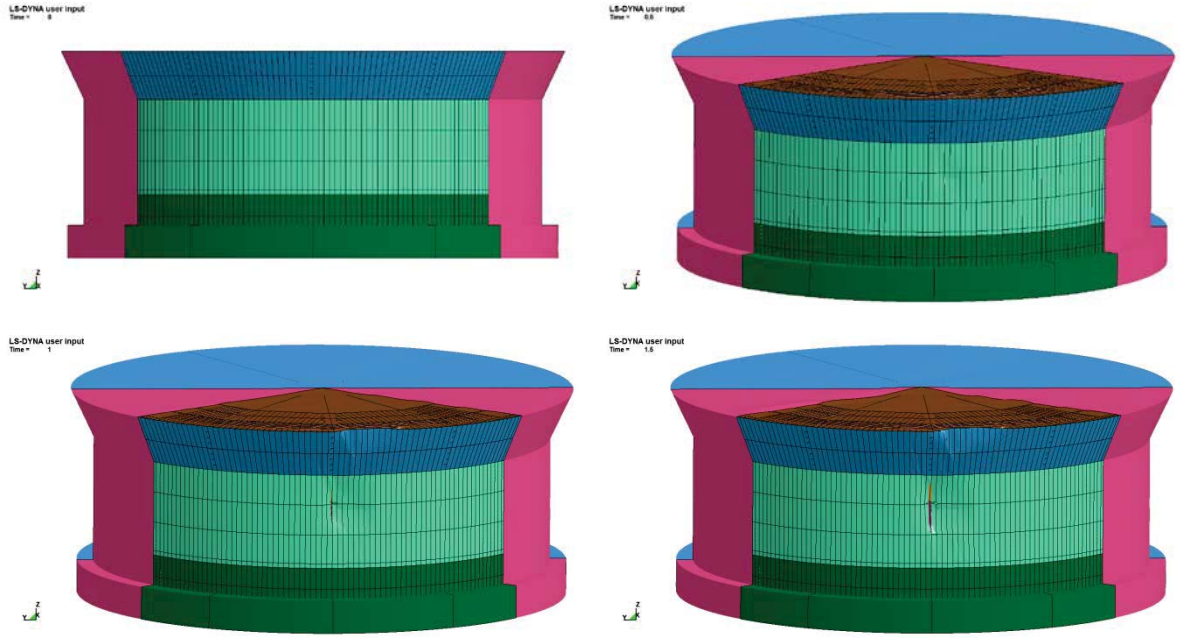

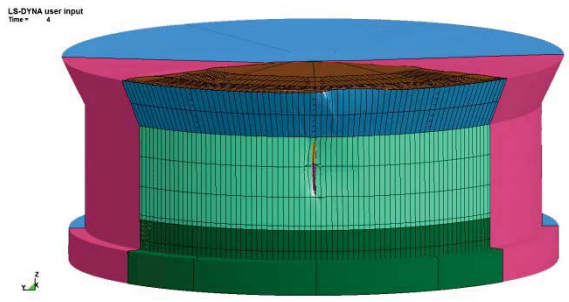

Figure A.4 Deformation of Platform_Glancing Angle_2m/s

A.3 Head on Collision_4m/s

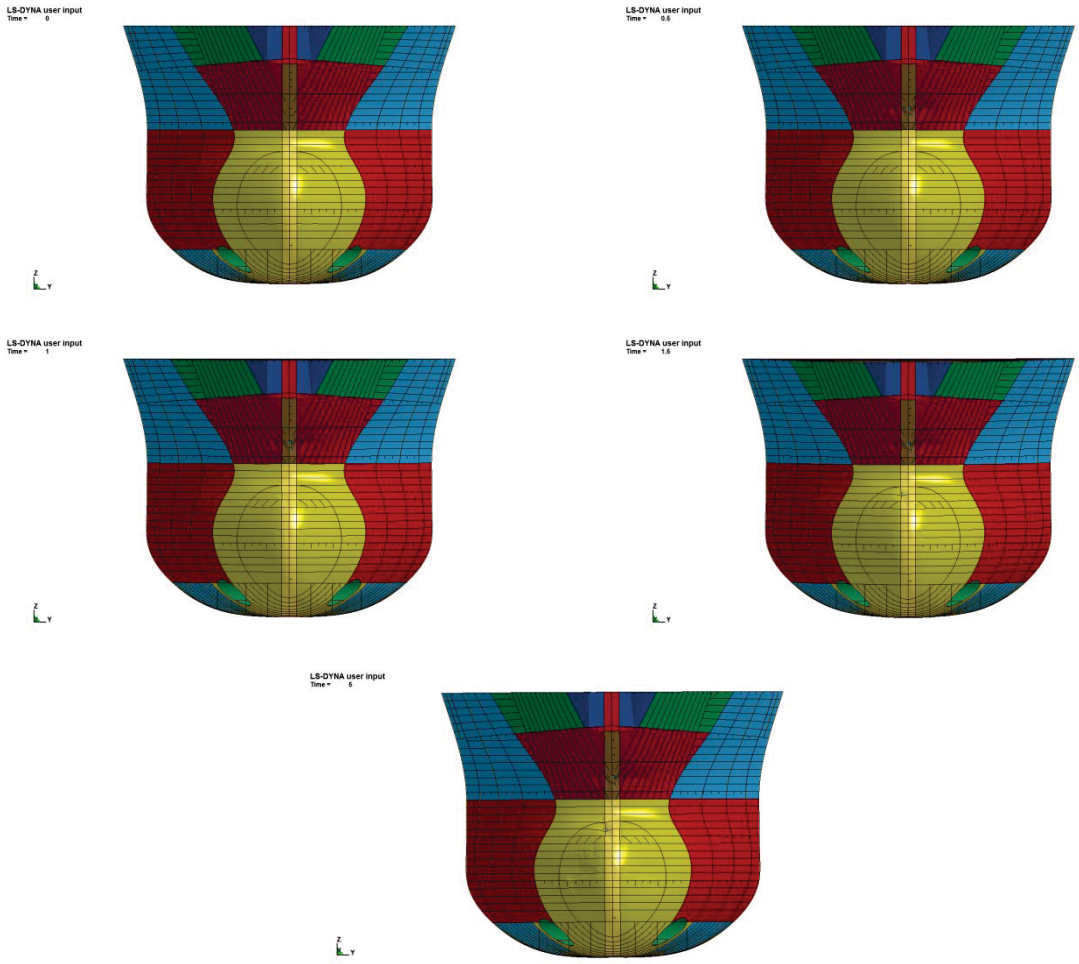

Figure A.5 Deformation of Tanker_Head on_4m/s

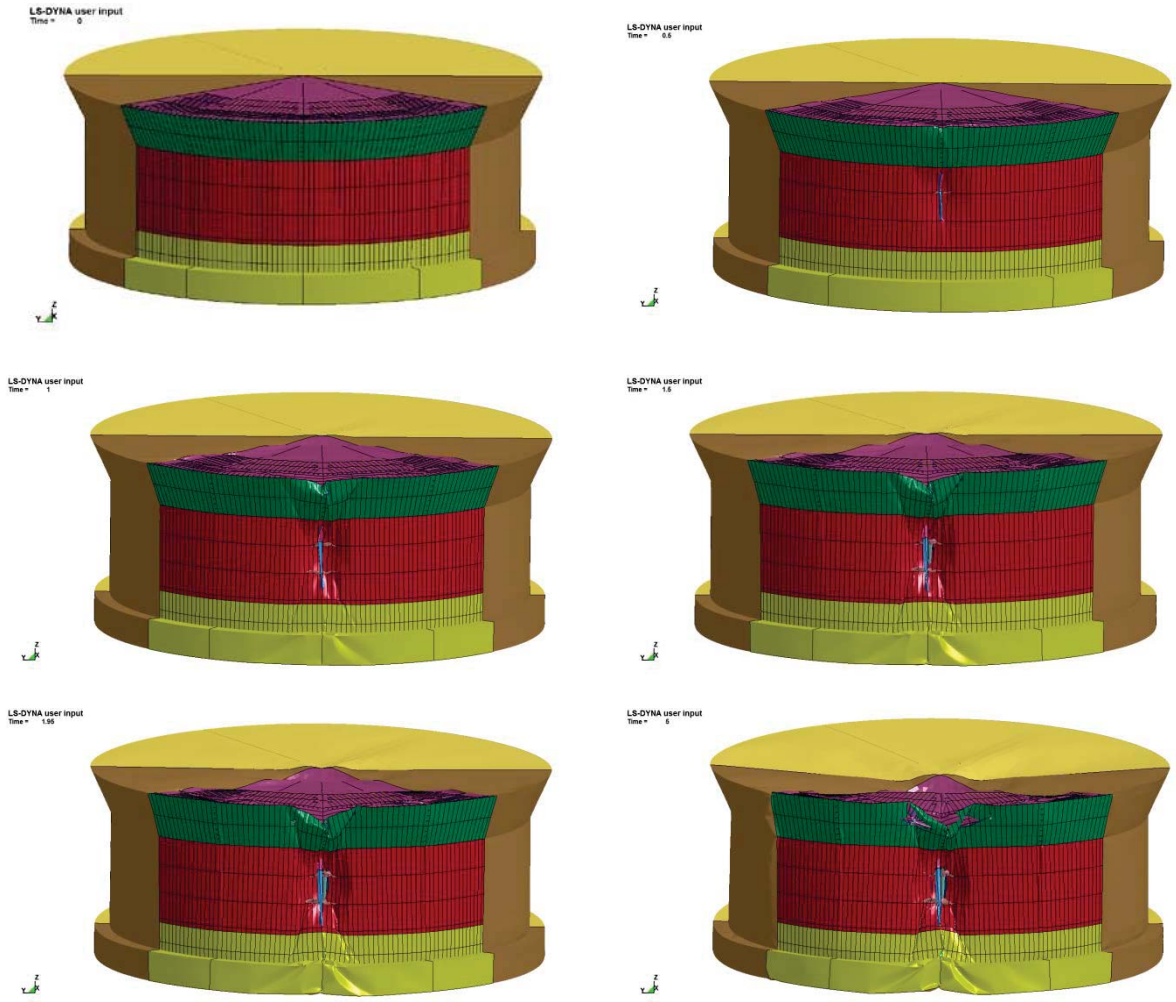

Figure A.6 Deformation of Platform_Head on_4m/s

A.4 30° Glancing Angle Collision_4m/s

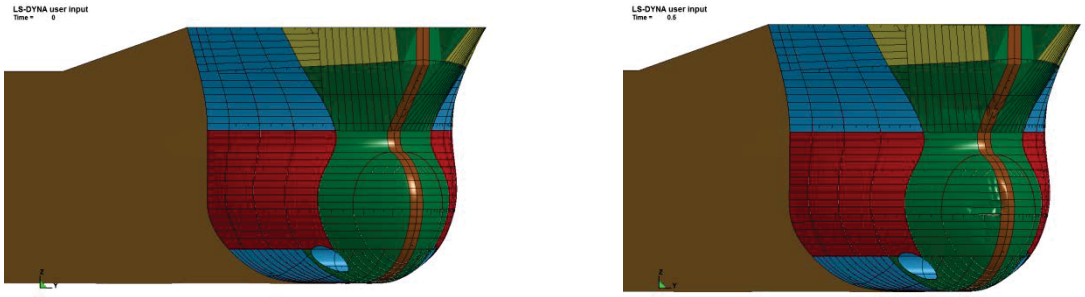

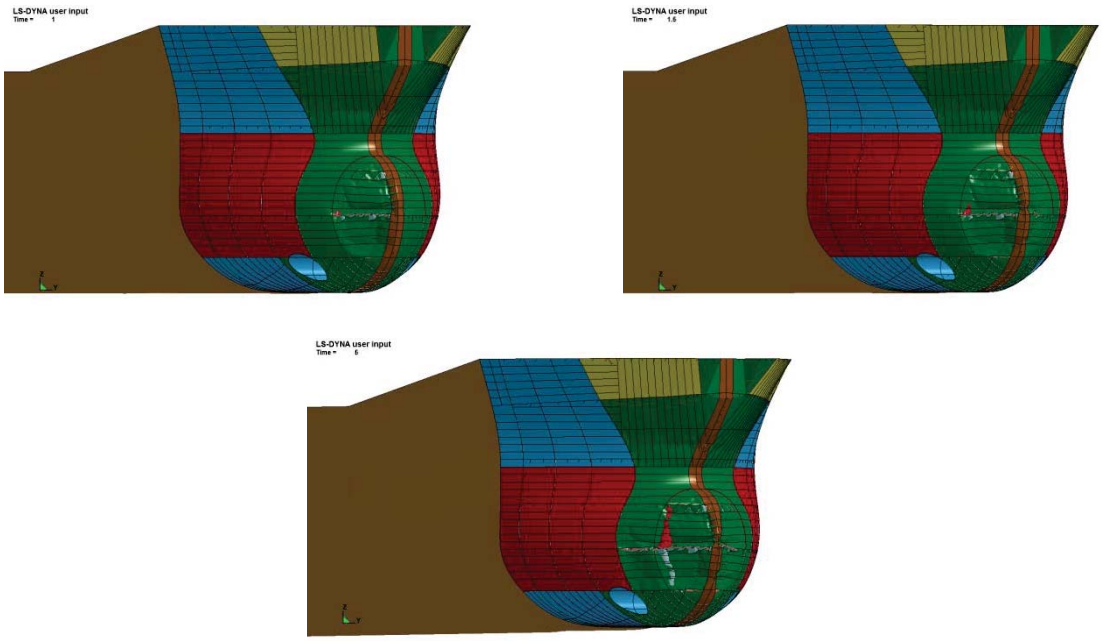

Figure A.7 Deformation of Tanker_Glancing Angle_4m/s

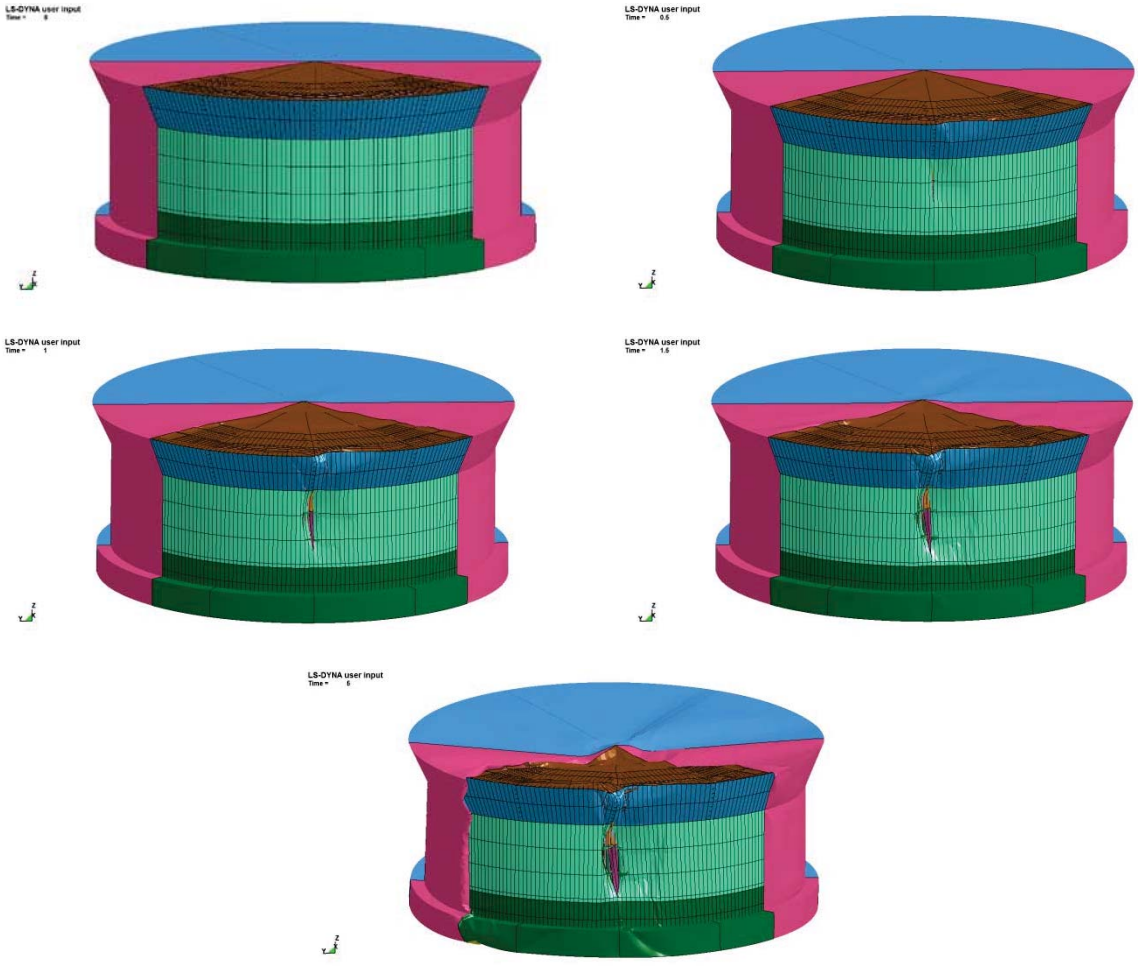

Figure A.8 Deformation of Platform_Glancing Angle_4m/s

B. Force-displacement Curve

B.1 Impact with Friction Coefficient 0.4

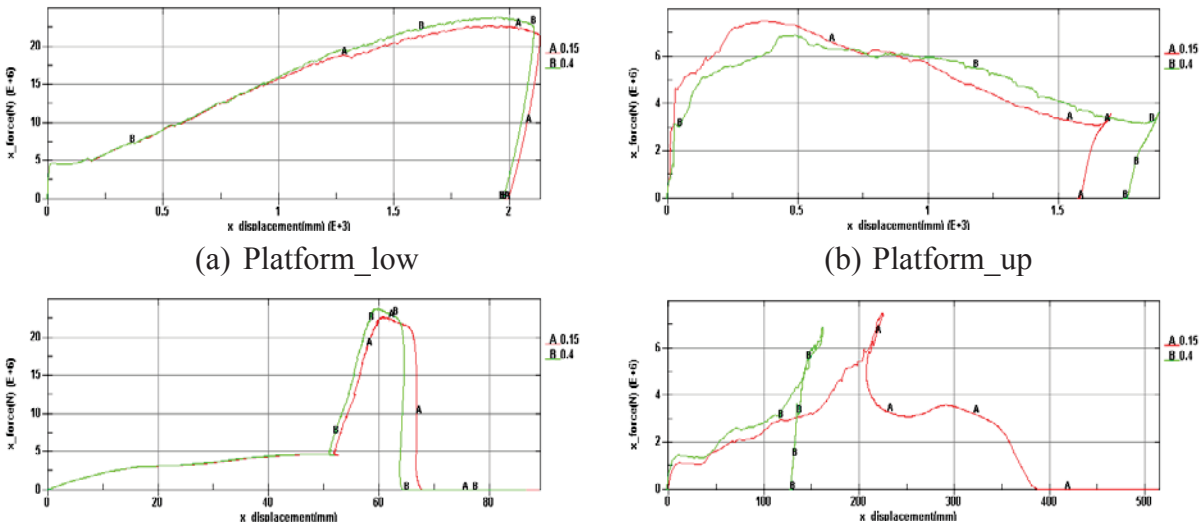

(a) Platform_low (b) Platform_up

(c) Tanker_low (d) Tanker_up

Figure B.1 Force-displacement Relationship Comparison_Friction Coefficient 0.4

B.2 Impact with New Elevation

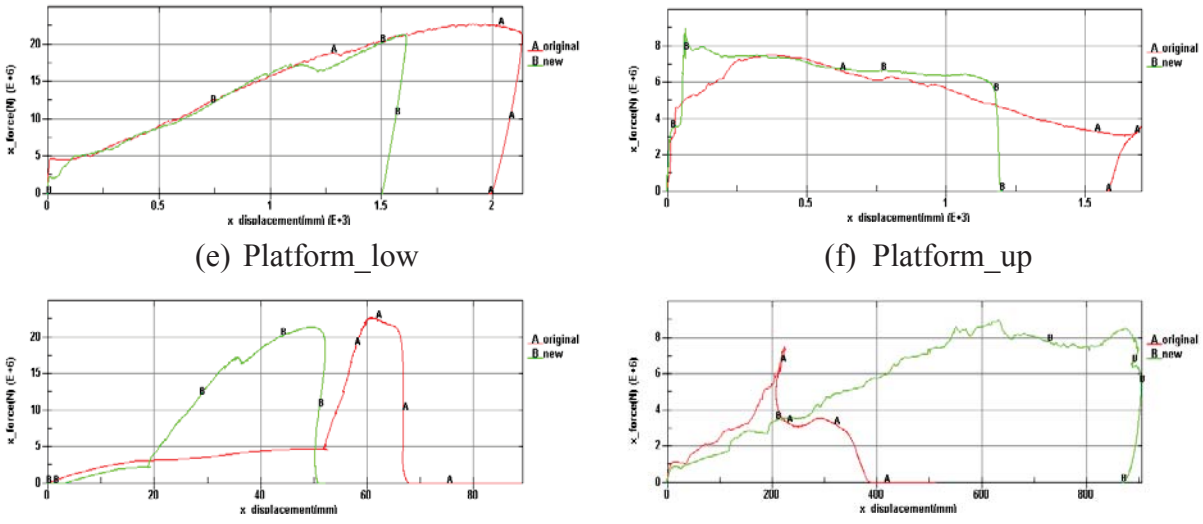

(e) Platform_low (f) Platform_up

(g) Tanker_low (h) Tanker_up

Figure B.2 Force-displacement Relationship Comparison_New Impact Elevation

C. Matlab Code for Liu's Method

C.1 Stronge Theory

```
function
[tt,ttm,dvv,ve_af,ve_bf,flag,miu,mass1,mass2]=stronge3d(Mass1,Mass2,Am,Bm,A
mr,Bmr,Ra,Rb,alpha,gama,betap,cp_a,cp_b,res,miu0,ve_a,ve_b)
%
% INPUT PARAMETERS
% Mass1 : mass of object a, no added mass included [kg]
% Mass2 : mass of object b, no added mass included [kg]
% Am    : translational added mass of object a under body frame of object a
% Bm    : translational added mass of object b under body frame of object b
% Amr   : rotational added mass of object a under body frame of object a
% Bmr   : rotational added mass of object b under body frame of object b
% Ra    : inertia radius square of object a under body frame of object a
%         [m2]
% Rb    : inertia radius square of object a under body frame of object b
%         [m2]
% alpha : waterline angle [deg]
% gama  : angle between body frame of object a and b [deg]
% betap : normal frame angle [deg]
% cp_a  : collision point under body frame of object a, array (3x1)
% cp_b  : collision point under body frame of object b,array (3x1)
% ve_a  : velocity of object a under body frame of object a,array (3x1)
% ve_b  : velocity of object b under body frame of object b,array (3x1)
% res   : restitution factor, res=0 (fully plastic), res=1 (fully elastic)
% miu0  : the static friction
%-------------------------------------------------------------------------
--------
% OUTPUT PARAMETERS
% tt    : total dissipated energy [J]
% ttm   : an array for dissipated energy in each direction [J]
% dvv   : relative velocity increase under the local frame n1n2n3
% ve_af : velocity after impact of object a under body frame of object a
% ve_bf : velocity after impact of object b under body frame of object b
% flag  : stick (1) or slide (2)
% miu   : static friction factor between object a and b
% mass1 : mass matrix for object a
% mass2 : mass matrix for object b
%
%-------------------------------------------------------------------------
```

```
--------
mass1=[1+Am(1) 0 0; 0 1+Am(2) 0; 0 0 1+Am(3)]*Mass1; % mass matrix for object
a
mass2=[1+Bm(1) 0 0; 0 1+Bm(2) 0; 0 0 1+Bm(3)]*Mass2; % mass matrix for object
b
rxa=Ra(1); % gyration radius square for a
rya=Ra(2); % gyration radius square for a
rza=Ra(3); % gyration radius square for a
rxb=Rb(1); % gyration radius square for b
ryb=Rb(2); % gyration radius square for b
rzb=Rb(3); % gyration radius square for b
Itrx1=[(1+Amr(1))*rxa 0 0;0 (1+Amr(2))*rya 0; 0 0 (1+Amr(3))*rza]*Mass1; %
Inertia matrix for a
Itrx2=[(1+Bmr(1))*rxb 0 0;0 (1+Bmr(2))*ryb 0; 0 0 (1+Bmr(3))*rzb]*Mass2; %
Inertia matrix for b
oba_g=[0 0 0]'; % gravity center of a under body frame of object a
obb_g=[0 0 0]'; % gravity center of b under body frame of object b
alpha=alpha/180*pi; %wanterline angle
gama =gama/180*pi;  % angle between body frame a and b
betap=betap/180*pi;
% calculate the relative impact vector under body frame a and b
rad1a=cp_a-oba_g;
rad2b=cp_b-obb_g;
% trasnformation matrix between body frame a and b
Mab=[cos(gama) sin(gama) 0;
    -sin(gama) cos(gama) 0;
    0 0 1];
% transformation matrix between local and global system for a
l=sin(alpha)*cos(betap);
m=cos(alpha)*cos(betap);
n=-sin(betap);
Mlg=[cos(alpha) -sin(alpha) 0;
    -sin(alpha)*sin(betap) -cos(alpha)*sin(betap) -cos(betap);
    l m n];
% transformation matrix between local and global system for b
Mtr2=Mlg*Mab;
% calculate the transformed inertia matrix
Rtrx1=inv(Mlg*Itrx1*inv(Mlg));
Rtrx2=inv(Mtr2*Itrx2*inv(Mtr2));
mass1f=inv(Mlg*mass1*inv(Mlg));
mass2f=inv(Mtr2*mass2*inv(Mtr2));
% calculate the impact vector under local frame
rad1=Mlg*rad1a;
rad2=Mtr2*rad2b;
```

```
% calculate the relative velocity under local system
rvl=Mlg*ve_a-Mtr2*ve_b;
% Input the reversed mass matrix
m11=(mass1f(1,1)+rad1(2)^2*Rtrx1(3,3)-2*rad1(2)*rad1(3)*Rtrx1(2,3)+rad1(3)^
2*Rtrx1(2,2))+ ...

(mass2f(1,1)+rad2(2)^2*Rtrx2(3,3)-2*rad2(2)*rad2(3)*Rtrx2(2,3)+rad2(3)^2*Rt
rx2(2,2));
m12=(mass1f(1,2)+mass2f(1,2))+(rad1(1)*rad1(3)*Rtrx1(2,3)-rad1(3)^2*Rtrx1(2
,1)-...
    rad1(1)*rad1(2)*Rtrx1(3,3)+rad1(2)*rad1(3)*Rtrx1(3,1))+...

(rad2(1)*rad2(3)*Rtrx2(2,3)-rad2(3)^2*Rtrx2(2,1)-rad2(1)*rad2(2)*Rtrx2(3,3)
+rad2(2)*rad2(3)*Rtrx2(3,1));
m13=(mass1f(1,3)+mass2f(1,3))+(rad1(1)*rad1(2)*Rtrx1(3,2)-...

rad1(2)^2*Rtrx1(3,1)-rad1(1)*rad1(3)*Rtrx1(2,2)+rad1(2)*rad1(3)*Rtrx1(2,1))
+...

(rad2(1)*rad2(2)*Rtrx2(3,2)-rad2(2)^2*Rtrx2(3,1)-rad2(1)*rad2(3)*Rtrx2(2,2)
+rad2(2)*rad2(3)*Rtrx2(2,1));
m22=(mass1f(2,2)+rad1(1)^2*Rtrx1(3,3)-2*rad1(1)*rad1(3)*Rtrx1(1,3)+rad1(3)^
2*Rtrx1(1,1))+...

(mass2f(2,2)+rad2(1)^2*Rtrx2(3,3)-2*rad2(1)*rad2(3)*Rtrx2(1,3)+rad2(3)^2*Rt
rx2(1,1));
m23=(mass1f(2,3)+mass2f(2,3))+(rad1(3)*rad1(1)*Rtrx1(1,2)-rad1(3)*rad1(2)*R
trx1(1,1)-...
    rad1(1)^2*Rtrx1(3,2)+rad1(1)*rad1(2)*Rtrx1(3,1))+...

(rad2(3)*rad2(1)*Rtrx2(1,2)-rad2(3)*rad2(2)*Rtrx2(1,1)-rad2(1)^2*Rtrx2(3,2)
+rad2(1)*rad2(2)*Rtrx2(3,1));
m33=(mass1f(3,3)+rad1(1)^2*Rtrx1(2,2)-2*rad1(1)*rad1(2)*Rtrx1(1,2)+rad1(2)^
2*Rtrx1(1,1))+...

(mass2f(3,3)+rad2(1)^2*Rtrx2(2,2)-2*rad2(1)*rad2(2)*Rtrx2(1,2)+rad2(2)^2*Rt
rx2(1,1));
m21=m12;
m31=m13;
m32=m23;
m=[m11,m12,m13;m12,m22,m23;m13,m23,m33];
syms dv1 dv2 dv3 dp1 dp2 dp3
rm=inv(m);
% calculate the extreme case for stick together get the critical value miu
```

```
dv1=-rvl(1);
dv2=-rvl(2);
dv3=-rvl(3)*(1-res);
dp1=subs(rm(1,1)*dv1+rm(1,2)*dv2+rm(1,3)*dv3,{dv1,dv2,dv3},{-rvl(1),-rvl(2)
,-rvl(3)*(1-res)});
dp2=subs(rm(2,1)*dv1+rm(2,2)*dv2+rm(2,3)*dv3,{dv1,dv2,dv3},{-rvl(1),-rvl(2)
,-rvl(3)*(1-res)});
dp3=subs(rm(3,1)*dv1+rm(3,2)*dv2+rm(3,3)*dv3,{dv1,dv2,dv3},{-rvl(1),-rvl(2)
,-rvl(3)*(1-res)});
miu=sign(dp1)*sqrt(dp1^2+dp2^2)/dp3;
miu2=dp2/dp1;
% friction matrix
flag='Stick';
if miu==0
    sm1=Inf;
else
    sm1=m11+m12*miu2+m13*sqrt(1+miu2*miu2)/miu;
    if miu2==0
        sm2=Inf;
    else
        sm2=m21/miu2+m22+m23*sqrt(1+miu2*miu2)/miu/miu2;
    end
end
sm3=m31*miu/sqrt(1+miu2*miu2)+m32*miu*miu2/sqrt(1+miu2*miu2)+m33;
if abs(miu)>=miu0 % sliding case
    flag='Slide';
    dv3=-rvl(3)*(1-res);
    fai=atan(miu2);
    if dp2==0
        fai=0/180*pi;
    end
    if miu0==0
        sm1=Inf;
    else
        sm1=m11+m12*miu2+m13*sqrt(1+miu2*miu2)/miu0;
        if miu2==0
            sm2=Inf;
        else
            sm2=m21/miu2+m22+m23*sqrt(1+miu2*miu2)/miu0/miu2;
        end
    end
    sm3=m31*miu0/sqrt(1+miu2*miu2)+m32*miu0*miu2/sqrt(1+miu2*miu2)+m33;
    AA=[miu0*cos(fai)*1e06 -rm(1,1) -rm(1,2);
        miu0*sin(fai)*1e06 -rm(2,1) -rm(2,2);
```

```
       1e06 -rm(3,1) -rm(3,2)];
    BB=[rm(1,3)*dv3 rm(2,3)*dv3 rm(3,3)*dv3]';
    CC=AA\BB;
    dp3=CC(1,1)*1e06;
    dv1=CC(2,1);
    dv2=CC(3,1);
    dp1=miu0*cos(fai)*dp3;
    dp2=miu0*sin(fai)*dp3;
end
%dpp=sqrt(dp1^2+dp2^2+dp3^2);
% energy on direction 1
%E1=abs(dp1/2.*(dv1+2*rvl(1)));
E1=abs(1/sm1/2*dv1*(dv1+2*rvl(1)));
% energy on direction 2
if miu2==0
    E2=0;
else
    %E2=abs(dp2/2.*(dv2+2*rvl(2)));
    E2=abs(1/sm2/2*dv2*(dv2+2*rvl(2)));
end
%E3=abs(dp3/2.*(dv3+2*rvl(3)));
E3=abs(1/sm3/2*dv3*(dv3+2*rvl(3)));
% velocity change vector
dvv=[dv1;dv2;dv3]; % this is in local frame
% total energy
% do control to output if NaN, usually a result of Inf*0
if isnan(E1)==1
    E1=0;
elseif isnan(E2)==1
    E2=0;
elseif isnan(E3)==1
    E3=0;
end
tt=E1+E3+E2;
ttm=[E1,E2,E3];
%% compute the velocity after impact at body frame a and b
FF=mass1+mass2*inv(Mtr2)*Mlg;
SS=mass1*ve_a+mass2*ve_b;
QQ=mass2*inv(Mtr2)*(rvl+dvv);
ve_af=inv(FF)*(SS+QQ);              % velocity of body a after impact under body
frame a
ve_bf=inv(Mtr2)*(Mlg*ve_af-(rvl+dvv)); % velocity of body b after impact under
body frame b
end
```

C.2 Liu's Method

Head on collision with impact velocity 2m/s is taken as an example herein.

```
clear all
close all
clc
%% The 3D collision mechanics based on Stronge's theory
%--------------dimension of the shuttle tanker------------
Ha=26.6;                % tanker height
La=278;                 % tanker length
Ba=46;                  % tanker breadth
Ta=9;                   % tanker waterdraft
%--------------dimension of the FPSO------------
Hb=27;
Db=65.15;
Tb=17;
%--------------tanker mass ballast [kg]---------------------------------
Mass1=90000000;
%--------------FPSO mass full [kg]-----------------------------
Mass2=51185000;
%--------------tanker added mass factor,assumptions-------
Amx=0.05;
Amy=1;
Amz=1;
Am=[Amx,Amy,Amz];
Amrol=0.1;
Ampit=1;
Amyaw=1;
Amr=[Amrol,Ampit,Amyaw];
%--------------ship inertia radius squared -------------------
%--------------empirical again and see reference in paper-----
rxa=(0.35*Ba)^2;
rya=(0.35*La)^2;
rza=(0.35*La)^2;
Ra=[rxa,rya,rza];
%--------------FPSO added mass experience value----------
Bmx=0.7;
Bmy=1;
Bmz=1;
Bm=[Bmx,Bmy,Bmz];
Bmrol=1;
Bmpit=1;
Bmyaw=1;
```

```
Bmr=[Bmrol,Bmpit,Bmyaw];
%--------------FPSO inertia radius squared-----
%-----------------------------------------------------------------
rxb=361;
%rx=0;
ryb=361;
%ry=0;
rzb=784;
Rb=[rxb,ryb,rzb];
%----------------varifying the frame angle--------------------
alpha=90;    % waterline angle
gama=0;     % the angle between body frame a and b
betap=0;    % the normal frame angle
%-------collision point of ship under ship's body frame-------
% for head on collision, draught is assumed
cp_a=[18.9 0 -3.51]';
%-------collision point of FPSO under FPSO's body frame---
cp_b=[-30 0 5.5]';
%----velocity of ship under ship's body frame-------------------
ve_a=[2 0 0]'; %[m/s]
%----velocity of iceberg under iceberg's body frame-------------
ve_b=[0 0 0]';   %[m/s]
miu0=0.15;      % static friction between ship and iceberg
res=0;        % restitution factor. 0-plastic, 1-elastic
%----call the 3d subroutine-------------------------------------
[tt,ttm,dvv,ve_af,ve_bf,miu,flag,mass1,mass2]=stronge3d(Mass1,Mass2,Am,Bm,A
mr,Bmr,Ra,Rb,alpha,gama,betap,cp_a,cp_b,res,miu0,ve_a,ve_b);
E0=(1/2*mass2(1,1)*ve_a(1,1)^2)/(1+mass2(1,1)/mass1(1,1));
    E=tt/E0;
    tt
    ttm
    dvv
    ve_af
    ve_bf
    E0
    E
    vpa(tt,6)
```

D. DVD

The contents of the DVD is as follows:

- Patran Database
  1. Platform model
  2. Shuttle tanker model

- LS-DYNA input files

1. Integrated_Head on collision_2m/s
2. Integrated_Glancing angle 30° collision_2m/s
3. Internal_Head on collision
4. Internal_Glancing angle 30° collision

- The DVD includes the animations of the four impact cases.
  1. Head on collision_2m/s_Impact
  2. Head on collision_2m/s_Platform deformation
  3. Head on collision_2m/s_Stress contours on platform
  4. Head on collision_4m/s_Impact
  5. Head on collision_4m/s_Platform deformation
  6. Head on collision_4m/s_Stress contours on platform
  7. Impact with glancing angle 30°_2m/s_Impact
  8. Impact with glancing angle 30°_2m/s_Platform deformation
  9. Impact with glancing angle 30°_2m/s_Stress contours on platform
  10. Impact with glancing angle 30°_4m/s_Impact
  11. Impact with glancing angle 30°_4m/s_Platform deformation
  12. Impact with glancing angle 30°_4m/s_Stress contours on platform